EFFECTS OF VARIATION OF AXIAL LOAD ON SEISMIC PERFORMANCE OF RC EXTERIOR BCJS

BY

UMAIS KHAN

A Thesis Presented to the
DEANSHIP OF GRADUATE STUDIES

KING FAHD UNIVERSITY OF PETROLEUM & MINERALS

DHAHRAN, SAUDI ARABIA

In Partial Fulfillment of the
Requirements for the Degree of

MASTER OF SCIENCE

In

CIVIL ENGINEERING

MAY 2016

KING FAHD UNIVERSITY OF PETROLEUM & MINERALS
DHAHRAN-31261, SAUDI ARABIA

DEANSHIP OF GRADUATE STUDIES

This thesis, written by **UMAIS KHAN** under the direction of his thesis advisor and approved by his thesis committee, has been presented and accepted by the Dean of Graduate Studies, in partial fulfillment of the requirements for the degree of **MASTER OF SCIENCE IN CIVIL ENGINEERING**

Dr. Salah U. Al-Dulaijan
Department Chairman

Dr. Mohammed Al-Osta
(Advisor)

Dr. Salam A. Zummo
Dean of Graduate Studies

Dr. Mohammed H. Baluch
(Member)

Kalimur Rahman

Dr. Muhammad K. Rahman
(Member)

15/5/16

Date

Dedicated to my beloved parents, sisters, brother

&

Martyred students of APS Peshawar

ACKNOWLEDGMENTS

First, I would like to praise Allah, the Almighty, for His blessings He bestowed on me; that He gave me the spirit, illuminating ideas, strength and endurance to go through all stages and accomplish this research.

My sincerest gratitude to King Fahd University of Petroleum and Minerals, Dhahran, Saudi Arabia for providing financial support and facilities through its well-equipped labs and well trained staff. Without this institutional support this research would not have been possible. Such support is a rare affluence in a world of limited resources, and I am grateful to have received it. I would also sincerely like to acknowledge support of Prainsa Precast Concrete Factory, along with its team, for supporting experimental phase of this research.

I would like to express my deepest appreciation to my thesis advisor, Dr. Mohammed Al-Osta, who has supported me throughout my research with his patience, knowledge and personal involvement whilst allowing me the room to work in my own way. I learned a lot through my rich experience with him on the academic and professional grounds. Moreover, I acknowledge my gratitude to Dr. Mohammed H. Baluch for his valuable contributions, guidance, moral support and encouragement. His valuable suggestions greatly helped to accomplish this research. I would like also to extend my gratitude to Dr. Muhammad K. Rahman for his instructive comments and support.

I would like to express my warmest gratitude to the faculty members of the Civil Engineering Department at KFUPM. I also want to thanks lab technicians Engr. Omer, Engr. Syed Imran Ali and Engr. Najam for their tireless efforts during experimental phase.

I would also like to extend my deepest gratitude to my friends Azhar Ali Khan, Baqir Muhammad, Mehboob Rasul, Muhammad Ajmal, Mohammed Al-Huri, Muhammad Luqman, Muhammad Umar, Muhammad Usman, Raja Awais and Wasem Razzaq. Their care and support helped me a lot throughout my graduate studies.

Finally, this journey would not have been possible without sacrifice, encouragement and eternal love of my parents who gave me an overwhelming support from cradle till today, I am forever indebted for their life-long efforts and struggle. Special words of thanks are due to my sisters and brother for their encouragement and unfailing support throughout these years of demanding studies.

TABLE OF CONTENTS

LIST OF TABLES

LIST OF FIGURES

LIST OF ABBREVIATIONS

AFRP : Aramid Fiber Reinforced Polymers

ALR : Axial Load Ratio

BCJ : Beam-Column Joint

BCJF : Beam-Column Joint Failure

BJF : Beam-Joint Failure

CAL : Column Axial Load

CFRP : Carbon Fiber Reinforced Polymer

CJF : Column Joint Failure

GFRP : Glass Fiber Reinforced Polymers

JAF : Joint Axial Failure

JF : Joint Failure

SMA : Shape Memory Alloy

UHPC : Ultra-High Performance Concrete

ABSTRACT

Full Name	:	Umais Khan
Thesis Title	:	Effects of Variation of Axial Load on Seismic Performance of RC Exterior BCJ's
Major Field	:	Civil Engineering
Date of Degree	:	May, 2016

Beam-column joints (BCJs) are the fundamental component of concrete buildings and their design and detailing in any moment resisting framed structure is decisive to the survival of such structure. Several earthquake reconnaissance all over the world reported that failure of BCJs is the most frequent reason of overall building collapse in major earthquakes.

The years since 1970s have seen many developments in field of earthquake engineering and come up with present advanced seismic design codes and regulations for different structural components, including beam column joints. Parameters that influence the performance of BCJs such as aspect ratio, material property, beam’s reinforcement ratio and anchorage of beam’s reinforcement are studied by many researches and are well understood, as a result theses parameters are incorporated in several joint shear strength model and consequently in the current design guidelines. However, column axial load (CAL) which is a key influencing parameter in predicting shear strength of BCJs is not considered explicitly so far and may be due to its complex effects on the shear strength of the joint this parameter is not well understood.

The main focus of this research work was to study the effects of various CAL levels on the behavior of reinforced concrete BCJs under monotonic and reverse cyclic loading. Literature review was carried out to establish an experimental test database to identify effects of important parameters influencing performance of BCJs and to evaluate available joint shear strength models. It is found that existing shear strength models are deficient in one or another way, including consideration of CAL. Thus a problem of interaction between shear strength of BCJ and axial load on column was first approached by developing a mechanistic model and then experimental test program was carried out on seven BCJs subassemblies subjected to monotonic and reverse cyclic loading with various level of CAL. Experimental results were then validated using FE software ABAQUS to advance study for various compressive strengths of concrete in order to get sufficient data population to develop a new shear strength model for BCJs that considers all the important parameters requires to predict shear strength of BCJs, including CAL.

The results depicted that CAL considerably effects the seismic performance of BCJs. Experimental results demonstrated that high axial load enhances the shear strength of the joint and reduces its ductility however after axial load ratio of 0.6-0.7 shear strength starts to decrease until pure axial failure of joint. High axial load also dictates the failure mode and development of crack patterns in BCJs. Reverse cyclic tests on BCJs showed that high axial load increases the initial stiffness but rate of stiffness degradation is found to be more in such cases also up to axial load ratio of 0.6 energy dissipation capacity increases due to confinement provided by axial load to BCJ. Finally, the developed shear strength model was validated with experimental database, which successfully predicted the shear strength of test specimens.

ملخص الرسالة

الاسم الكامل: اوميس خان

عنوان الرسالة: آثار تباين القوة المحورية على الأداء الزلزالي للمفاصل الخرسانية المسلحة الخارجية

التخصص: هندسة مدنية

تاريخ الدرجة العلمية: مايو 2016 م

المفاصل شعاع المفاصل الخراسنية المسلحة هي العنصر ألاساسي للمباني الخرسانية وتعتبرتصميمها وتفاصيل تسليحها في الهيكل الانشائي حاسمة لبقاء هذا الهيكل. حيث اشار عدد من الاستطلاعين في جميع أنحاء العالم أن فشل المفاصل الخرسانية للمنبى هي السبب الأكثر شيوعا لنهيار المبنى بشكل عام في حالة الزلازل الكبرى.

شهدت السنوات منذ 1970م العديد من التطورات في مجال هندسة الزلازل ويأتي هذا مع الاكود المتقدمة للتصميم الزلزال والانظمة المختلفة للمكونات الهيكلية ، بما في ذلك المفاصل الخرسانية لمنطقة اتصال العمود والجسور. يتم دراسة العوامل التي تؤثر على أداء المفاصل الخرسانية مثل نسبة الارتفاع وخواص المواد ، ونسبة حديد تسليح والتثبيت للجسور في المفاصل من قبل العديد من الأبحاث وفهمها جيدا، ونتيجة لذلك أدرجت هذة العوامل في قوة القص للمفصل وبالتالي في الشروط التصميمة الحالية. ومع ذلك، لم يعتبر حمل العمود المحوري المفتاح والمؤثرعلى قوة القص للمفاصل صراحة حتى الآن، وربما يرجع ذلك إلى آلاثار المعقدة على قوة القص للمفصل نتجية هذا العامل ليست مفهومة جيدا حتى الان.

كان التركيز الرئيسي من هذا العمل البحثي لدراسة الآثار المترتبة على مختلف المستويات للحمل المحوري للعمود على سلوك المفاصل الخرسانية المسلحة تحت التحميل الثابت والعكسي والدوري. وقد ادت مراجعة للابحاث العلمية إلى إنشاء قاعدة بيانات اختبار تجريبية لتحديد آثار المعاملات الهامة التي تؤثر على أداء المفاصل الخرسانية المسلحة وتقييم النماذج المتاحة لتحديد قوة القص للمفصل. وتبين أن النماذج القائمة لتحديد قوة القص للمفصل تعاني من نقص في واحد أو وسيلة أخرى، بما في ذلك تأثير الحمل المحوري للعمود. وهكذا فأن مشكلة التفاعل ما بين قوة القص للمفاصل الخرسانية المسلحة وحمولة العمود المحورية قد تم الوصول لها من خلال تطوير نموذج واجراء اختبار

تجريبي لعدد سبعة من المفاصل الخرسانية المسلحة والمعرضة لتحميل ثابت وعكسي ودوري مع مستويات مختلفه من الحمل المحوري للعمود. وتم التحقق من النتائج التجريبية في المعمل باستخدام النمذج امتنهية في الصغرى باستخدام برنامج ABAQUS للمضي قدما في دراسة الاثار المختلفة لقوة الخرسانة في الضغط من أجل الحصول على بيانات كافية لتطوير نموذج قوة القص الجديدة للمفاصل الخرسانية المسلحة والذي يضم جميع المعاملات الهامة والمطلوبة للتنبؤ لقوة القص للمفاصل ، بما في ذلك تأثير الحمل المحوري للعمود .

وضحت النتائج ان الحمل المحوري للعمود يؤثر بشكل كبير على الأداء الزلزالي للمفاصل الخرسانية المسلحة. أظهرت النتائج التجريبية أن حمولة العمود المحورية العالية يعزز قوة القص للمفصل، ويقلل من ليونتها ولكن بعد نسبة حمولة محورية للعمود من 0.6-0.7 قوة القص تبدأ في الانخفاض حتى الانهيار المحوري الصافي من المفصل. كما يملي حمولة العمود المحورية العالية لحالة الانهيار وتطوير أنماط التشرخات للمفاصل الخرسانية المسلحة. أظهرت الاختبارات العكسية والدورية على المفاصل الخرسانية المسلحة أن الحمولة المحورية العالية يزيد من الصلابة الأولية ولكن معدل تدهور الصلابة وجدت تكون أكثر في مثل هذه الحالات وقد وجد أيضا انه في نسبة حمولة محورية 0.6 بأن الطاقة تزيد بسبب الاحتواء الناتج من الحمل المحوري للمفاصل الخرسانية المسلحة. وأخيرا تم التحقق من صحة نموذج قوة القص المطور مع قاعدة البيانات التجريبية، الذي تنبأ بنجاح قوة القص من عينات الاختبار.

CHAPTER 1

INTRODUCTION

1.1. General

BCJ's are the fundamental component of concrete buildings and their design and detailing in any moment resisting framed structure is decisive to the survival of such structure. Several earthquake investigations all over the world reported that deficient BCJs is the frequent reason of overall building failure in major earthquakes.

Since 1970's a lot of experimental and analytical research work has been done to understand key parameters influencing the performance of BCJs which mainly includes material property, type and amount of reinforcement, bond conditions between reinforcement and concrete, BCJ aspect ratio, anchorage details and application of strengthening composites e.g. [1]–[10]

However, very scarce information is present in literature and in the design guidelines regarding the consequence of CAL on behavior of BCJs. In actual practice when any building experiences an earthquake, axial force in the exterior column of a building experience varying axial loads due to overturning moment and vertical component of an earthquake, together with the varying effect of dead load. Not only an axial load have consequences on the column capacity but it also greatly effects the performance of a joint, as shear concentration at joint panel is dependent on an axial load present on a column therefore it has remarkable effect on a shear capacity of joint panel. Thus consideration of axial load on column in accessing the behavior of BCJ is not only essential for studies considering different retrofitting techniques for deficient joints but is equally important to be incorporated in current design standards.

1.2. Motivation

BCJ is one of the most critical component of any moment resisting building exposed to seismic excitation as it is responsible to transfer forces between the beams and column and thus failure of BCJ dictates the collapse of complete structural system. In past earthquakes, all over the world many buildings collapsed due to BCJs failure resulted in huge life and economic loss. Some of the important examples of such earthquakes are Algeria, 1980; El-Ansam; Mexico, 1999 and Athens, Greece, 1999 other includes:

Northridge earthquake in California, 1994 in which Kaiser building which is designed and constructed before 1970's collapsed due to BCJs failure. The photographs of this building are shown in Figure 1-1.

Figure 1-1 Collapse of structure due to BCJs failure, Northridge earthquake, 1994

Earthquake in Izmit, Turkey in 1999 is another examples in which buildings collapsed due to failure of BCJ. Partial collapse of building in this earthquake is shown in Figure 1-2.

Figure 1-2 BCJ failure of building in during earthquake in Izmit, Turkey, 1999 [11]

In Chi-Chi, Taiwan, 1999 earthquake 15 story building collapsed due to failure of BCJs as shown in Figure 1-3.

Figure 1-3 Building failure due to BCJ Chi-Chi, Taiwan, 1999 earthquake [12]

Moehle and Mahin [13] observed several buildings collapse due to BCJs failure while studying performance of reinforced concrete buildings during earthquakes. One of the building collapse is as shown in Figure 1-4.

Figure 1-4 Structural failure caused by beam-column joint failure [13]

Therefore, BCJ which is the influential factor in deciding the performance of reinforced concrete buildings during earthquake requires the complete understanding and consideration of parameters associated with its failure mechanism.

1.3. Need for Research

Substantial amount of research work has been performed to understand the seismic behavior of BCJs but an axial load on the column which is a key influencing parameter in predicting shear strength of BCJ is not considered explicitly so far and may be due to its complex effects on the shear strength this parameter is not well understood. Axial load on column is a core parameter that effect the performance of BCJs which can be varied under earthquake due to overturning moment, vertical component of ground motion and due to different level of axial load on column in a high rise building. These effects are very important to consider in the seismic design of the BCJs in order to avoid inadequate and non-conservative design approach.

Thus, a comprehensive study is required to take into account all the important components of an earthquake to understand completely the behavioral response of BCJs under earthquake and to develop appropriate design methods.

1.4. Research Objectives

The main focus of this research work was to investigate the effects of varying CAL levels on the behavior of RC exterior BCJs under monotonic and reverse cyclic loading applied to the beam.

The specific objectives are:

1. Development of a suitable mechanistic model to understand interaction between shear strength and column axial stress
2. Experimental investigation on effect of magnitude of CAL on shear strength and failure modes of the BCJs under monotonic and cyclic loading.
3. Simulation of BCJs in ABAQUS environment to envisage the performance and failure modes of the joint. Calibration of numerical models with the experimental results to advance the study.
4. Development of new design equation to estimate shear strength of unconfined joints.

CHAPTER 2

LITERATURE REVIEW

2.1. Introduction

This chapter explores and review the seismic deficiencies in reinforced concrete buildings followed by parameters influencing the seismic performance of BCJs. Several empirical and analytical shear strength models for BCJs are also reviewed to investigate the adequacy of existing models for parameters influencing the shear strength of BCJs. Finally, past researches on numerical modelling of BCJs are reviewed to investigate the feasibility of employing finite element method to BCJs.

2.2. Overview of Seismic Deficiencies in Reinforced Concrete Buildings

Strength of a structure, its ductility or deformability and energy dissipation capacity are prime building blocks of an advanced seismic design. Most of the buildings in the world designed before 1970s are deficient both in strength and deformability capacity due to lack of knowledge and understanding of seismic behavior of structures and thus absence of proper seismic design guidelines at that time. Many of these deficient buildings house important facilities like hospitals, schools, offices and shopping malls. Damage observed due to catastrophic earthquakes that hit the different parts of the world like 1970 Tong Hai earthquake, 1971 San Fernando earthquake, and 1975 Lice earthquake created a concern among the government officials and building owners that how these deficient buildings will perform under the earthquakes. This concern gave a boost to research in earthquake engineering to understand the seismic behavior of structure under earthquake.

Structural engineer's association of California (SEAOC) first introduced the ductile requirements in 1963 for high rise buildings that are above 48 meters but damage observed due to deadly earthquake following that, SEAOC extended those ductility requirements for all the buildings under seismic zone. Development of these ductility requirements paved a way for the development of Uniform Building Code 1976 which was the first formal building code to implement ductile requirements for the buildings under seismic risk in United States. In parallel Japan based on years of research updated its first "Earthquake resistant construction regulations 1924" in the form of "New Earthquake resistant building standards 1981". The years since then have seen many developments in field of earthquake engineering and come up with present advanced seismic design codes and regulations.

The major design deficiency in buildings built before the development of advanced seismic design is inelastic or non-ductile mechanism which is not appropriate for deformation response needed from the structure under earthquake loading. This inelastic response in such buildings is mainly due lack of proper detailing of structural components including BCJs. Absence of adequate hoop reinforcement with in a joint, inadequate development length of beam longitudinal bars, deficient splice lengths of column longitudinal reinforcement and use of plain steel bars are most common deficiencies in the BCJ's of deficient buildings.

A lot of experimental and analytical research work has been done to understand behavior and performance of BCJ and as a result of these researches advanced design concepts have been formulated to ensure reliability of BCJs to perform adequately under seismic excitation. Apart from developing new seismic design concepts and codes many research works investigated the ways to retrofit deficient joints. These retrofitting techniques include CFRP sheets, steel jacketing, GFRP sheets, AFRP, ultra-high performance concrete (UHPC), SMA and many other retrofitting procedures. However, to understand completely the behavior of BCJs it is very imperative to understand the key parameters influencing the behavior of BCJs in order to advance studies not only in successful retrofitting schemes but to reinforce new design concepts.

2.3. Parameters Influencing the Seismic Performance of BCJ

Since 1970's a lot of research has been performed to understand the key parameters influencing the performance of BCJ which mainly includes material property, type and amount of reinforcement, bond conditions between reinforcement and concrete, geometry of BCJ, anchorage details and application of strengthening composites. BCJs that were not designed to resist earthquake forces are very common in the seismic regions all over the world and due to their vulnerability against seismic excitation a lot of research work has been done on such joints.

Hakuto et al [3] in 2000 studied two exterior BCJs categorized as unit 06 and unit 07. Each unit had one tie in the joint but they differ from each other in detailing of beam longitudinal reinforcement within a joint. In unit 06 beam steel was hooked in the joint while in unit 07 it was bent outside the joint in to the column as shown in Figure 2-1 other design parameters are summarized in Table 2-1. In unit 07 early degradation of joint was observed with joint failure mode. Unit 06 in contrast had mixed failure and shown much better performance in terms of ductility and shear response. This study illustrates the significance of bending the beam main steel inside the joint rather than in to the column. Figure 2-1 illustrates the steel details, hysteresis curves and failure mechanism in both the units.

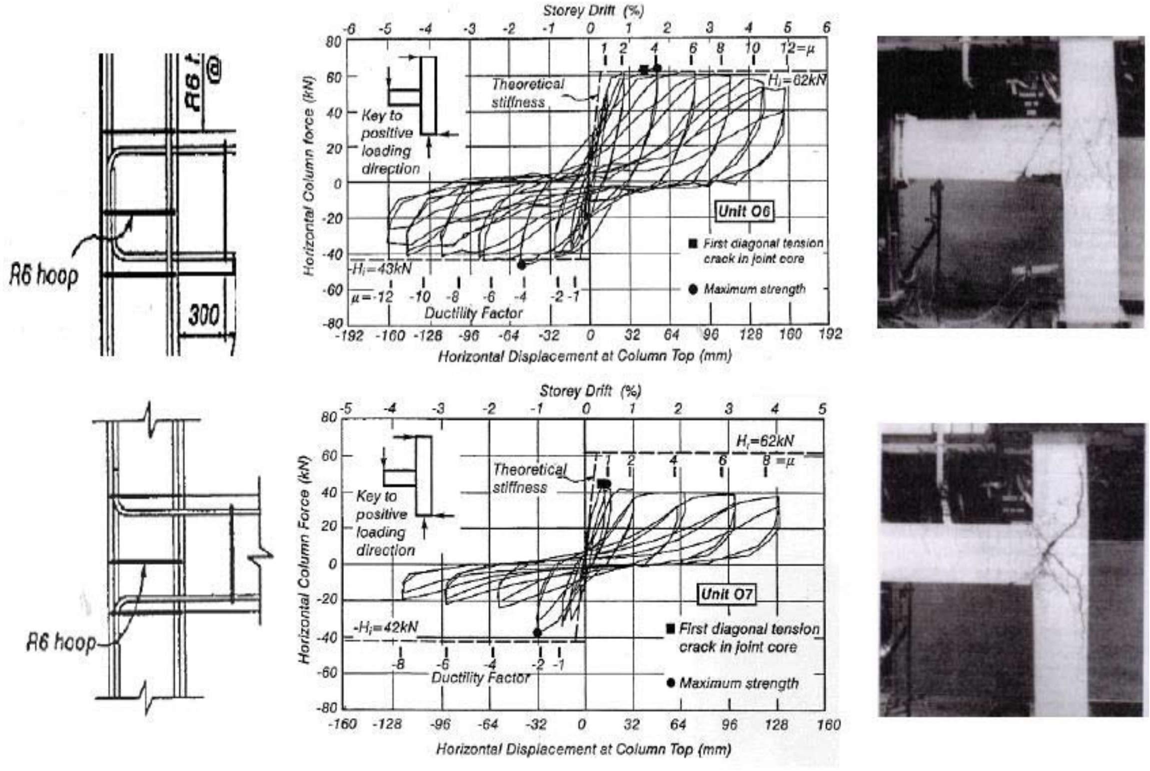

Figure 2-1 Reinforcement details, hysteresis curve and failure modes of specimens [3]

Gokgoz [14] investigated the seismic behavior of BCJs with transverse beam on each sides of the joint with a slab in one of the specimen as shown in Figure 2-2 Joints were designed according to pre-1970’s construction details practiced in United States Figure 2-3

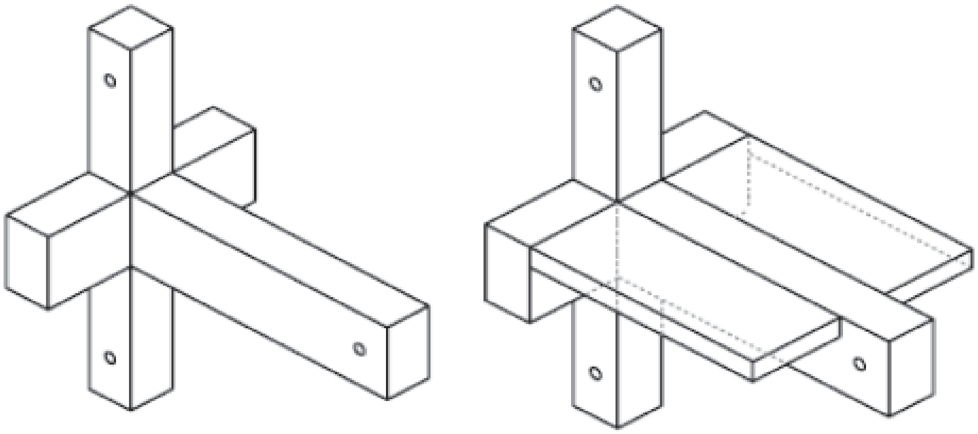

Figure 2-2 Exterior BCJs with and without slab [14]

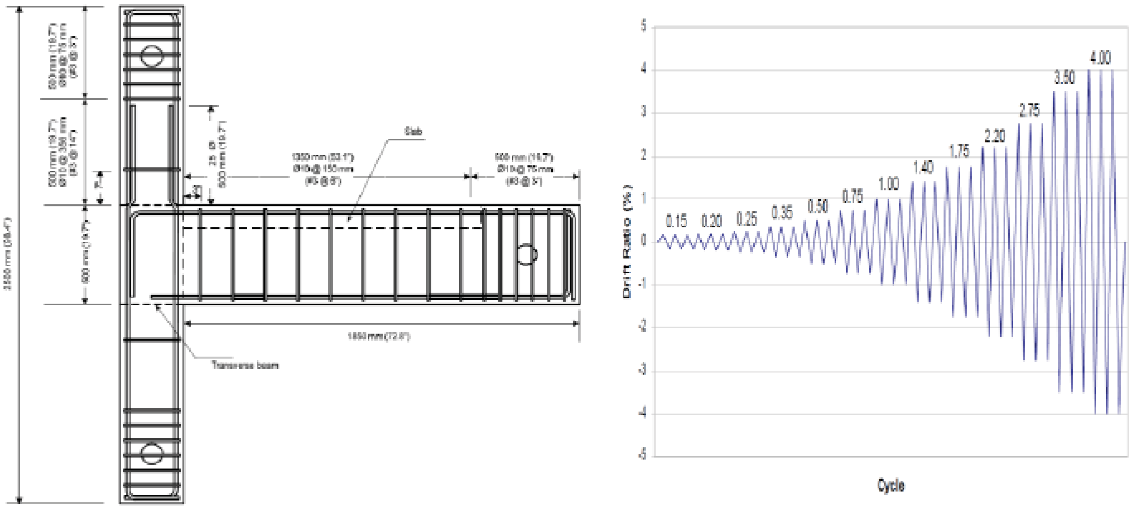

Figure 2-3 Reinforcement details and loading protocol [14]

Seismic performance of these specimens was compared with previously reported similar specimens without transverse beams (US-C-Control). Results of this study demonstrates that presence of transverse beams (US-E-Control) increases the deformation capacity and strength of BCJ. Inclusion of slab (US-ES-Control) considerably enhanced the strength and stiffness.

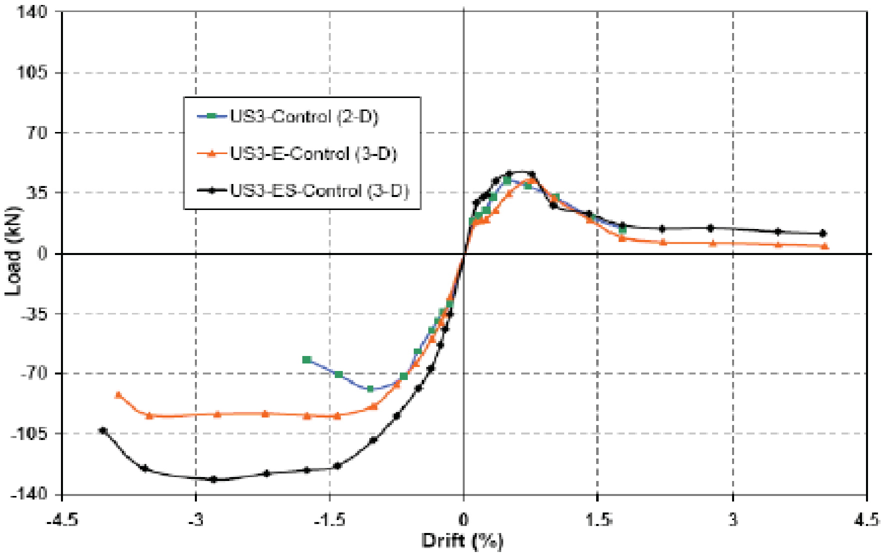

Figure 2-4 Backbone curves of test specimens [14]

Ghobarah and Said [15] studied the performance of CFRP retrofitted BCJs with seismically deficient reinforcement details Table 2-1. Their control specimen had shown high vulnerability against seismic excitation and failed in a conventional shear mode with substantial strength loss. The same joint experienced complete loss of load carrying capacity at displacement ductility co-efficient of 2.5.

Many researchers also focused on the BCJs considering the effect of some comprehensive clarifications on performance and failure. As an example:

Park et al. in 2002 [8] discussed the improvement in performance of seismically substandard BCJs of pre 1970’s construction by comparing them with the performance of BCJs designed according to current design concept and details, considering the various anchorage of beam steel in BCJ and reinforcement type both plane and deformed. However, in their review axial compressive load on column was zero except for the two specimens that had an ALR of 0.25. The specimens with axial load had demonstrated a significant enhancement in stiffness and strength because of delayed premature failure of joint by diagonal tension cracking.

The influence of axial compressive load which is one of the key influencing parameter in seismic performance of BCJ has not given due consideration in most of the studies available in literature whether concerned with study of deficient joints or with performance of joints designed according to current design practice like Hakuto et al [3] and Park et al. [8]. Very few studies has demonstrated the seismic behavior of BCJs considering the effect of CAL and even in those studies this effect is not completely understood due to lack of detailed explicit study like:

Clyde et al. [16] studied the seismic behavior of four half scaled BCJs without confinement ties in the joint and transverse beams. Effect of two different ALR was considered that were (0.10 and 0.25) other test parameters are summarized in Table 2-1. The beam and column was designed such that failure occurred in the joint. At the initial yielding of beam steel joint withstand the shear failure. Increase of 8% joint shear capacity was observed due to increased CAL. Displacement ductility observed at ALR of 0.10 and 0.25 was 2.7 and 1.6 respectively. Hysteresis measured at both axial load are shown in Figure 2-5

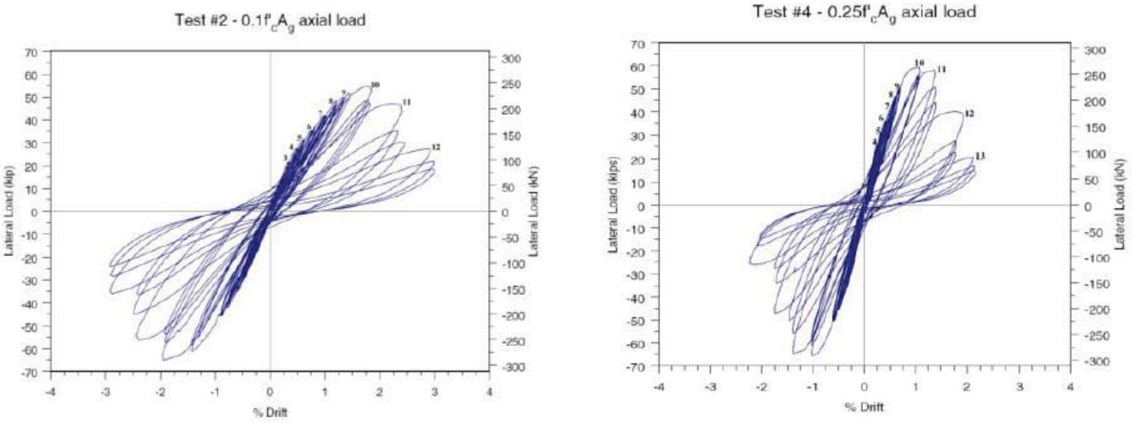

Figure 2-5 Hysteresis response measured at different axial load levels [16]

Barnes and Jigorel [17] reported the results of two tests on exterior BCJs with transverse slabs having no confinement reinforcement in the joint. Joints were designed such that column reinforcement yields, which is a very common failure mechanism in older buildings. In test 1 ALR was 0.40 which was reduced to 0.20 f'$_c$ A$_g$ in test 2. The results of this study demonstrated rapid strength degradation in test 1 with high axial load than that observed in test 2 with low axial load. However, increase of around 11% ultimate joint shear capacity was observed due to increased CAL. Comparison of hysteresis response for both the tests is presented in Figure 2-6

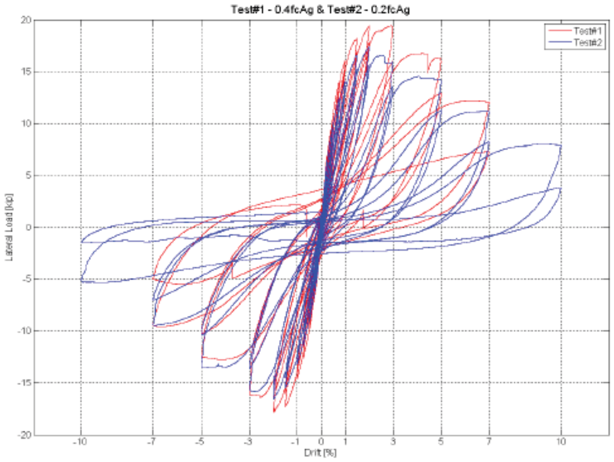

Figure 2-6 Hysteresis response for test 1 and test 2 with different axial load [17]

Wong [18] studied mainly the influence of column and beam reinforcement in BCJs. Total eleven exterior BCJs without confining ties were studied as displayed in Figure 2-7. All the specimens had an ALR of 0.15 except for two that was tested at ALR of 0.03, design details of these specimens are presented in Table 2-1. Specimens with a certain amount of intermediate column reinforcement resulted in 24% rise in the joint shear capacity. However, with an increase in column intermediate reinforcement had a very minor effect in increasing joint shear resistance capacity implying the threshold limit. Results of these experiments also demonstrated that increasing an axial compressive load on column results in an increase of joint shear capacity.

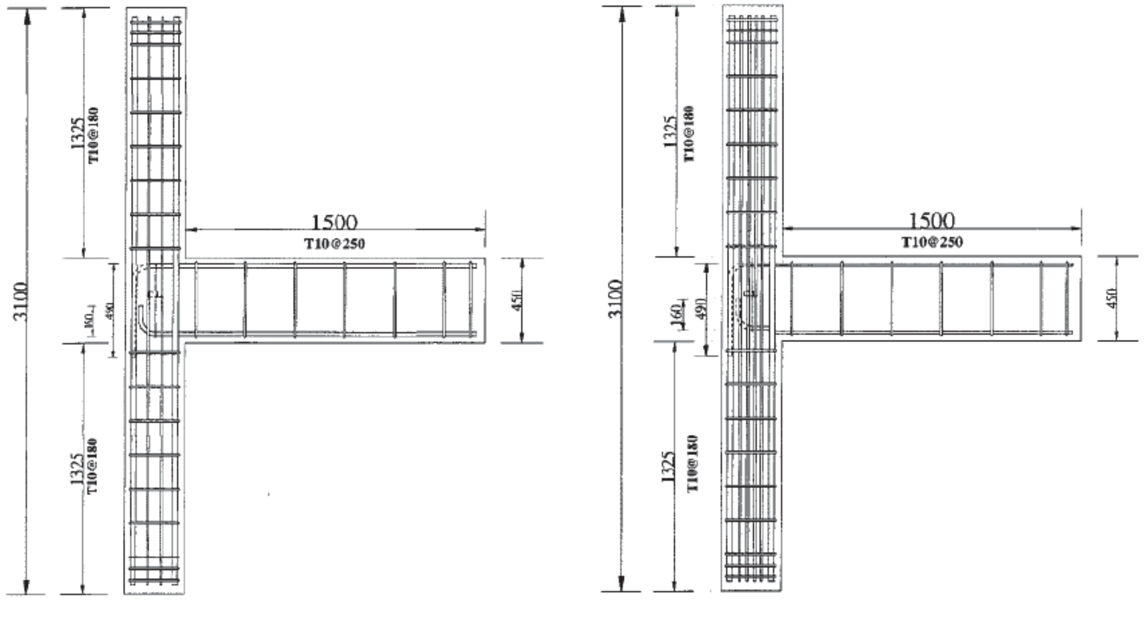

Figure 2-7 Details of exterior BCJ with column intermediate reinforcement [18]

Antonopoulos and Triantafillou [19] investigated eighteen 2/3 scale BCJ specimens with two control specimens (without FRP) to evaluate shear capacity of BCJ using fiber reinforced polymers. The specimen details utilized are presented in the Figure 2-8.

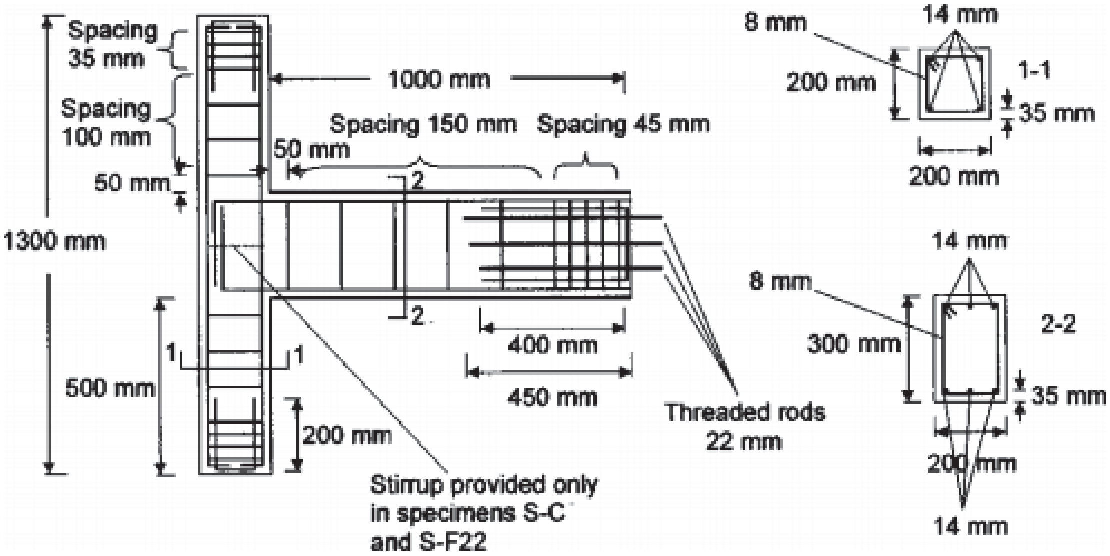

Figure 2-8 Geometry of specimens and reinforcement details [19]

In this study, all of the specimens had same CAL of 46 kN except for one specimen which received an axial load of 115 kN and on basis of their test results they have found a positive effect of high CAL on shear capacity of BCJ. According to their findings, strength of BCJ because of high axial load increased by 65% to 85% and energy dissipation increased by 50% to 70%.

Pantelides et al. [20] studied the six exterior BCJs without confinement reinforcement in the joint. The study focused to investigate the performance of different types of beam bars anchorage details in to the joint under ALR of 0.10 and 0.25. Figure 2-9 shows the three different types of anchorage for beam steel including small embedment length in to the joint, extended up to the outer face of column and beam bars bent in BCJ.

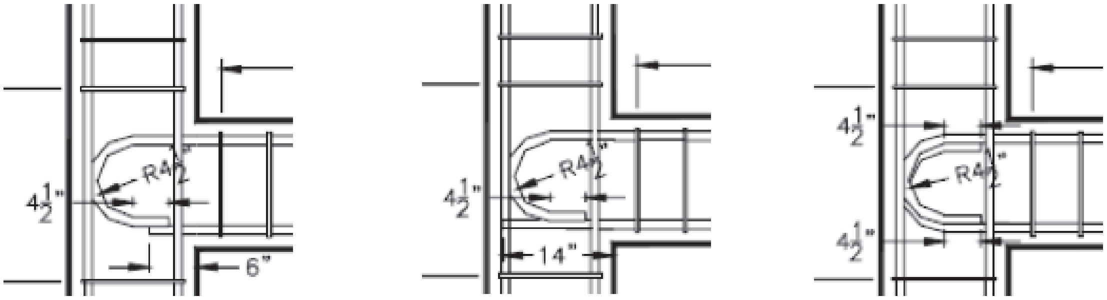

Figure 2-9 Schematic view of test setup [20]

Joints with insufficient embedment lengths suffered the bond slip failure however by increasing ALR from 0.10 to 0.25 improved the strength up to 35% as bars sustained the bond failure due to higher CAL. The shear capacity of other two joints with straight and hooked beam bars in to BCJ increased up to 15% with an increase in axial load.

Table 2-1 Summary

Researchers	Specimens	Joint Type	Joint aspect ratio	f'_c MPa	Beam			Column		V_{Test} (MPa)
					ρ_{bb} (%)	ρ_{tb} (%)	f_{yb} MPa	ρ_c (%)	f_{yc} MPa	
Hakuto [3]	06	Exterior	1.10	31.0	0.66	1	308	0.86	308	3.75
	07	Exterior	1.10	31.0	0.66	1	308	0.86	308	4.06
Gokgoz [14]	US3-E	Ext. 2 TB	1.67	23.5	0.59	0.72	359	2.10	441	4.35
	US3-ES	Ext. 2TB	1.67	23.5	0.59	1.08	359	2.10	441	6.12
Clyde et al. [16]	SP 2	Exterior	0.89	46.2	2.45	2.45	454	2.23	469	6.26
	SP 6	Exterior	0.89	40.9	2.45	2.45	454	2.23	469	6.26
	SP 4	Exterior	0.89	37.0	2.45	2.45	454	2.23	469	7.07
	SP 5	Exterior	0.89	40.1	2.45	2.45	454	2.23	469	6.83
Barnes [17]	Test 1	Ext. 2 TB	1.50	46.1	1.00	1.94	448	3.20	469	11.05
	Test 2	Ext. 2TB	1.50	40.9	1.00	1.94	448	3.20	469	11.57
Pantelides et al. [20]	SP 1	Exterior	1.00	33.0	1.90	1.90	459	2.45	469	5.39
	SP 2	Exterior	1.00	33.0	1.90	1.90	459	2.45	469	5.24

Researchers	Specimens	Joint Type	Joint aspect ratio	f'_c MPa	Beam			Column		V_{Test} (MPa)
					ρ_{bb} (%)	ρ_{tb} (%)	f_{yb} MPa	ρ_c (%)	f_{yc} MPa	
Pantelides et al. [20]	SP 3	Exterior	1.00	34.0	1.90	1.90	459	2.45	469	5.08
	SP 4	Exterior	1.00	34.0	1.90	1.90	459	2.45	469	5.66
	SP 5	Exterior	1.00	31.6	1.90	1.90	459	2.45	469	5.46
	SP 6	Exterior	1.00	31.6	1.90	1.90	459	2.45	469	5.46
Wong [18]	BS-L	Exterior	1.50	30.8	0.94	0.94	520	2.25	520	4.05
	BS-U	Exterior	1.50	30.9	0.94	0.94	520	2.25	520	4.06
	BS-LL	Exterior	1.50	42.1	0.94	0.94	520	2.25	520	5.39
	BS-L-LS	Exterior	1.50	31.6	0.94	0.94	520	2.25	520	5.06
	BS-V2T10	Exterior	1.50	32.6	0.94	0.94	520	2.25	520	3.19
	BS-V4T10	Exterior	1.50	28.3	0.94	0.94	520	2.25	520	4.79
	BS-L600	Exterior	2.00	36.4	0.68	0.68	520	2.25	520	3.38
	JA-NN03	Exterior	1.33	44.9	0.46	0.46	520	2.25	520	3.38
	JA-NN15	Exterior	1.33	46.0	0.46	0.46	520	2.25	520	3.87
	JB-NN03	Exterior	1.00	47.3	0.65	0.65	520	2.25	520	3.89

Researchers	Specimens	Joint Type	Joint aspect ratio	f'_c MPa	Beam			Column		V_{Test} (MPa)
					ρ_{bb} (%)	ρ_{tb} (%)	f_{yb} MPa	ρ_c (%)	f_{yc} MPa	
Wong [18]	BS-L-300	Exterior	1.00	34.1	1.53	1.53	520	2.25	520	6.01
Ghobarah and Said [15]	T 1	Exterior	1.00	30.9	1.20	1.20	425	1.80	425	5.58
	T 2	Exterior	1.00	30.9	1.20	1.20	425	1.80	425	5.63
Antonopoulos and Triantafillou [19]	C1	Exterior	1.50	19.4	0.77	0.77	585	1.54	460	2.57
	C2	Exterior	1.50	23.7	0.77	0.77	585	1.54	460	2.95

Note: Axial load ratio (ALR) =$\frac{N}{A_g f'_c}$; V_{Test} = Shear strength from experiment; f'_c = Concrete compressive streng

reinforcement percentage; ρ_{tb} = Beam top reinforcement percentage; ρ_c = Column reinforcement percentage; f_{yb}

yield strength; f_{yc} = Column reinforcement yield strength, Aspect ratio = $\frac{beam\ depth}{Column\ depth}$, N = column axial loa

sectional area.

2.4. Beam-Column Joint Shear Strength Models

Several models are currently available to characterize seismic behavior of BCJs. In this section, the existing joint shear strength models proposed by several researches and design guidelines are reviewed.

2.4.1. Shear Strength Model of Vollum and Newman

Vollum and Newman [21] has developed the model to estimate the shear strength of exterior BCJs:

$$V_c = 0.642\beta \left(1 + 0.555\left(2 - \frac{h_b}{h_c}\right)\right) b_{eff}\, h_c \sqrt{f_c} \tag{2.1}$$

$$V_j = V_c + (A_{sje} f_y - \alpha b_{eff} h_c \sqrt{f_c}) \tag{2.2}$$

The above joint shear capacity $V_j$should be less than the following:

$$V_j < 0.97 \left(1 + 0.555\left(2 - \frac{h_b}{h_c}\right)\right) b_{eff}\, h_c \sqrt{f_c} < 1.33 b_{eff}\, h_c \sqrt{f_c} \tag{2.3}$$

where Vj is the overall joint shear strength including stirrups. α depends on joint aspect ratio, column load, amount of stirrups and strength of concrete and is taken conservatively as 0.2. β is a co-efficient taken as 1 for standard 90 degree hooks and 0.9 for U shaped bend of beam main steel in the joint. This model while considered influence of anchorage details of beam steel in BCJ and joint aspect ratio as significant parameters did not explicitly consider the effect of CAL.

2.4.2. Shear Strength Model of Bakir and Boduroglu

Bakir and Boduroglu [22] proposed an empirical model considering mainly the effect of anchorage details and amount of beam steel, aspect ratio of joint and amount of stirrups in the joint. The effects of above parameters are incorporated in the model based on the parametric study and by calibrating each parameter independently from the other. The shear strength equation considering the effects of above parameters is as follow:

$$V_c = 0.71\beta\gamma\left(\frac{100A_{sb}}{b_b d}\right)^{0.4289}\left(\frac{b_c+b_b}{2}\right)\left(\frac{h_b}{h_c}\right)^{-0.61} h_c\sqrt{f_c} + \alpha A_{sje} f_y \tag{2.4}$$

where β can be taken as 0.85 for joints with U shaped anchorage of beam reinforcement and 1 for the standard 90-degree hook. γ can be taken as 1.37 and 1 for inclined bars in the joint and 1 for other cases. The proposed joint shear strength equation does not take in to an account the effect of CAL. According to the analysis of Bakir and Boduroglu [22] CAL has no effect on the BCJ shear strength.

2.4.3. Shear Strength Model of Sarsam and Phillips

Shear strength equation proposed by Sarsam and Phillips [23] is based on test databank of exterior BCJs subjected to monotonic loading. Parameters like aspect ratio of joint, axial load on column and column steel percentage are lumped in to the following shear strength equation:

$$V_j = 5.08\left(f'_c\rho\right)^{0.33}\left(\frac{d_c}{d_b}\right)^{1.33}\left(1 + 0.29\frac{N}{A_g}\right)^{0.5} b_c d_c \tag{2.5}$$

where V_j is the shear strength of BCJ. According to the above model joint shear capacity enhances with an increase in CAL however a limit of axial load ratio $\frac{N}{A_g f'_c} \leq 0.42$ was set due to unavailability of experimental results in literature above this limit.

2.4.4. Shear Strength Model of Ilki et al 2011

According to Ilki et al [24] shear failure of BCJ is assumed to occur on the onset of diagonal cracking which occurs when the principal tensile stresses reaches the tensile strength of concrete. The shear strength equation proposed by Ilki et al [24] is as follow:

$$\tau_{vc} = 0.5\sqrt{f'_c}\ \sqrt{1 - \frac{N}{0.5\sqrt{f'_c}A_g}} \tag{2.6}$$

$$V_c = \tau_{vc}\, b\, d \tag{2.7}$$

where V_c is the shear capacity of concrete in the joint. According to this model joint shear strength enhances with an increase in CAL.

2.4.5. Current Design Guidelines

ACI-ASCE Committee 352 [25] recommended the following joint nominal shear strength equation:

$$v_n = 0.083\, \gamma \sqrt{f'_c}\, b_j\, h_c \tag{2.8}$$

where h_c is the depth of column in direction of load and b_j is the effective joint width

$$= \text{smallest of} \begin{cases} \frac{b_{beam} + b_{col}}{2}, \\ b_{beam} + \sum \frac{mh}{2}, \\ b_{col} \end{cases} \tag{2.9}$$

m is the co-efficient that catered for the effect of eccentricity which can be taken as 0.3 when eccentricity between column centroid and beam center line exceeds $b_{col}/8$ and 0.5 for all other cases. γ is constant that depends on the type either Type 1 or Type 2 joints and classification based on confinement of the joint.

2.5. Summary of Parameters Influencing Seismic Performance of BCJ

Review of the experimental studies performed on BCJs as discussed in the previous sections reveals that several important parameters influence the seismic behavior of exterior BCJs. These parameters comprise the anchorage of beam steel ratio, aspect ratio of the joint, loading protocol on beam column join assemblies, effect of slab on performance of BCJs, and effect of presence of transverse beams on confinement and thus on performance of the joint. The effects of above parameters are studied by many researches and are well understood and incorporated in many joint shear strength model and consequently in the current design guidelines. But CAL which is a key influencing parameter in predicting shear strength of BCJ is not considered explicitly so far and may be due to its complex effects on the shear strength of BCJ this parameter is not well understood. Very few researches studied the effect of CAL in predicting seismic behavior of BCJ as summarized in Table 2-1 and even in these studies range of axial load ratio is very narrow, in most of the cases variation of studied ALR is not more than approximately 0.15 and maximum axial load considered and well documented in form of shear strength equation is 0.42 $f'_c A_g$ as in case of Sarsam and Phillips [23]. Due to lack of detailed study on effect of CAL on BCJ researchers working in this area have different opinions. Some researchers [16]–[20], [23] find that with increase in CAL joint shear strength enhances, while another group of researchers [21], [22] believe that joint shear strength is not effected by CAL.

2.6. Previous Research on Numerical Modelling of BCJs

Research work of Will et al. in 1972 [26] was one of the first numerical study of joint region in which elastic behavior of concrete in compression and tension was considered. In 1981 Noguchi [27] simulated reinforced concrete BCJs using discrete crack model to predict cracks in concrete. Since then many research work has been done on numerical modelling of BCJs which resulted in a lot of improvement in terms of material models for concrete and interaction between steel and concrete. Few examples of this research work includes:

Baglin and Scott in 2000 [28] modelled sixteen reinforced concrete BCJs using non-linear finite element code SBETA. Different failure mechanisms were apprehended from numerical models which includes beam failure, shear failure of joint and anchorage failure; depending on the type of reinforcement and strength of concrete. Results of finite element modelling was in close agreement with that of experiment both in terms of strength and failure mechanism.

Sagbas [29] used a nonlinear finite element program VecTor2 to model several BCJ subassemblies. In this research smooth reinforcement bars with unconfined seismically deficient BCJs were considered with different rehabilitation schemes. In numerical modelling concrete was modelled using Hognestad parabola for pre-post behavior and “Modified Park-Kent” model available in VecTor2 was utilized to model the post-peak behavior whereas default linear option was used for tensile behavior of concrete. Mohr-

Coulomb criteria was considered for modelling concrete cracking. Numerically obtained results were successfully matched with experiment in term of load capacity, ductility and failure mechanism.

Ahmed et al. [30] utilized DYANA software to model exterior BCJs with low strength concrete that were experimentally tested in Istanbul Technical University. In numerical modelling of BCJs Drucker-Prager failure criteria was considered for concrete. Numerical results showed good match in terms of strength and failure. Calibrated models were then used to advance research in modelling shear critical BCJs with normal strength concrete.

Mitra et al [31] utilized DIANA 9.1 to simulate BCJs. Drucker-Prager model was used for compression response whereas fixed crack model [32] with Hordijk softening [33] was utilized for modelling tensile behavior. Mitra [31] with above combination of material models concluded that above combination of software and material models are capable of representing behavior of fairly complex problems but could not captured cracking and crushing of concrete simultaneously due to numerical unstable algorithms and lack of martial models in DIANA 9.1 software. Thus he recommended the explicit non-linear FE codes like LS-DYNA and ABAQUS for simulation of complex problems considering local inelastic mechanisms.

CHAPTER 3

THEORY AND MECHANICS OF BCJ

3.1. Introduction

In this chapter first theoretical preliminaries of BCJs are presented. Then mechanics of BCJs is discussed which encompasses comprehensive mechanistic model to estimate shear strength of joint considering axial load on column.

3.2. Geometrical Types of BCJs

BCJs have different geometrical shapes depending upon their location in a building. This research work is concerned with exterior BCJs as displayed in Figure 3-1.

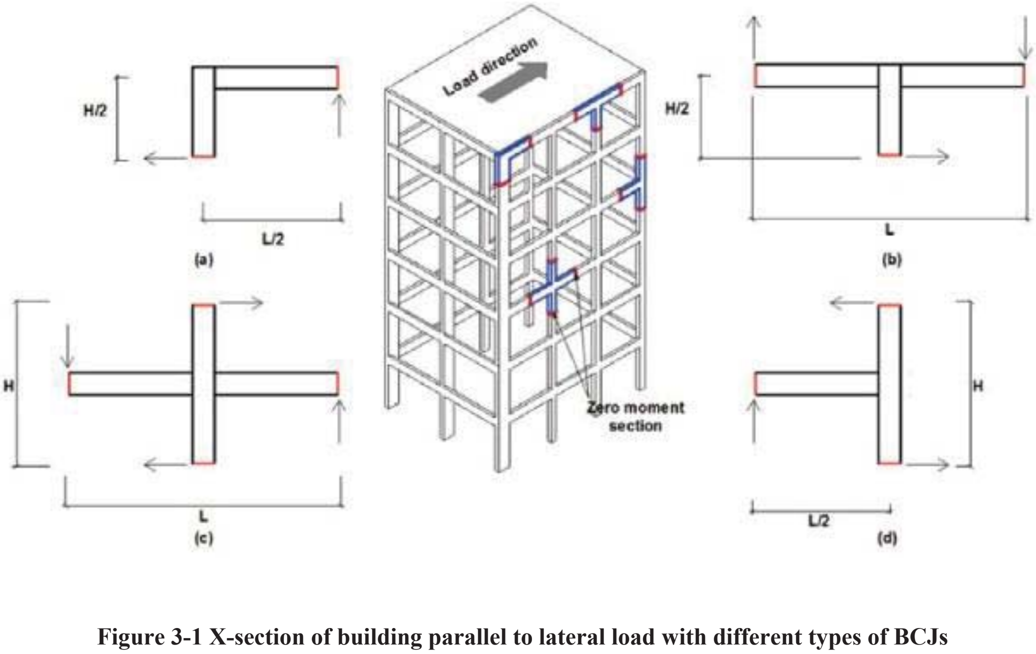

Figure 3-1 X-section of building parallel to lateral load with different types of BCJs

a) Roof-Exterior; b) Roof Interior; c) Interior; d) Exterior

3.3. BCJs Failure Mechanisms

Based on the literature review in the previous chapter, following BCJs failure mechanism are established:

3.3.1. Joint Failure

Joint Failure (JF) mode takes place when columns and beams are adequately designed and reinforced to take seismic forces. Thus BCJ which is responsible to take both horizontal and vertical forces becomes a weakest link and fails in pure shear. This failure mechanism of joint is most brittle and gives true shear capacity and is most common in seismically deficient buildings.

3.3.2. Beam-Joint Failure

Beam-Joint Failure (BJF) occurs if beam main steel yields followed by shear cracking of joint. This failure mechanism is more ductile as compared to JF mode owing to yielding of beam longitudinal steel.

3.3.3. Column-Joint Failure

Column-Joint Failure (CJF) occurs when column reinforcement yield which initiates shear cracking in the joint. This failure mechanism is very common in non-seismically designed buildings in which weak column and strong beams are most frequent.

3.3.4. BCJ Failure

BCJF is the combination of BJF and CJF where yielding in beam and column reinforcement starts simultaneously followed by intense shear cracking of joint.

3.3.5. Joint Axial Failure

Joint Axial Failure (JAF) is a crushing failure that occurs either due large lateral displacements or due to very high CAL during seismic excitation especially in case of unconfined joints.

3.4. Mechanics of BCJs

BCJ is a key structural component which is used to transfer vertical and lateral forces from column and beams respectively. Axial load N on column creates an axial stresses σ_N whereas load on beam V creates a shear stresses τ_v in the joint. These stresses can be converted to principal joint stresses σ_1 and σ_2 respectively using Mohr's circle as shown in Figure 3-2.

Principal joint stresses can be calculated as follow:

$$\sigma_1 = \frac{\sigma_x + \sigma_y}{2} + \sqrt{\left(\frac{\sigma_x - \sigma_y}{2}\right)^2 + {\tau_{xy}}^2} \tag{3.1}$$

$$\sigma_2 = \frac{\sigma_x + \sigma_y}{2} - \sqrt{\left(\frac{\sigma_x - \sigma_y}{2}\right)^2 + {\tau_{xy}}^2} \tag{3.2}$$

where $\sigma_x = \sigma_N$ and $\sigma_y = 0$ which is stress in beam longitudinal direction therefore Equation [3.1] and Equation [3.2] can be written as:

$$\sigma_1 = \frac{\sigma_N}{2} + \sqrt{\left(\frac{\sigma_N}{2}\right)^2 + {\tau_{xy}}^2} \tag{3.3}$$

$$\sigma_2 = \frac{\sigma_N}{2} - \sqrt{\left(\frac{\sigma_N}{2}\right)^2 + {\tau_{xy}}^2} \tag{3.4}$$

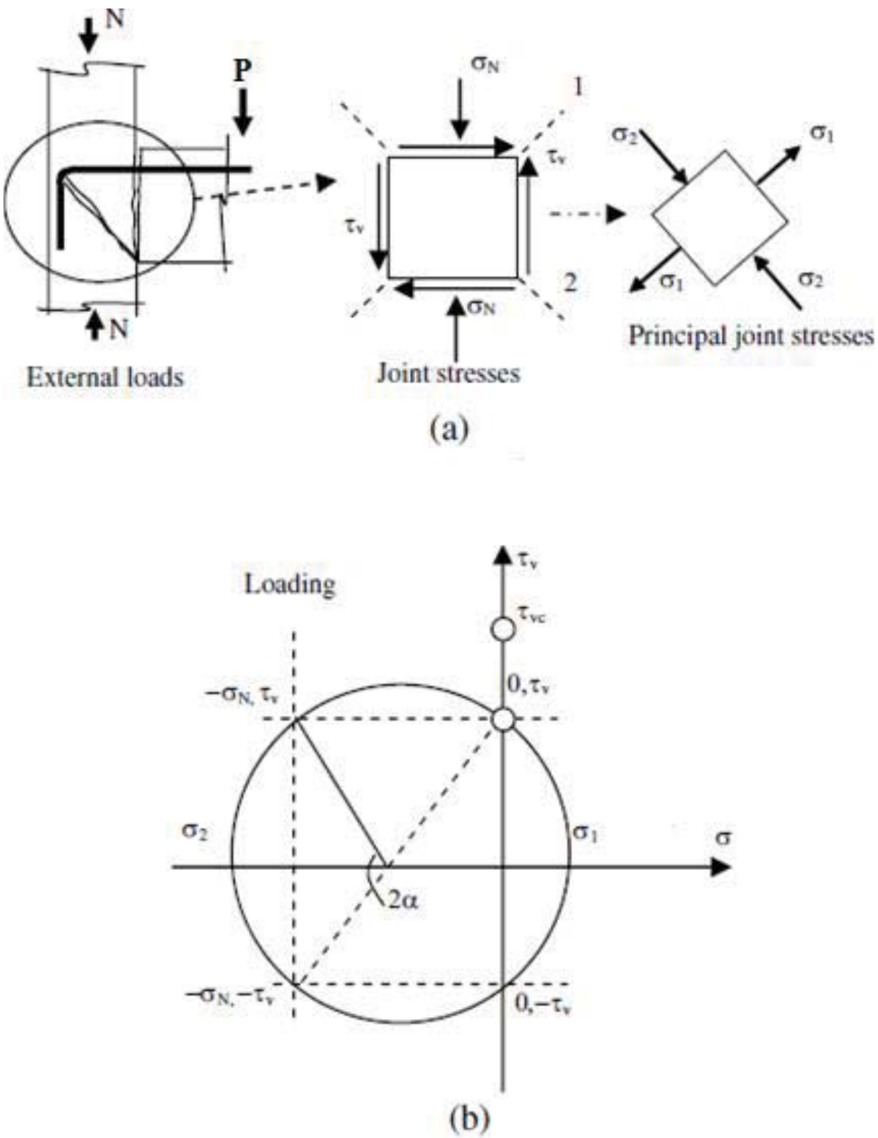

Figure 3-2 a) Applied loads, stresses in joints and principal stresses; b) Mohr's circle

σ_1 Figure 3-2a when surpasses the tensile capacity of the concrete f_t a crack is formed as shown in Figure 3-3. Similarly joint axial failure occurs if σ_2 increases the f'_c.

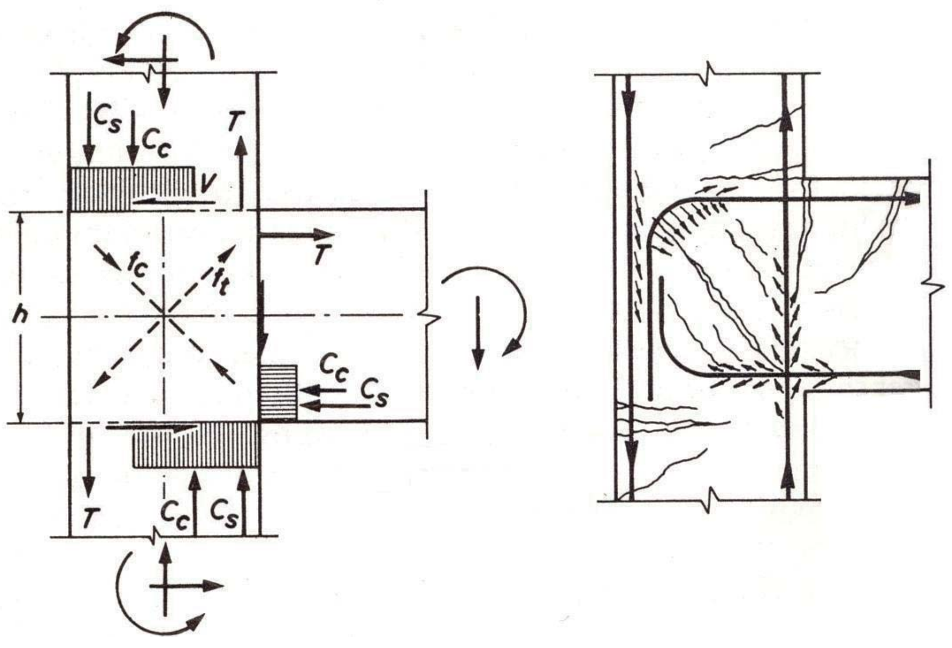

Figure 3-3 Diagonal shear crack mechanism in BCJ

William and Warnke [34] failure criteria as employed by many commercially available nonlinear finite element codes like ANSYS is used to define failure of concrete. As per William and Warnke failure criteria two strength parameters that is tensile strength f_t and compressive strength f'_c are required to define the failure surface of concrete. Cracking failure occurs if principal stress σ_1 surpasses the tensile capacity of the concrete f_t similarly crushing failure occurs if principal stress σ_2 increases the f'_c. Failure surface by William and Warnke is shown in Figure 3-4

In Figure 3-4 slope of line in fourth quadrant can be written as:

$$m = \frac{y_2 - y_1}{x_2 - x_1} \tag{3.5}$$

Substituting values we get

$$m = \frac{0-\left(-\frac{\sigma_2}{f'_c}\right)}{\frac{\sigma_1}{f_t}-0} \tag{3.6}$$

where $\frac{\sigma_1}{f_t}$ and $\frac{\sigma_2}{f'_c}$ equals to unity, thus $m = 1$

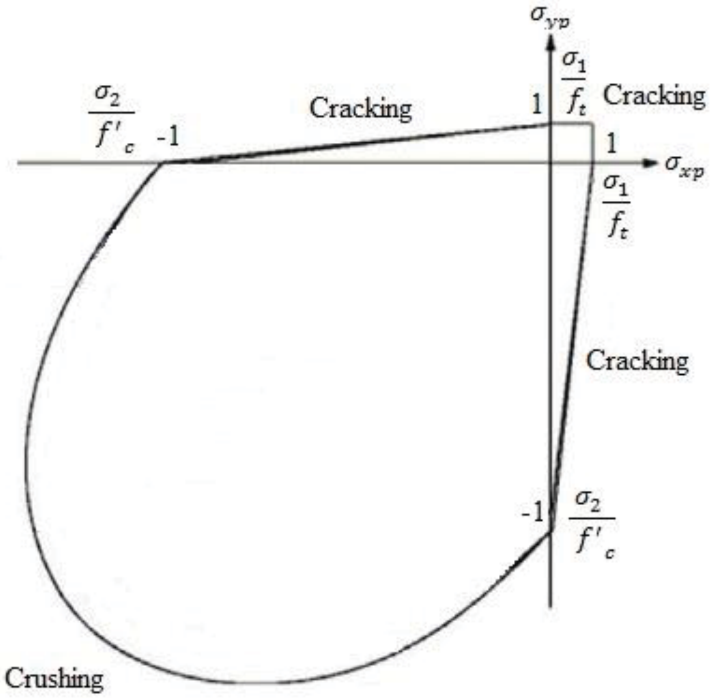

Figure 3-4 Failure surface of concrete

Therefore, equation of line can be written as:

$$y = mx + c \tag{3.7}$$

Substituting values in above equation

$$\frac{\sigma_2}{f'_c} = \frac{\sigma_1}{f_t} - 1$$

or

$$\frac{\sigma_1}{f_t} - \frac{\sigma_2}{f'_c} = 1 \tag{3.8}$$

σ_2 can be written in terms of σ_1 as:

$$\sigma_2 = c\,\sigma_1 \tag{3.9}$$

where $1/c$ = -1 for pure shear thus

$$-\sigma_2 = \sigma_1 \tag{3.10}$$

Similarly $1/c$ = 0 for pure compression thus

$$\sigma_1 = 0 \tag{3.11}$$

Therefore $1/c$ ranges [-1, 0]

Substituting Equation [3.9] in to Equation [3.8] σ_1 and σ_2 can be written as:

$$\sigma_1 = \frac{f_t\, f'_c}{f'_c - c f_t} \tag{3.12}$$

$$\sigma_2 = \frac{c\, f_t\, f'_c}{f'_c - f_t} \tag{3.13}$$

Solving Equation [3.3] and Equation [3.12] or Equation [3.4] and [3.13] simultaneously with various values of σ_N ranges [0- f'_c] and $1/c$ ranges [-1, 0] shear stress at failure can be obtained against each value of σ_N. Thus plotting σ_N against calculated value of $\tau_{xy} = v_j$ interaction diagram as shown in Figure 3-5 can be established for various strengths of concrete.

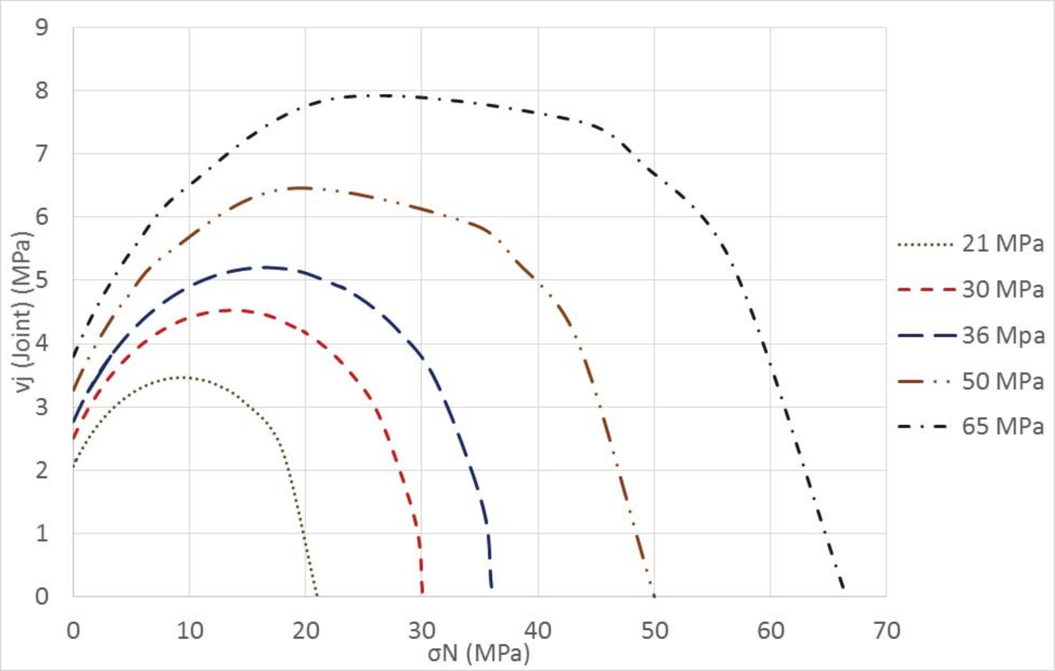

Figure 3-5 Shear strength - axial stress interaction for different concrete strengths

CHAPTER 4

EXPERIMENTAL PROGRAM

4.1. Introduction

This chapter delineates the experimental program conducted at “Heavy Structures Testing Laboratory” at KFUPM. The test program mainly composed of seven 1/3 scale exterior BCJs. The main focus of the test program was to understand the effects of different magnitude of CAL on seismic behavior of exterior BCJs. ALR was varied from 0.0 to 0.7 to gain insight of its effects and to understand susceptibility to axial and shear failure of BCJs. Both monotonic and reversed cyclic loading was applied to evaluate the actual shear capacity and stiffness degradation under seismic excitation respectively. All the specimens were highly equipped and instrumented to capture important aspects of performance under different types of loading.

4.2. Objectives of Experimental Program

The primary objectives of experimental program are as follow:

1. Effects of different magnitude of axial load on seismic behavior of BCJs.
2. Understand and ascertain different failure mechanisms in BCJs under different axial loads.
3. Analyze the shear capacity of joints under monotonic and reversed cyclic loading.
4. Comprehend the overall seismic behavior of BCJs.

5. To obtain sufficient data to calibrate FE model in order to extend the research in subject area.

4.3. Specimens Design and Details

In order to achieve better understanding of effects of axial load and its role in joint performance design characteristics such as BCJ dimensions and reinforcement were kept same in seven specimens. The component design of specimens are discussed in following paragraphs.

4.3.1. Design of Beam

Reinforcement ratio in a beam was kept high to promote joint failure mechanism and to avoid beam reinforcement yielding. Development length and anchorage of beam steel was satisfied according to current ACI 318-14 [35] to ensure proper shear transfer from beam to the joint.

4.3.2. Design of Column

Column dimensions and reinforcement details were kept constant in all the specimens to study the effects of CAL on performance of BCJs. ACI 318-14 [35] was used to design column whereas CSiCOl software was used to develop the interaction diagram as shown in Figure 4-1. Column was designed such that its flexural capacity was around 2 times higher than demand imposed by the beam for all load combinations used in experimental program.

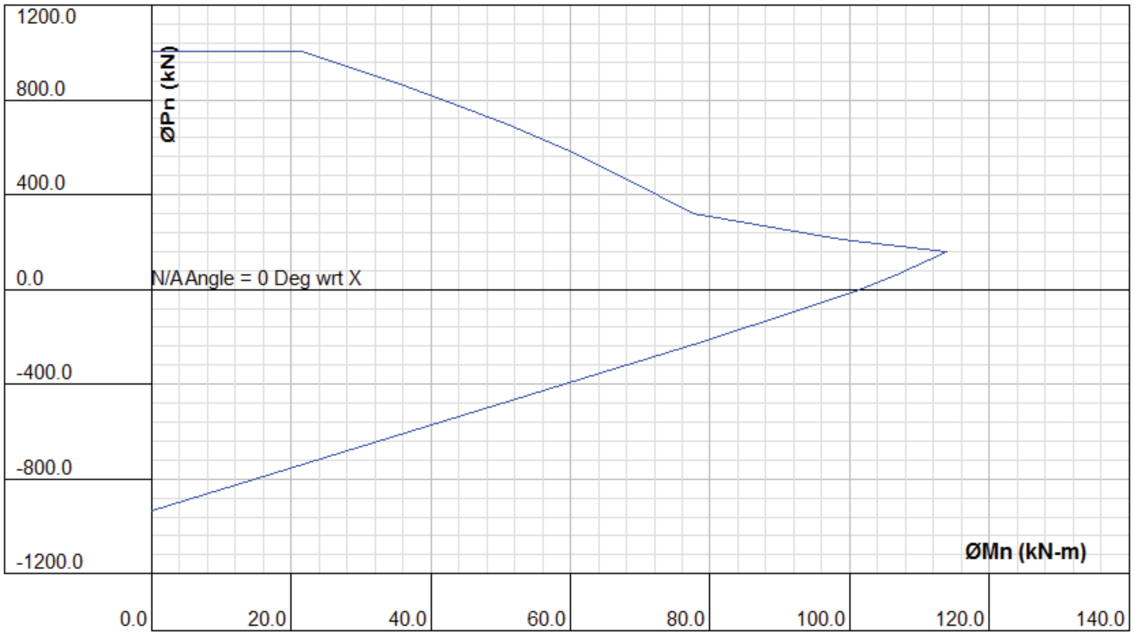

Figure 4-1 Interaction diagram of column

4.3.3. Design of BCJ

In order to examine the effects of CAL dimensions of BCJs were selected to promote joint failure mechanism. Aspect ratio h_b/h_c of BCJ was selected as 1 which is the most common case as found in literature review.

4.3.4. Design Details

Details of beam and column design are tabulated in Table 4-1 whereas Figure 4-2 displays concrete outline and reinforcement layout of specimens.

Table 4-1 Beam and column design details

Specimen	Dimensions (mm)		Reinforcement				
			Beam			Column	
	Beam	Column	Top	Bottom	Stirrups	Main	Ties
SP1-SP7	200 x 250	200 x 250	4- Ø20	4- Ø20	Ø8 @ 50	6- Ø20	Ø8 @ 50

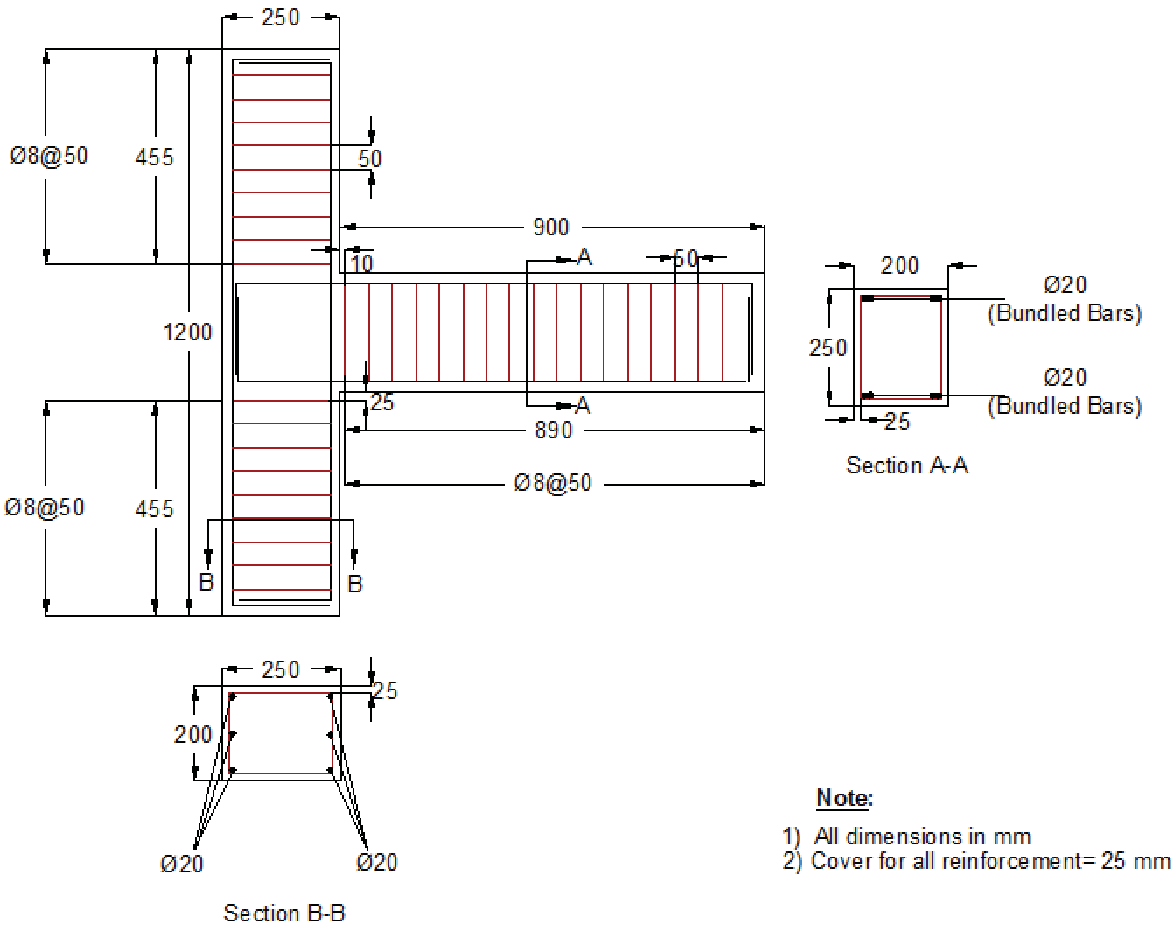

Figure 4-2 Concrete outline and reinforcement layout

4.4. Specimens Construction

Specimens were constructed at “Prainsa precast concrete factory, Dhahran” to maintain high standards in construction. Wooden forms Figure 4-3 were prepared and special attention was given to dimensions, concrete cover, reinforcement spacing and alignments which were finally checked at the day of casting. Steel cages Figure 4-4 for all the specimens were made at the same time to avoid effects associated with different batches of reinforcement. Concrete was ordered from “Saudi Ready-mix Concrete Company” and casting of five specimens as shown in Figure 4-5 was done on the same day except for two specimens which were casted two weeks later . Simultaneously during the preparation of steel cages strain gauges were installed, labeled and continuously monitored till casting to ensure their functionality. After casting special attention was given to curing of specimens to avoid loss of moisture from surface that could adversely affect concrete strength.

Figure 4-3 Preparation of formwork

Figure 4-4 Installation of reinforcement

Figure 4-5 Casting of specimens

After completion of 28 days curing period as shown in Figure 4-6 specimens were carefully transported from “Prainsa precast concrete factory” to “Heavy Structures Testing Laboratory” at KFUPM.

Figure 4-6 Specimens at 28days of curing period

4.5. Material Properties

4.5.1. Concrete

Concrete was delivered by “Saudi Ready-mix Concrete Company”. The targeted concrete strength was 20 MPa however to ensure actual concrete strength at 28 days and at test dates twenty one concrete cylinders (75 mm in diameter and 150 mm in height) were prepared during casting of the specimens as a representatives of actual strength of concrete as presented in Figure 4-7.

Figure 4-7 Sampling of concrete during casting

4.5.1.1. Concrete Compressive Strength Test

Compression strength test of concrete was conducted on test date of each specimen according to ASTM C39M [36] at a loading rate of 0.25 MPa/s as displayed in Figure 4-8.

Figure 4-8 Concrete compressive strength test

Three cylinders were tested for each specimen and results are tabulated in Table 4-2.

Table 4-2 Concrete compressive strength for SP1 - SP-7

Specimen ID	Compressive Strength f'$_c$ (MPa)
SP-1	21.01
SP-2	20.31
SP-3	21.09
SP-4	21.20
SP-5	21.58
SP-6	30.47
SP-7	29.71

Compressive stress-strain behavior for specimen SP-1 to SP-7 are as follow:

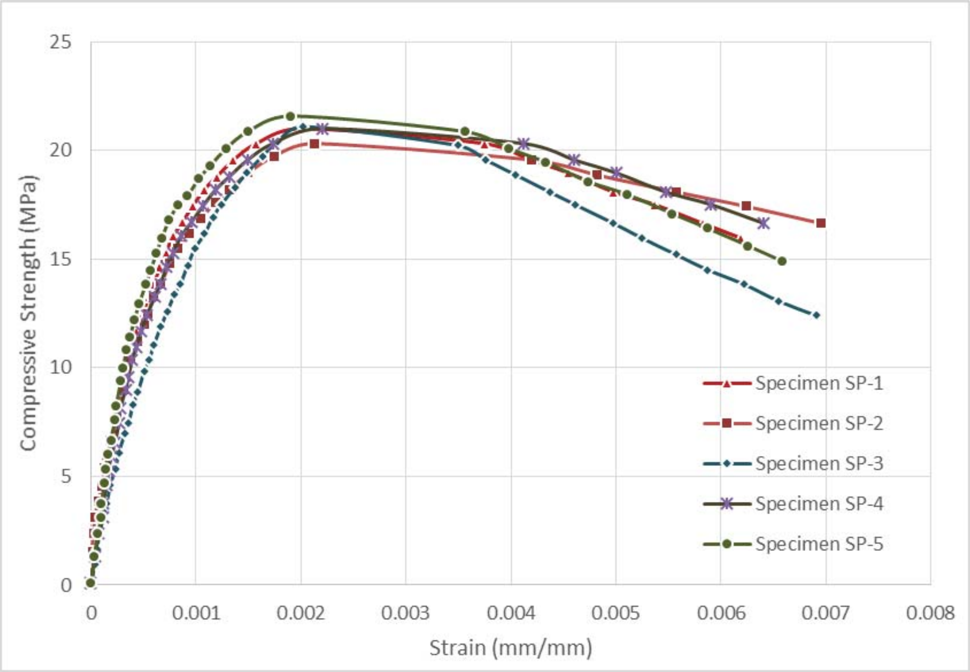

Figure 4-9 Concrete compressive stress-strain behavior for specimen SP-1 - SP-5

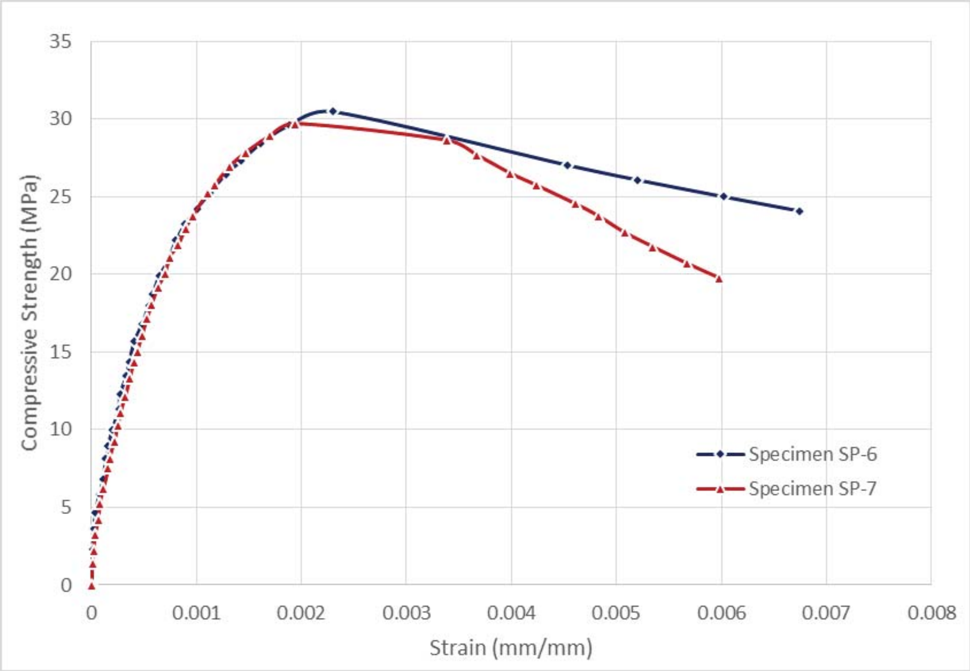

Figure 4-10 Concrete compressive stress-strain behavior for specimen SP-6 and SP-7

4.5.1.2. Modulus of Elasticity and Poisson’s Ratio.

Test for modulus of elasticity of concrete and Poisson’s ratio was conducted according to ASTM C469 [37] which requires uniaxial cyclic compression test on concrete cylinders as shown in Figure 4-11. Results of cyclic behavior of concrete for specimens SP-1 and SP2 and SP3 to SP5 tested on adjacent dates is shown in Figure 4-12 and Figure 4-13 respectively while that for specimen SP-6 and SP-7 is shown in Figure 4-14

Figure 4-11 Cyclic test on concrete cylinders

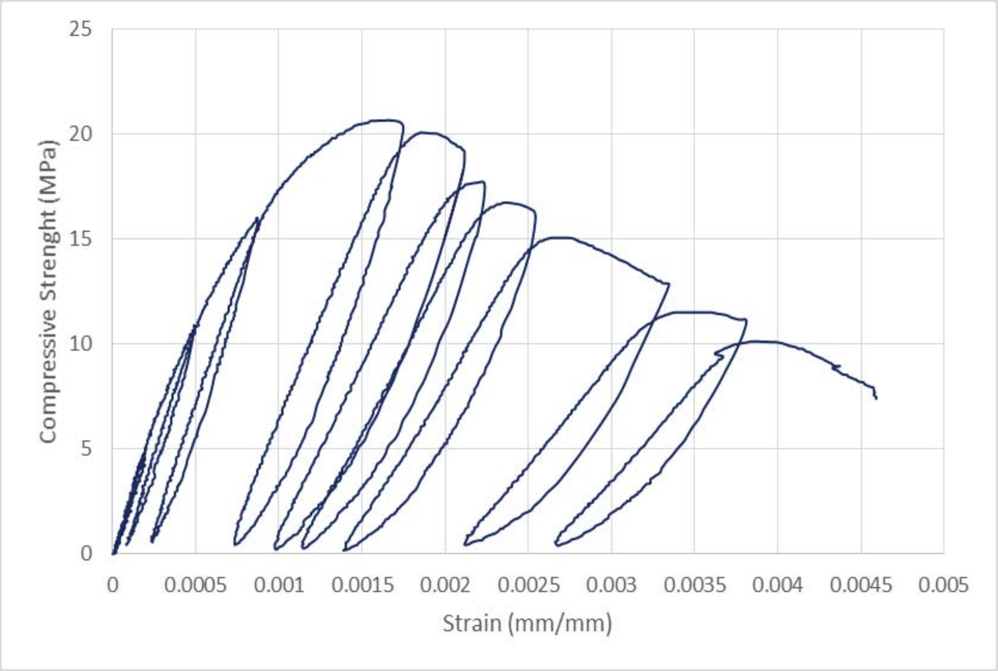

Figure 4-12 Behavior of concrete under cyclic compressive loading for SP1 and SP2

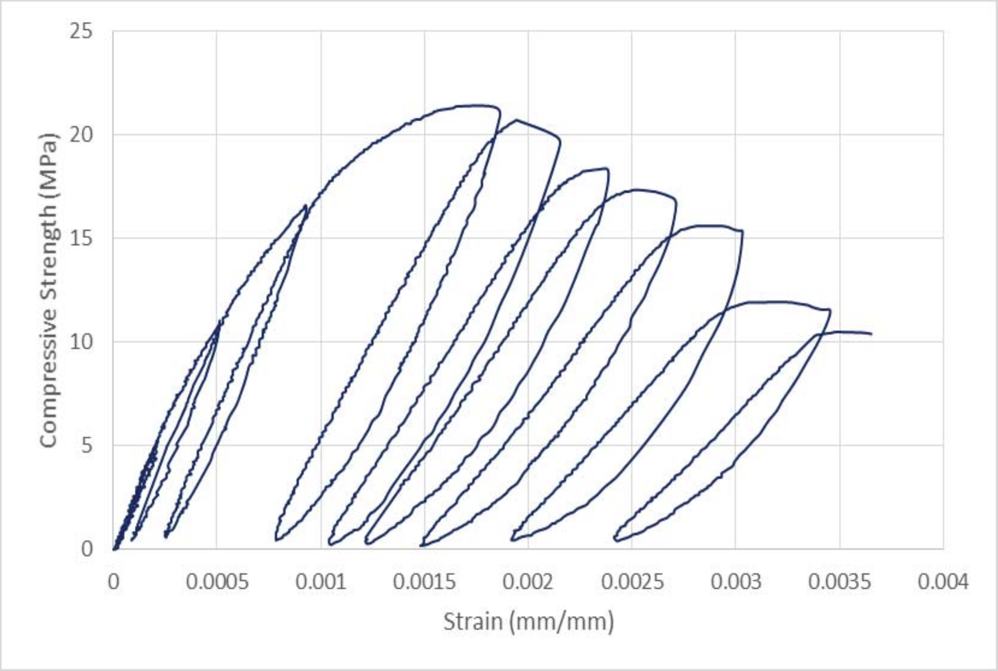

Figure 4-13 Behavior of concrete under cyclic compressive loading for SP3 - SP5

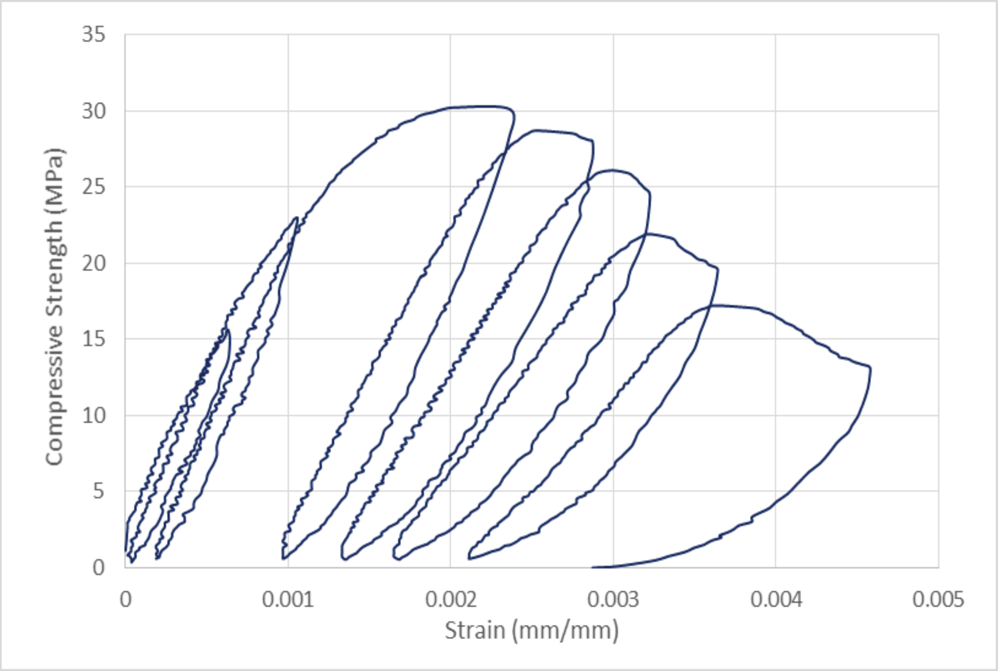

Figure 4-14 Behavior of concrete under cyclic compressive loading for SP6 and SP7

Modulus of elasticity is calculated according to following relation:

$$E = (S_2 - S_1)/(\epsilon_2 - 0.000050) \tag{4.1}$$

where E is modulus of elasticity, S_2 is stress at 40% of failure load, S_1 is stress at longitudinal strain $\epsilon_1 = 0.000050$ and ϵ_2 is the longitudinal strain correspond to S_2.

Poisson's ratio is calculated as follow:

$$\mu = (\epsilon_{t2} - \epsilon_{t1})/(\epsilon_2 - 0.000050) \tag{4.2}$$

where ϵ_{t2} and ϵ_{t1} are transverse corresponds to stress of S_2 and S_1 respectively.

Results of this test are tabulated in Table 4-3.

Table 4-3 Elastic modulus and Poisson's ratio

Specimen ID	Modulus of Elasticity (MPa)	Poisson’s Ratio
SP-1 – SP-2	21542	0.20
SP-3 – SP-5	21528	0.20
SP-6 – SP7	25700	0.19

4.5.1.3. Concrete Tensile Strength Test

Concrete tensile strength was calculated indirectly by split cylinder test conducted according to test procedure laid down by ASTM C496 [38] as displayed in Figure 4-15.

Figure 4-15 Split cylinder strength test

Average split tensile strength was calculated by conducting three split cylinder tests on 21 MPa (SP1-SP5) and 30 MPa (SP6-SP7) concrete respectively according to following relation:

$$f_t = \frac{2\,P}{\pi\,l\,d} \tag{4.3}$$

where P is applied load, l and d are length and diameter of cylinder and f_t is the split tensile strength. Tensile strength of concrete according to Equation [4.3] is tabulated in Table 4-4

Table 4-4 Tensile strength of concrete

Specimen ID	Tensile Strength (MPa)
SP-1 – SP-5	2.81
SP-6 – SP7	3.08

4.5.2. Steel reinforcement

ASTM A615 deformed reinforcement was utilized for column and beam reinforcements which were tested in "Structural Mechanics Lab" of KFUPM Figure 4-16.

Figure 4-16 Testing of reinforcing steel

Ø8 bar was used as ties and stirrups in column and beam respectively whose yield strength was found to be 580MPa at strain of 0.0030 mm/mm Figure 4-17 giving E = 193600 MPa whereas Ø20 bar was used as main longitudinal reinforcement for beam and column whose yield strength was found to be 605MPa at strain of 0.0031 mm/mm as shown in Figure 4-18 giving E = 195161 MPa.

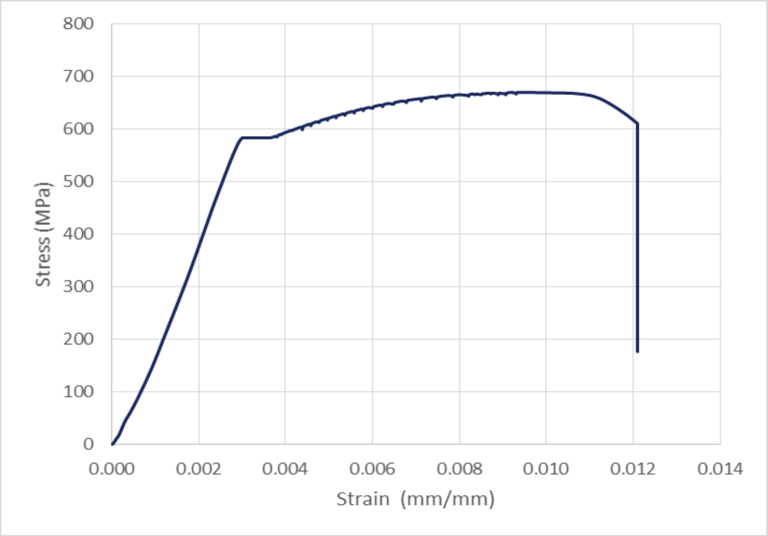

Figure 4-17 Stress-strain curve for Ø8 reinforcing bar

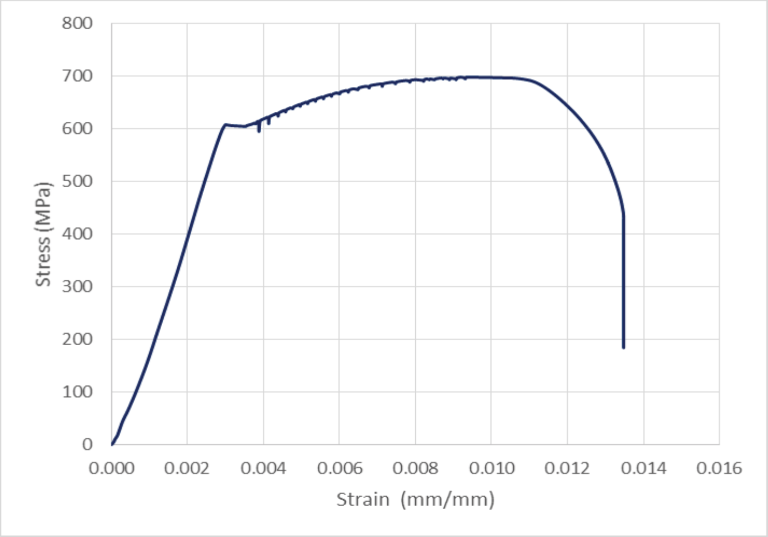

Figure 4-18 Stress-strain curve for Ø20 reinforcing bar

Tensile strength test results of steel reinforcement are summarized in Table 4-5.

Table 4-5 Results of steel tensile test

Specimen	Bar Size	Stress (MPa)		Strain (mm/mm)		Modulus of Elasticity, E (MPa)
		f_y	f_u	ϵ_y	ϵ_u	
SP1-SP7	Ø8	580	667	0.0030	0.0105	193600
	Ø20	605	695	0.0031	0.0106	195161

4.6. Test Setup Details

Test setup is designed to simulate forces and boundary conditions to which BCJ is subjected under seismic excitation. Moment release is provided at beam's end and at top and bottom ends of the column to simulate the three inflection points in the actual structure as shown in Figure 4-19a. which is the deformed shape of BCJ sub-assembly under seismic action. Figure 4-19b. shows the test idealized arrangement in which both ends of the column are restrained with pin while load at beam's is applied to simulate load reversal which perfectly simulate the forces and boundary conditions except the P-Δ effect, which do not have consequences on performance of BCJ.

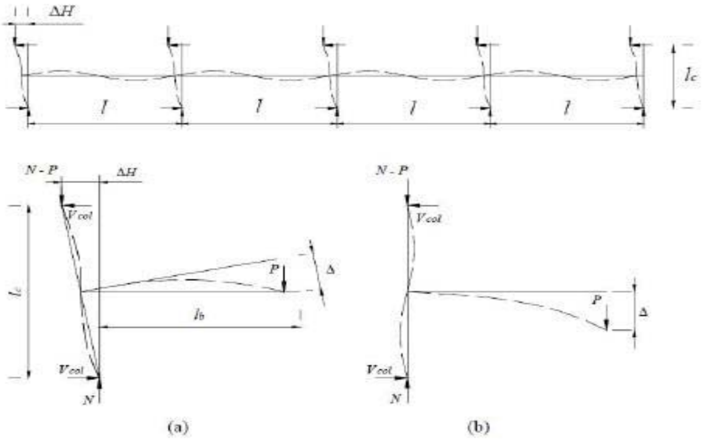

Figure 4-19 a) Deformed shape of BCJ under seismic action; b) Test idealization

Test setup comprises of steel reaction frame, hydraulic jacks and supports. Steel reaction frame takes load from two hydraulic jacks one at the column and other at the beam tip. The jack at the column with loading capacity of 1200 kN is used to apply loads of different magnitude on column according to loading protocol whereas jack at the beam tip with loading capacity of 300 kN is used to apply load reversal to simulate seismic loads. Two specially designed pin supports are also connected to the frame to support column and to allow application of loads from both the jacks. Figure 4-20 and Figure 4-21 shows the schematic diagram and BCJ test setup respectively at KFUPM.

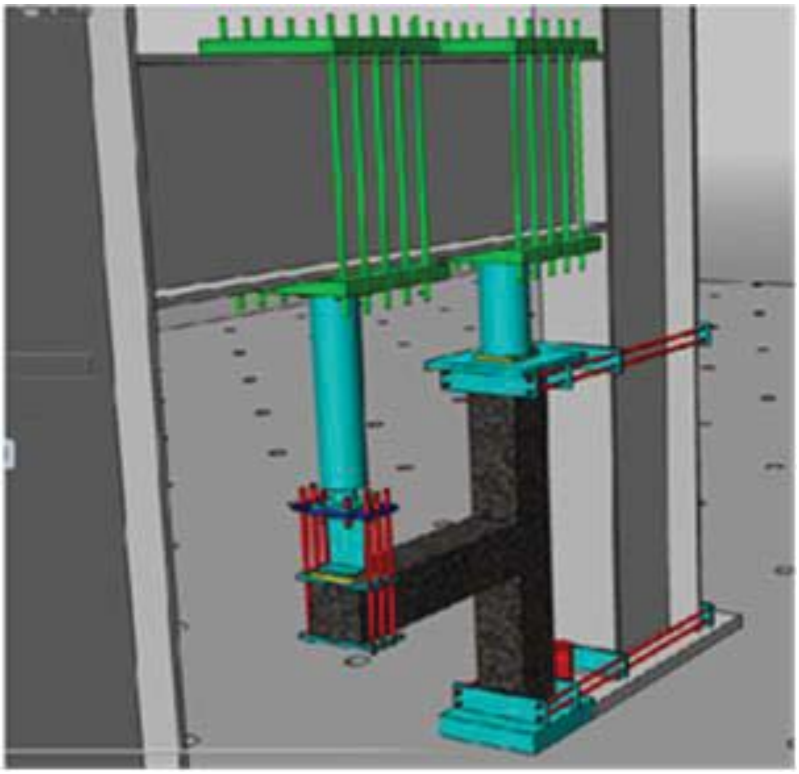

Figure 4-20 Schematic diagram of BCJ test setup at KFUPM

Figure 4-21 Test setup at KFUPM

4.7. Instrumentation

4.7.1. Introduction

Specimens were highly equipped to capture all the required aspects of experiment like over-all structural response, local distortions, and strains in concrete and steel. Instrumentation was similar for all the specimens and done in two stages. First stage instrumentation was done before casting which includes the installation of electrical steel stain gauges which were continuously monitored till casting to ensure their functionality. Second stage instrumentation was done in laboratory which includes installation of external equipment like concrete strain gauges, (Linear Variable Differential Transformer, LVDT's) and extensometer. Apart from specimen instrumentation frame was also equipped with LVDT's to measure any possible over-all rigid movements of the specimen.

4.7.2. First Stage Instrumentation

In first stage instrumentation steel strain gauges of 120Ω electrical resistance were installed and protected with waterproofing materials. Column bars were gauged just above and below the joint which is the most critical flexural zone for column reinforcement. Beam longitudinal reinforcement both top and bottom layers were gauged near the joint interface to measure the strains for two-fold reason, one of the reason is to measure the strains which is used in shear capacity calculation of joint and the other is to investigate the possible reinforcement yielding to judge failure mechanism. First stirrup at shear critical section of beam was also equipped with strain gauge to measure any likely yielding. Locations of steel strain gauges are shown in Figure 4-22.

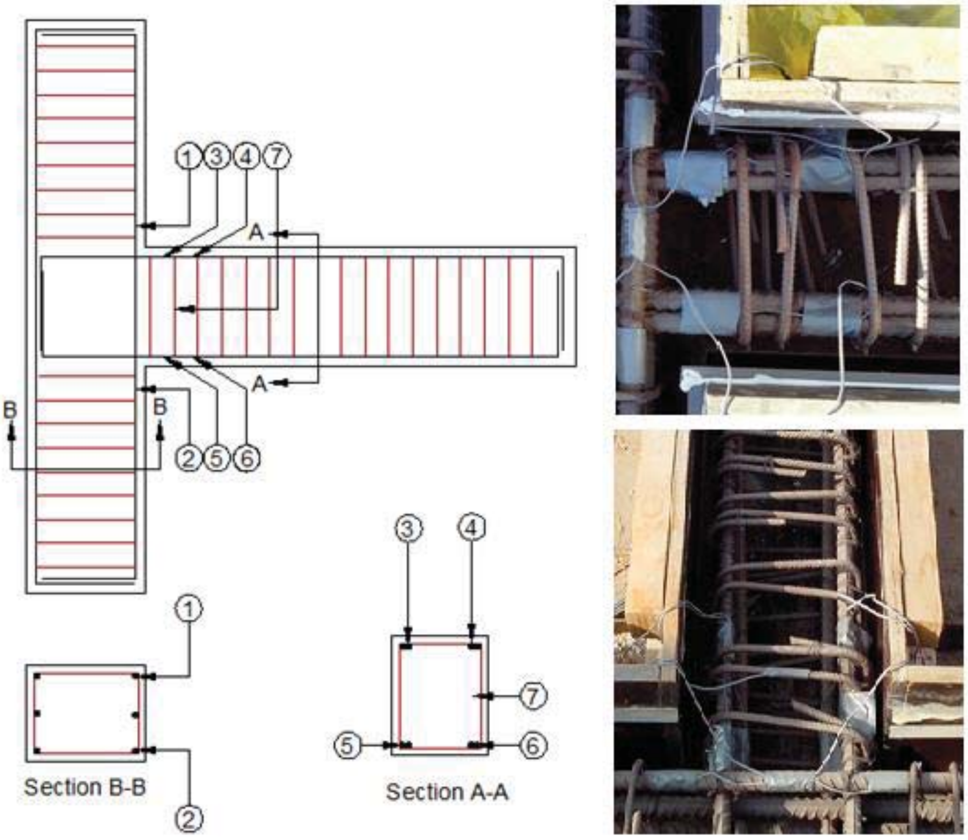

Figure 4-22 Location of steel strain gauges

4.7.3. Second Stage Instrumentation

Second stage instrumentation includes installation of external equipment like concrete strain gauges, LVDT's, extensometer etc.

Concrete strain gauges were mounted in vertical direction on all the sides of the column to ensure concentric application of axial load as far as possible. Portion of columns just above and below the joint which is the most critical flexural zone was also gauged. Concrete cross-strain gauges were mounted on both faces of joint to measure stains. One concrete strain gauge was mounted at column face beside the joint to measure strains at onset of reinforcement rotation. Along with concrete strain gauges LVDT's were installed on joints to measure shear deformation in the joint. Two LVDT's were installed at top and bottom clamp support of the column to measure any possible rigid body motion of the specimen. One extensometer was attached at the beam tip to measure deflection under application of load. External instrumentation of specimen Figure 4-23 and Figure 4-24.

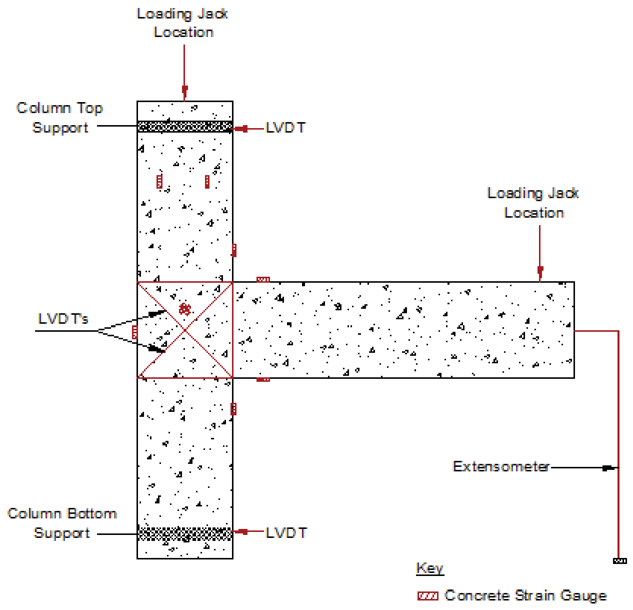

Figure 4-23 Schematic diagram of external instrumentation

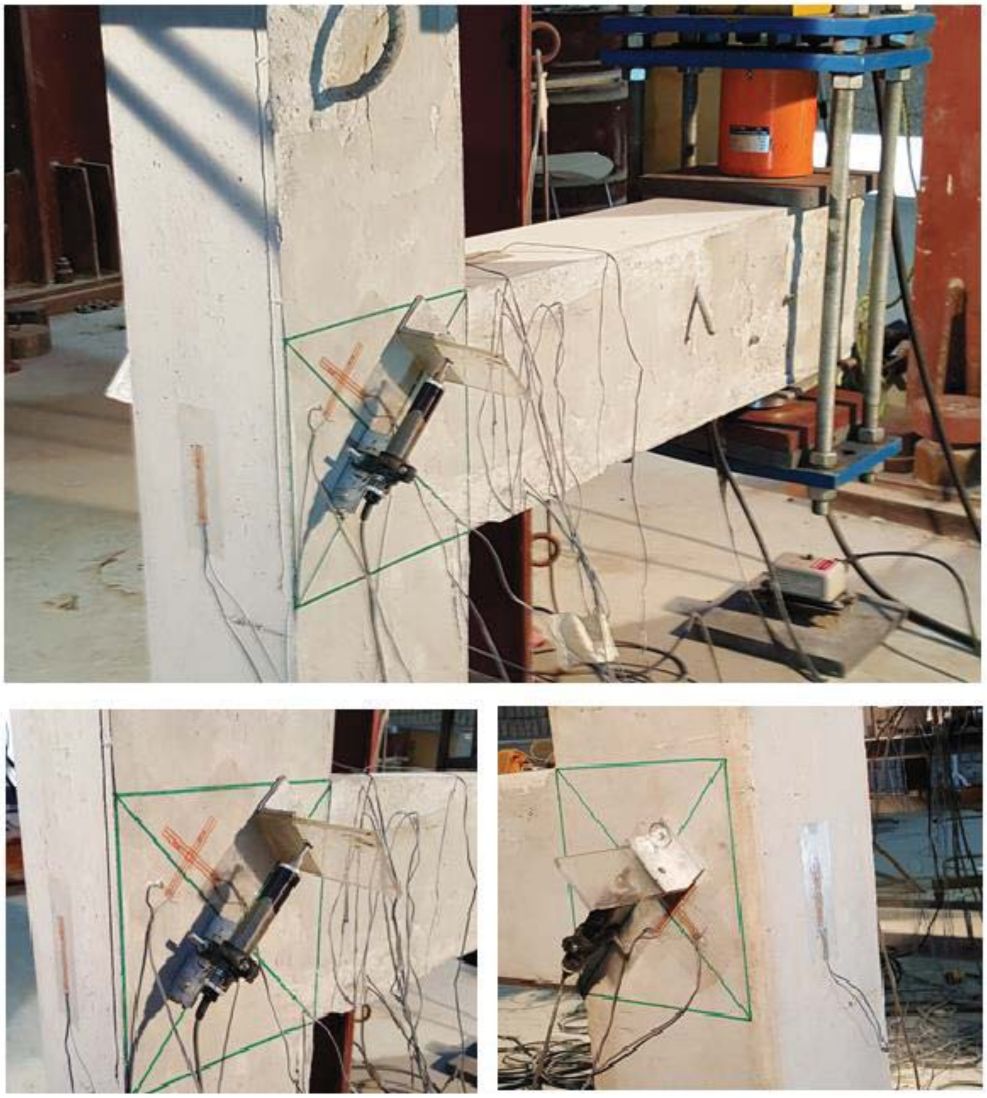

Figure 4-24 External instrumentation

4.8. Test Program

4.8.1. Introduction

Both monotonic and reversed cyclic loading was considered in test program to estimate the actual shear capacity and stiffness degradation under seismic excitation respectively. Monotonic test was conducted on four specimens to precisely monitor the effect of different magnitude of column axial load on strength and failure mechanism whereas reversed cyclic loading was applied on three BCJ to understand the ductility, stiffness degradation and energy dissipation capacity of BCJs.

4.8.2. Monotonic Load Tests

Four specimens with same details were subjected to different magnitudes of axial load on column according to axial load protocol as tabulated in Table 4-6. Load on beam tip was applied until failure of BCJ. Range of ALR 0.0 to 0.7 was considered to capture the behavior over entire range.

Table 4-6 Axial loading scheme

S. No.	Specimen ID	Magnitude of Axial Load (kN)	Axial load ratio (ALR), $\frac{N}{A_g f'_c}$
1	SP-1	0	0.00
2	SP-2	200	0.19
3	SP-3	600	0.57
4	SP-6	1050	0.70

4.8.3. Reverse Cyclic Load Tests

Reverse cyclic load test was done on three specimens to understand the performance of BCJs subjected to different magnitude of axial and cyclic loads to simulate actual scenario to which BCJs are subjected under seismic excitation. In these tests axial load of different magnitudes was applied on column whereas reverse cyclic load was applied at beam tip until complete failure of BCJs.

CAL on specimen SP-4 and SP-5 was 200 kN and 600 kN respectively. Reverse cyclic loading protocol for SP-4 and SP-5 Table 4-7.

Table 4-7 Loading protocol for specimen SP-4 and SP-5

Cycle Number	Drift Ratio %	Push (mm)	Pull (mm)
1	0.11	1	-1
2	0.22	2	-2
3	0.33	3	-3
4	0.44	4	-4
5	0.56	5	-5
6	0.67	6	-6
7	0.78	7	-7
8	0.89	8	-8
9	1.00	9	-9
10	1.11	10	-10
11	1.22	11	-11
12	1.33	12	-12
13	1.44	13	-13
14	1.56	14	-14
15	1.67	15	-15
16	1.78	16	-16
17	1.89	17	-17
18	2.00	18	-18
19	2.22	20	-20
20	2.44	22	-22
21	2.78	25	-25
22	3.11	28	-28
23	3.56	32	-32
24	4.00	36	-36
25	4.56	41	-41

Note:

1) Drift Ratio Percentage = (Beam Tip Displacement/ Beam Length) x 100.
2) Each cycle is repeated in specimen SP-4.

Figure 4-25 and Figure 4-26 shows the reverse cyclic loading protocol graphically.

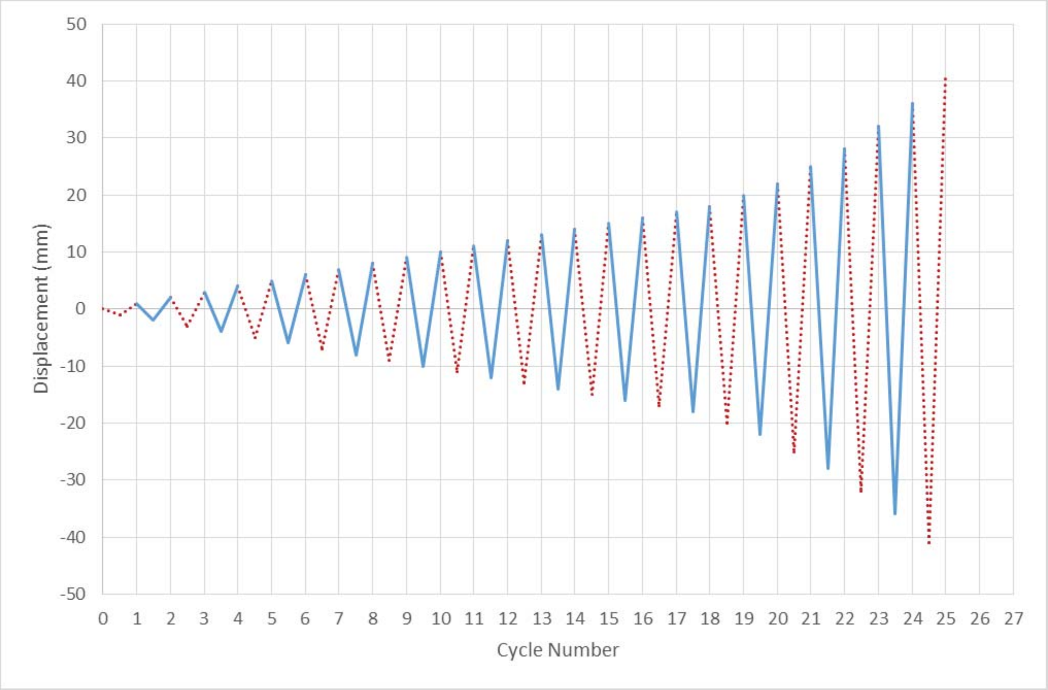

Figure 4-25 Loading protocol for specimen SP-4

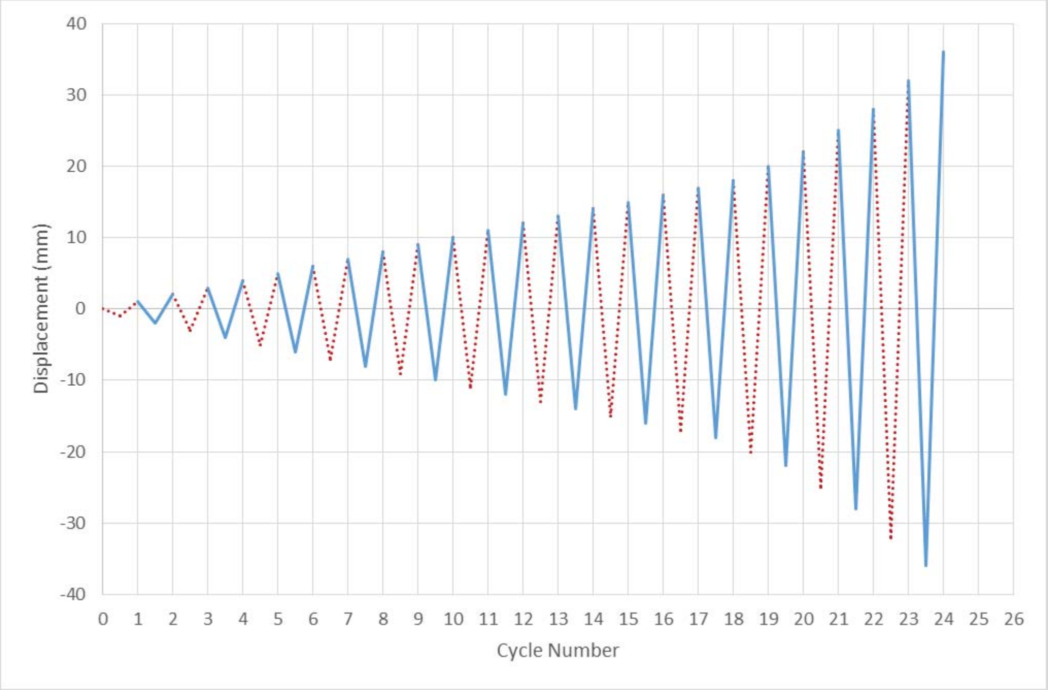

Figure 4-26 Loading protocol for specimen SP-5

Column axial load on specimen SP-7 was 1050 kN. Reverse cyclic loading protocol is tabulated in Table 4-8.

Table 4-8 Loading protocol for specimen SP-7

Cycle Number	Drift Ratio %	Push (mm)	Pull (mm)
1	0.11	1	-1
2	0.33	3	-3
3	0.56	5	-5
4	0.78	7	-7
5	1.00	9	-9
6	1.33	12	-12
7	1.67	15	-15
8	2.00	18	-18
9	2.44	22	-22
10	3.00	27	-27

Figure 4-27 shows the reverse cyclic loading protocol for specimen SP-7 graphically.

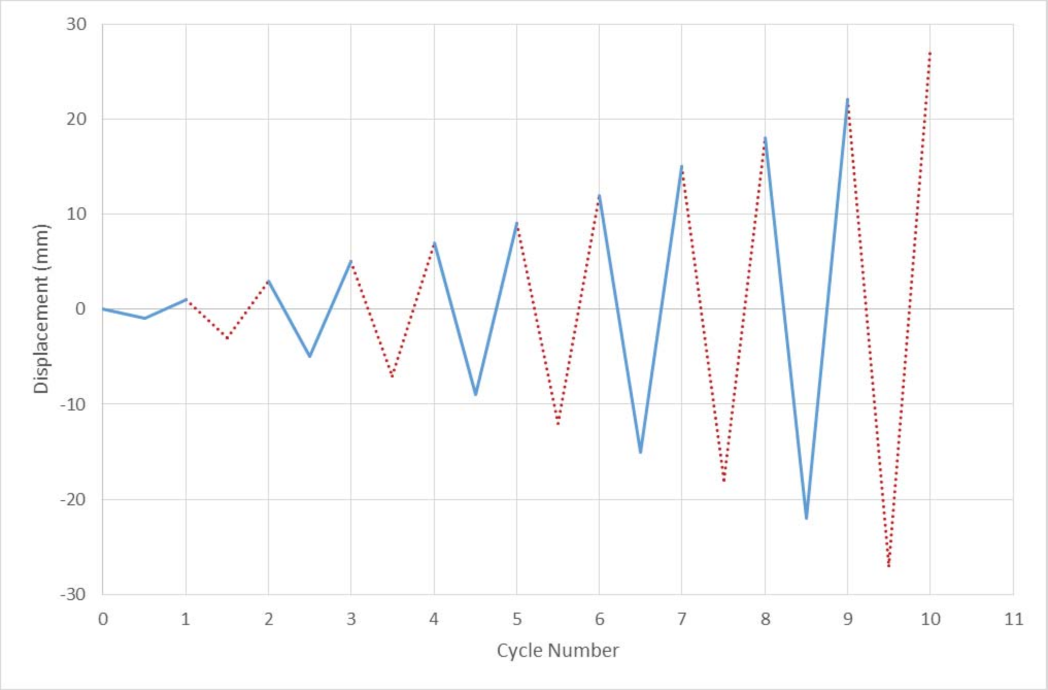

Figure 4-27 Loading protocol for specimen SP-7

4.8.4. Summary of Test Loading Scheme

Loading scheme of all the specimens are tabulated in Table 4-9.

Table 4-9 Summary of test loading scheme

S. No.	Specimen ID	Magnitude of Axial Load (kN)	Axial load ratio (ALR), $\frac{N}{A_g f'_c}$	Test Method
1	SP-1	0	0.00	Monotonic
2	SP-2	200	0.19	Monotonic
3	SP-3	600	0.57	Monotonic
4	SP-4	200	0.19	Reverse Cyclic
5	SP-5	600	0.57	Reverse Cyclic
6	SP-6	1050	0.70	Monotonic
7	SP-7	1050	0.70	Reverse Cyclic

CHAPTER 5

EXPERIMENTAL RESULTS AND DISCUSSIONS

5.1. Introduction

This chapter delineates the result of experimental program as described in the previous chapter. In this chapter first the seismic performance of each experimentally tested specimen will be discussed which will be judged on parameters like joint failure mechanism, joint crack pattern and its propagation, load-drift relationship, joint shear strength and joint ductility and energy dissipation capacity. Secondly theses performance parameters will be compared to understand the effect of different magnitude of CAL and beam loading history.

5.2. Specimen’s Performance under Monotonic Loading

5.2.1. Specimen SP-1

Specimen SP-1 was tested under monotonic loading without CAL. Figure 5-1 presents the load-deformation response whereas Figure 5-2 shows the crack pattern of SP-1. The crack at interface of joint and the first shear crack in the BCJ was detected simultaneously at load of 16 kN at beam tip, corresponding to displacement of 1.34 mm. With increase of displacement at beam tip shear cracks in BCJ extended towards the outer edge of column and the maximum load of 37.55 kN was reached at displacement of 19.44 mm giving a shear strength of 2.74 MPa. With further increase of displacement at beam tip width of shear cracks increased without any increase in the load describing the joint failure.

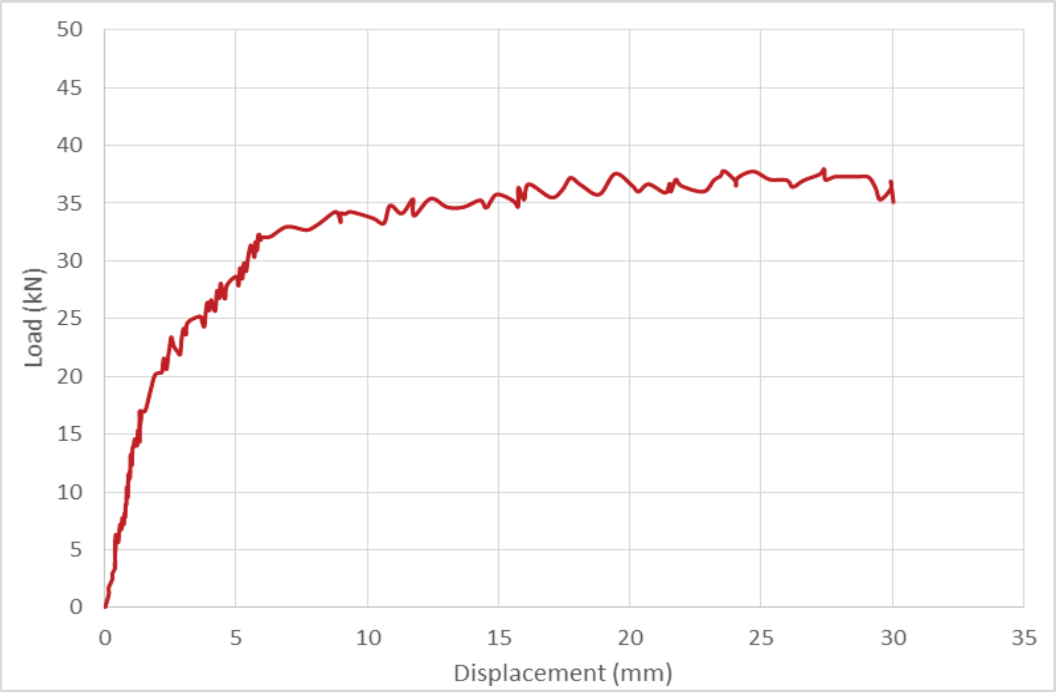

Figure 5-1 Load-displacement response of specimen SP-1

First the crack appeared at the center of joint which propagated toward the outer edge of column in upward direction and toward the lower beam-joint interface in downward direction giving the inclination of main diagonal crack at 45°. At the later stage of loading some vertical cracks at outer face (face of joint opposite to beam) was also observed due to rotation of beam reinforcement hooks in the joint. Apparently no cracks were detected in the beam also the maximum strain observed in beam top reinforcement was 0.00066 mm/mm which is considerably lower than the yield strain of reinforcement. This condition dictates the pure joint failure mode in this specimen.

Figure 5-2 Crack pattern of specimen SP-1

5.2.2. Specimen SP-2

Specimen SP-2 was tested under monotonic loading with CAL of 200 kN (ALR = 0.19 f'_c A_g). Figure 5-3 shows the load-deformation response. The first vertical crack in beam and the diagonal crack at the center of joint (on both faces) appeared simultaneously at a load of 29 kN at displacement of 3.8 mm. With increase in displacement at beam tip the second crack appeared at beam-joint interface at a load of 32 kN and displacement of 4.49 mm. The third crack at front face of the joint was observed parallel to the first diagonal crack at 40 kN at displacement of 7.02 mm which increased in width and length until the maximum failure load of 51 kN at displacement of 19.48 mm. Just before the failure fourth crack appeared in the joint on both the faces in vertical direction which extends in to the column Figure 5-4. The shear strength against load of 51 kN is found to be 3.45 MPa.

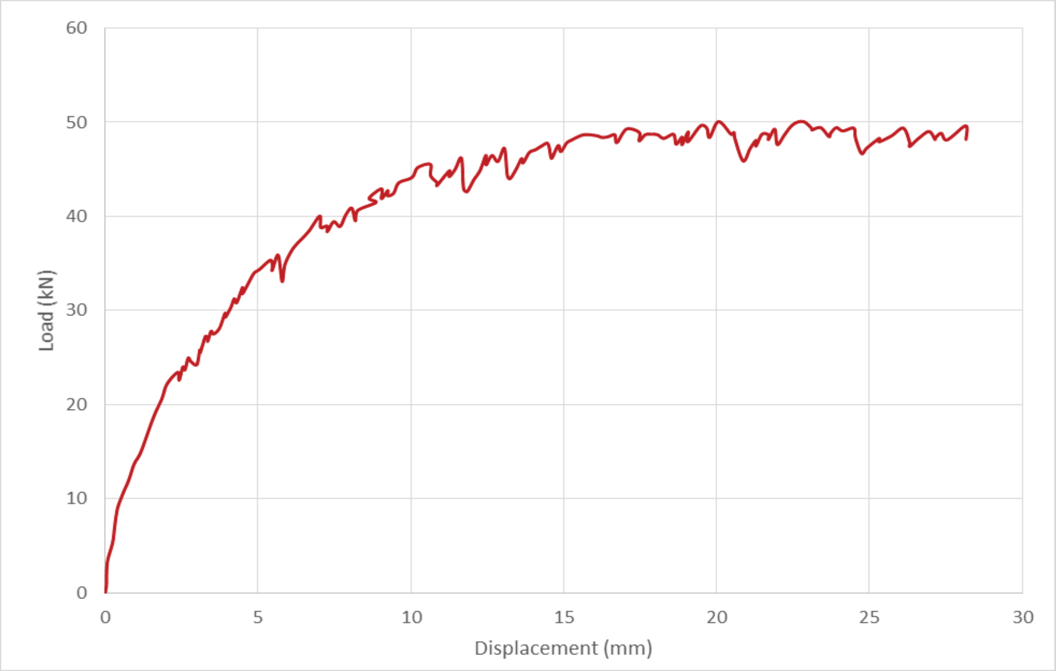

Figure 5-3 Load-displacement response of specimen SP-2

Figure 5-4 shows the crack pattern in the joint observed at different stages of loading. It is important to note that with increase of an ALR from 0.0 to 0.19 the crack initiation at joint delayed that is first crack in the joint appeared at 29 kN as compared to Specimen SP-1 where first crack appeared at 16 kN. Cracking of beam-joint interface also delayed as crack in interface of specimen SP-2 was observed at 32 kN as compared to 16 kN in case of specimen SP-1 due to more confinement provided by CAL to the beam reinforcement. Also the shear strength increases considerably that is from 2.75 MPa to 3.45 MPa with increase of ALR from 0.0 to 0.19. Inclination of main diagonal shear crack also increased to 50°. Similar to specimen SP-1 vertical cracks appeared at the outer face of joint at later stages of loading also very few hair line cracks were also detected in the beam. The maximum strain in beam reinforcement was found to be 0.00081 mm/mm which is significantly lower than the yield strain of reinforcement. Specimen SP-2 failed in joint failure mode.

Figure 5-4 Crack pattern of specimen SP-2

5.2.3. Specimen SP-3

Specimen SP-3 was tested under monotonic loading with CAL of 600 kN (ALR = 0.57 f'_c A_g). Figure 5-5 shows the load-displacement response. In specimen SP-3 first crack seemed in the beam at load of 17 kN corresponding to displacement of 1.03 mm at some distance from the interface then the second crack appeared at 21 kN at displacement of 1.32 mm. Third crack in beam and crack in beam-joint interface occurred simultaneously at 38 kN corresponding to displacement of 4.11 mm. With further increase of displacement at beam tip the fourth and fifth crack appeared in the joint at load of 43 kN at displacement of 5.38 mm. Forth crack appeared at very high inclination of about 75° while the fifth crack was perfectly at 90° as shown in the Figure 5-6. Both these cracks then increased in length and width until failure of joint which arose at load of 56.87 kN at corresponding to 17.86 mm.

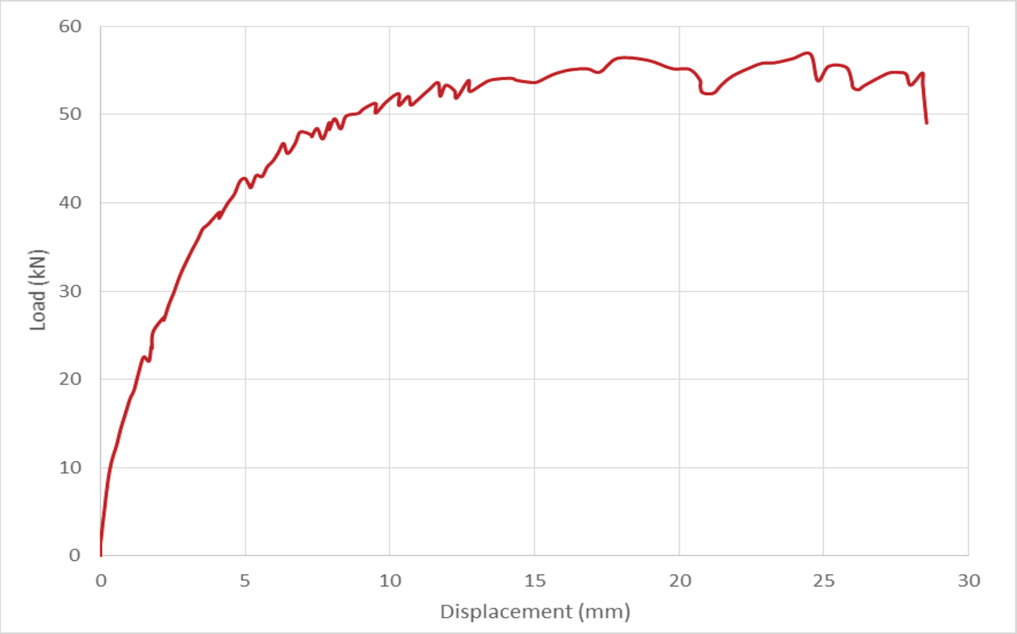

Figure 5-5 Load-displacement response of specimen SP-3

The shear strength against load of 56.87 kN is found to be 4.23 MPa.

Figure 5-6 shows the crack pattern in the joint observed at different phases of loading. It is essential to note that with increase of an ALR to 0.57 $f'_c A_g$ the crack initiation and pattern considerably changed. First crack in the joint appeared at 43 kN as compared to 16 kN and 29 kN in case of specimens SP-1 and SP-2. Secondly the cracks in the joint appeared after reasonable amount of cracks in the beam which was not the case in the previous two specimens. Thirdly the inclination of main shear cracks was found to be very high that is around 75° and 90°. With increase of axial load enhancement in joint shear strength is observed that is shear strength in specimen SP-3 further increased to 4.23MPa as compared to 2.75 MPa and 3.45 MPa in case of specimen SP-1 and SP-2 respectively.

Although considerable number of thin cracks appeared in the beam but maximum strain observed in the beam longitudinal reinforcement was 0.000986 mm/mm which is greater than the previous two cases but far less than the yield stress of reinforcement. The maximum strain observed in the column longitudinal reinforcement is found to be 0.00148 mm/mm which means that reinforcement in not yielding the above facts dictates that up to ALR of 0.57 $f'_c A_g$ no flexural or axial failure of joint is observed.

The joint of specimen SP-3 also failed in joint shear failure mode like the previous two cases however the performance of joint changed considerably due to increase in axial load on column not only in term of strength and cracking behavior but also in terms of stiffness. Continuous increase in stiffness is observed with increase in ALR from 0.00 to 0.57 which will be deliberated in detail later in this chapter.

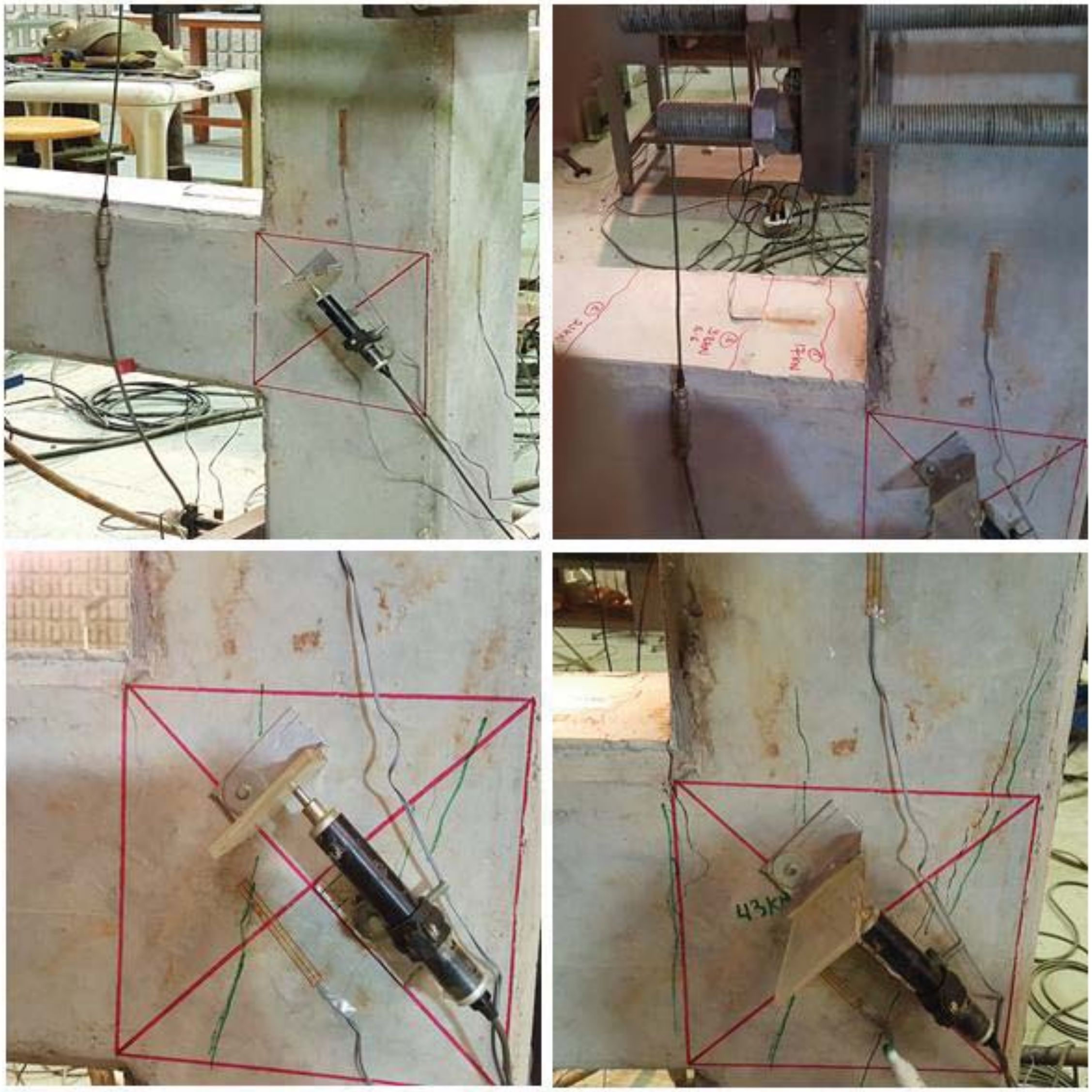

Figure 5-6 Crack pattern of specimen SP-3

5.2.4. Specimen SP-6

Specimen SP-6 was tested under monotonic loading with CAL of 1050 kN (ALR = 0.70 $f'_c A_g$). Figure 5-7 displays the load-displacement curve. In this specimen first number of cracks were observed in beam at load of 20 kN at beam tip then the two main vertical cracks in BCJ and crack in the beam-joint interface appeared simultaneously at 45 kN corresponding to displacement of 3.05 mm. With further increase of displacement crack at beam-joint interface increased in width while vertical cracks in BCJ extended towards the column and then increased in width until the failure load for this specimen reached that is 66.89 kN corresponding to the displacement of 8.55 mm. The joint shear strength is found to be 5.20 MPa.

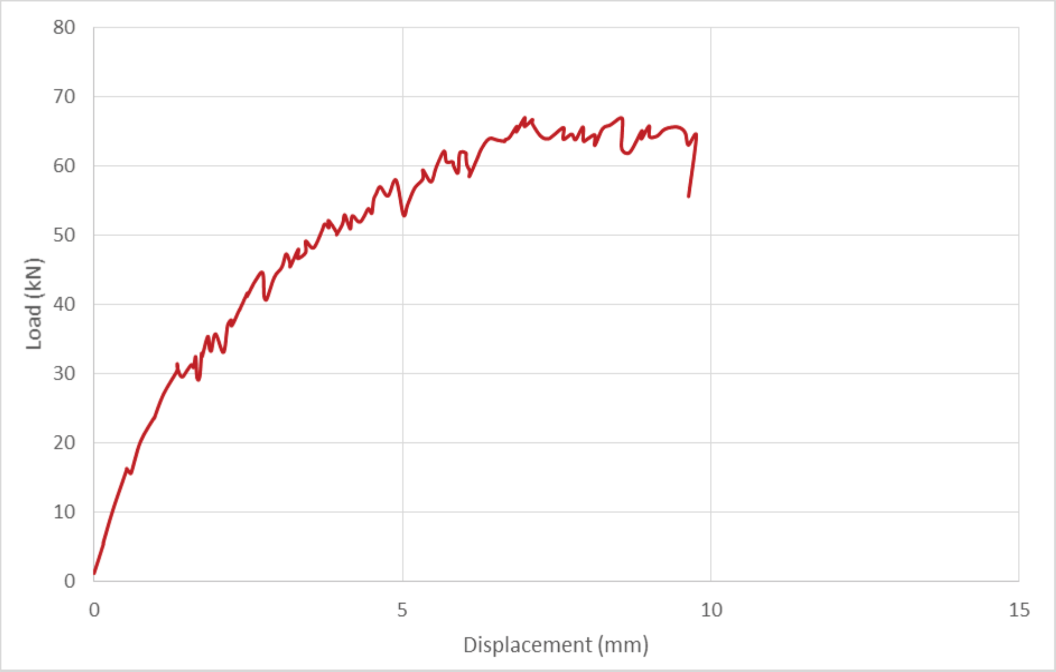

Figure 5-7 Load-displacement response of specimen SP-6

It is important to note that crack initiation and propagation pattern for specimen SP-6 Figure 5-8 considerably changed as compared to previous specimen. First all the crack appeared in the joint were almost inclined at 90°. Secondly the crack at beam appeared at some distance from the interface because of confinement effect of CAL which enables the beam longitudinal reinforcement to gain more strains. Some vertical cracks also seemed on the outer face of the joint and in the column just above the beam top at later phases of loading.

Figure 5-8 Crack pattern of specimen SP-6

Maximum strain recorded in the beam and column longitudinal reinforcement was 0.001199 mm/mm and 0.001625 mm/mm respectively which is lower than the yield strain of reinforcement. Thus joint in the specimen SP-6 also failed in joint failure mode.

5.3. Specimen's performance under Reverse Cyclic Loading

5.3.1. Specimen SP-4

Specimen SP-2 was tested under reverse loading with an CAL of 200 kN (ALR = 0.19 $f'_c A_g$). Specimens were tested under reverse cyclic loading primarily to gain in depth knowledge of their seismic performance and to compare the cyclic behavior with their monotonic counterparts.

Figure 5-9 displays the hysteresis response of specimen SP-4 while Figure 5-10 and Figure 5-11 displays the crack pattern and development observed during the test. JF mode was observed in this specimen both in positive (push) and negative (pull) direction of loading.

The first diagonal crack seemed in the joint at 21 kN during push corresponded to the fourth positive cycle at a displacement of 2.80 mm and during pull in fifth negative cycle at a displacement of 3.80 mm at load of 26 kN.

The maximum load in the positive direction reached at 40.9 kN at displacement of 15.07 mm giving the shear strength of joint as 2.98 MPa whereas maximum load of 43 kN was achieved in the negative direction of loading at displacement of 15.22 mm which corresponded to shear strength of 3.09 MPa.

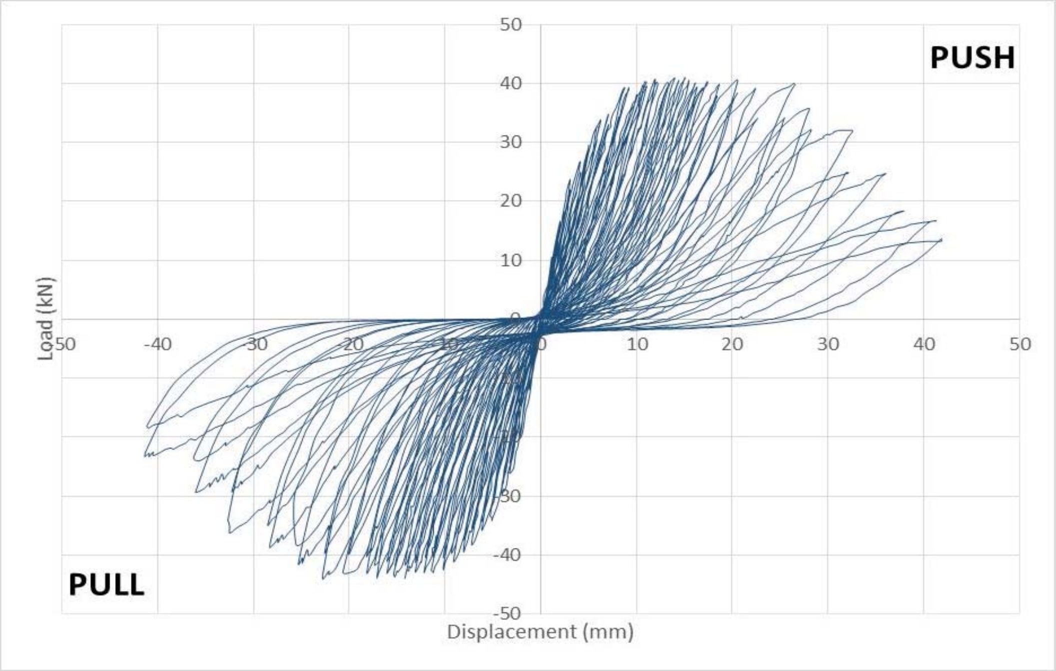

Figure 5-9 Hysteresis curve of specimen SP-4

Figure 5-10 shows the crack pattern observed at initial stages of loading. The first crack appeared in the beam during push in the second cycle at 20 kN whereas the second crack appeared near the interface during pull in the third cycle at a load of 27 kN. Diagonal cracking in the joint started in fourth and fifth cycle during push and pull respectively. The main crack seemed right at the center of the joint and with increase in loading cycles propagated towards the outer edge of the column. Increase in width of diagonal shear cracks and development of several parallel cracks was also detected with the progress of the test.

Main diagonal shear cracks in the joints were inclined almost at 45°. Other parallel cracks in both directions appeared with subsequent loading in both directions (push and pull) formed a net of cracks.

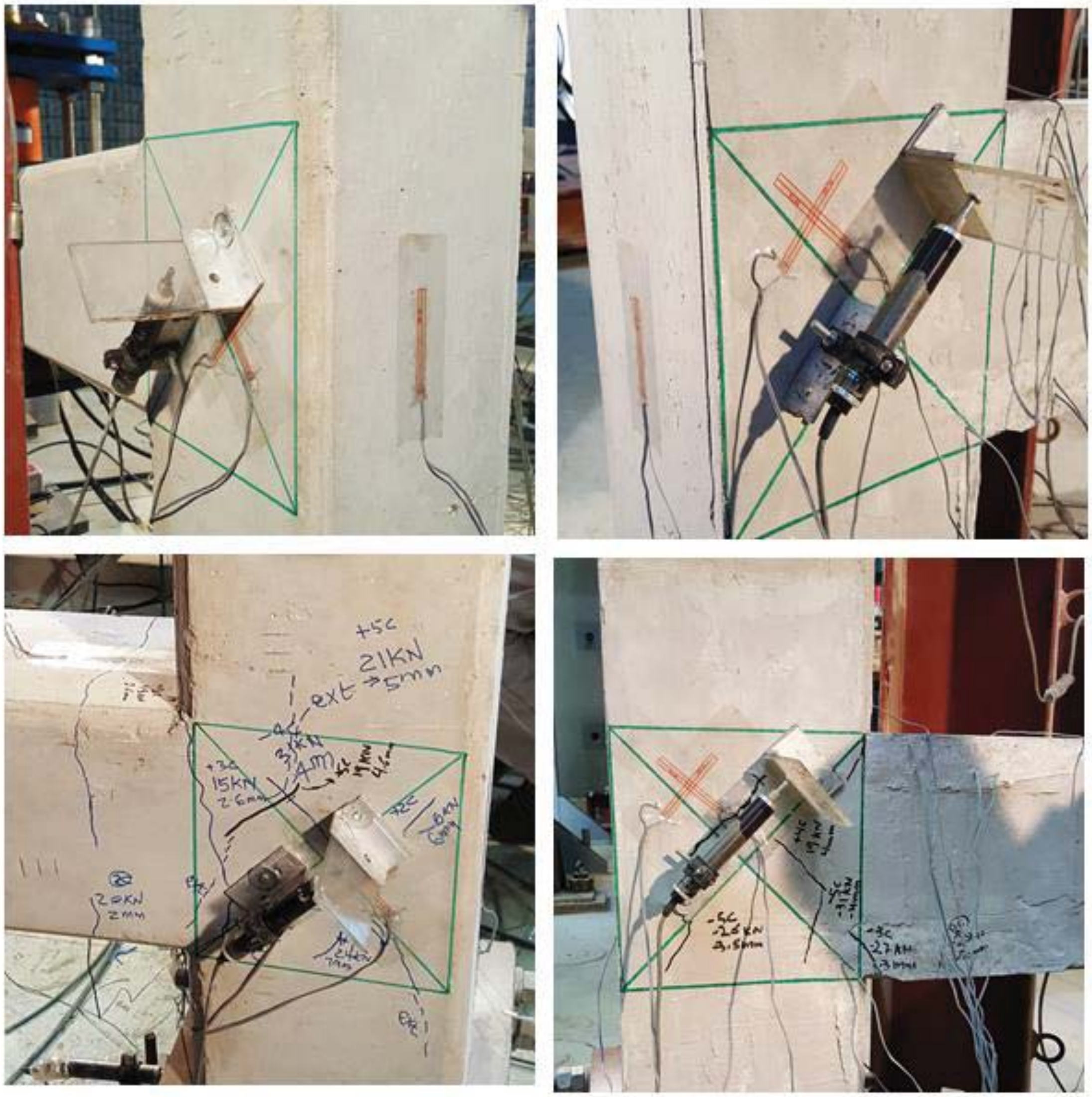

Figure 5-10 Development of cracks in initial loading stage of specimen SP-4

After a peak load 40.9 kN and 43 kN in push and pull respectively cracks in both directions increased in width and propagated towards the column. Vertical cracks at the outer edge of joint were initiated and crack at beam-joint interface also increased excessively at later phases of loading. BCJ of specimen SP-4 failed in joint failure mode with typical wedge crack pattern.

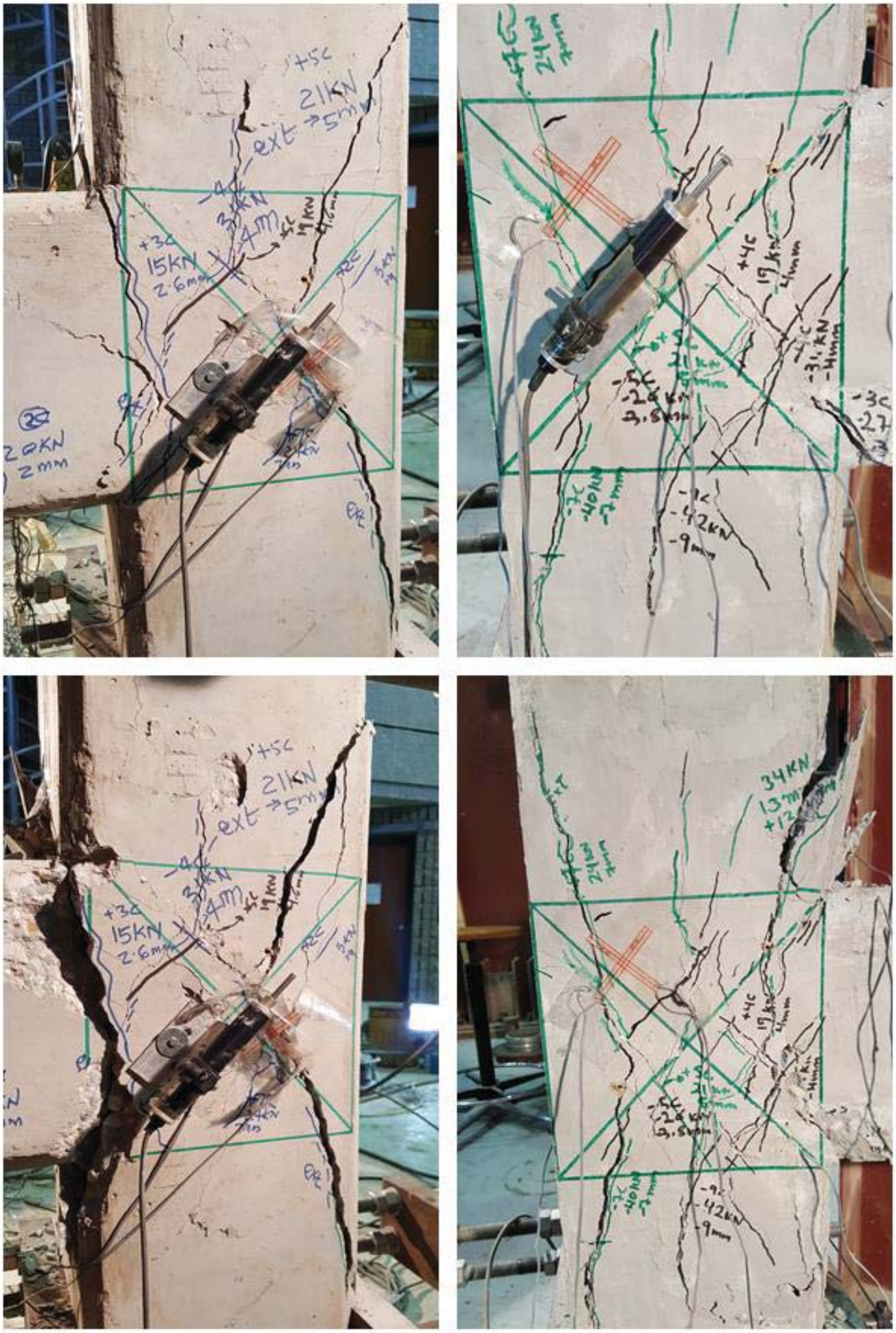

Figure 5-11 Crack pattern at intermediate and final loading stage of specimen SP-4

Pronounced pinching effect of hysteresis is observed due to formation of large number of shear cracks in the joint and bond-slip failure between reinforcement and the concrete. The phenomenon of pinching is more prominent at high displacements due to severe shear damage of joint and bond between concrete and reinforcement.

Figure 5-12 displays the load-displacement curve envelope of specimen SP-4. The maximum load achieved in push and pull was 40.9 kN and 43 kN respectively against 51 kN as obtained in the monotonic counterpart of this specimen. Thus the shear strength obtained is 2.98 MPa and 3.09 MPa in push and pull respectively against 3.45 MPa obtained in specimen SP-2 with monotonic loading due to continuous stiffness degradation in each cycle of loading.

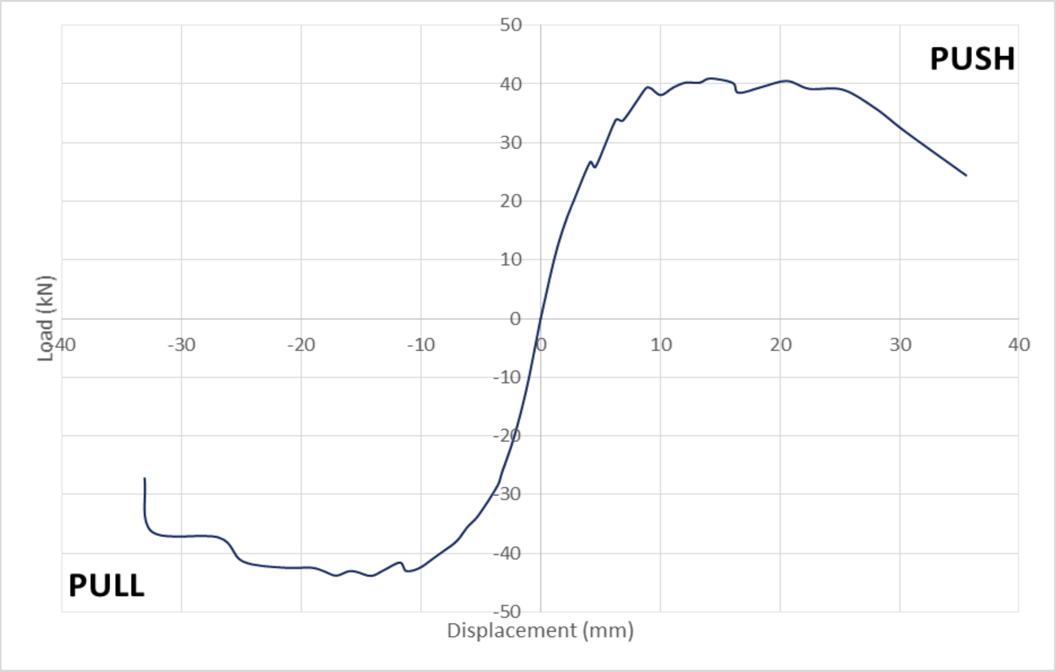

Figure 5-12 Load-displacement envelope curves of test specimen SP-4

Figure 5-13 shows the stiffness degradation curve of specimen SP-4. Peak to peak stiffness k_p is calculated as a slope of line joining the peak of negative load step of previous cycle with the peak of positive load step of current one. Stiffness degraded continuously from the first to the last cycle of loading which is calculated as 98 %. Degradation in stiffness is more pronounced in the initial stages of loading due to formation of cracks whereas in later stages of loading the stiffness degradation is comparatively more gradual as large displacements are required for the further crack propagation and damage of BCJ.

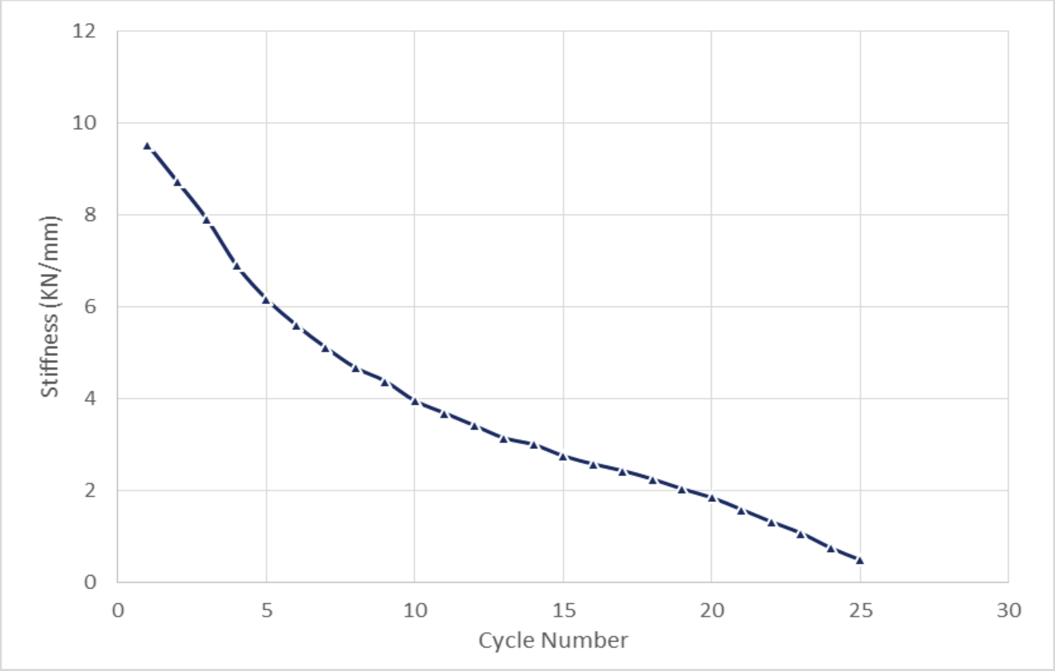

Figure 5-13 Stiffness degradation curve of specimen SP-4

Figure 5-14 shows the cumulative energy dissipation curve of specimen SP-4. Energy dissipation can be calculated as area enclosed by load-displacement plots of each cycle. Increase in total energy is observed however this increase is not proportional to the applied displacement due to degradation of strength associated with each loading cycle.

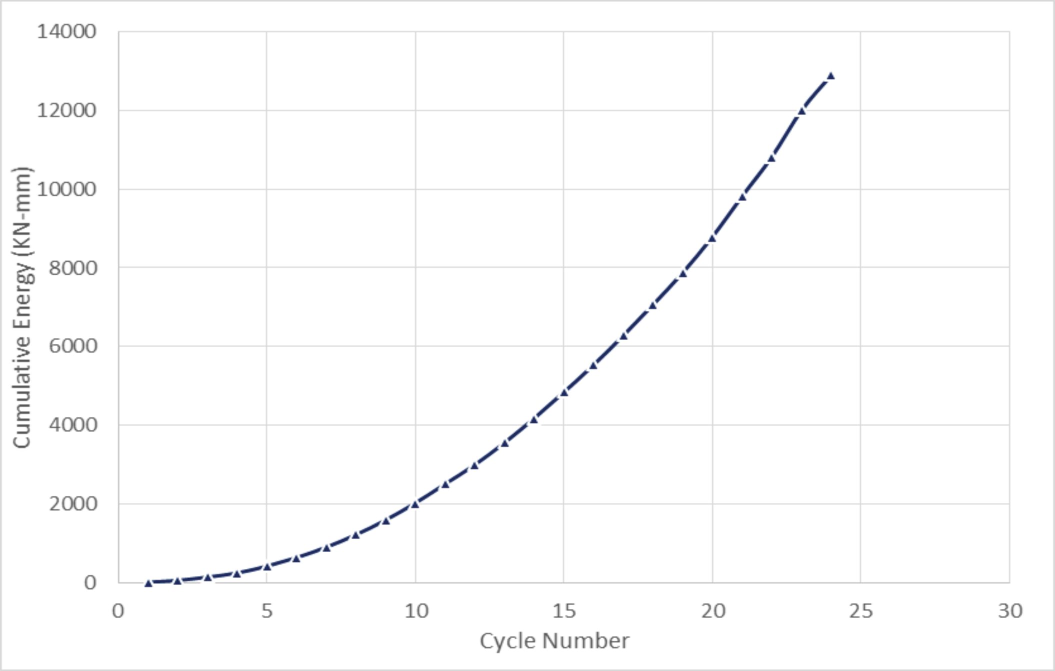

Figure 5-14 Cumulative energy dissipation curve of specimen SP-4

5.3.2. Specimen SP-5

Specimen SP-5 was tested under reverse loading with an axial load of 600 kN on column (ALR = 0.57 f'_c A_g) having a concrete compressive strength of 21 MPa. Figure 5-15 displays the hysteresis response of specimen SP-5 while Figure 5-16 and Figure 5-17 displays the crack pattern and development observed during the test. JF mode was observed in this specimen both in push and pull.

First diagonal crack appeared in BCJ at 36 kN during push corresponded to the fifth positive cycle at a displacement of 5.12 mm and during pull in fourth negative cycle at a displacement of 4.00 mm at 32 kN.

The maximum load in the positive direction reached at 47.3 kN at 13.60 mm giving the shear strength of joint as 3.43 MPa whereas maximum load of 50.0 kN was achieved in the negative direction of loading at displacement of 11.47 mm giving shear strength of 3.50 MPa.

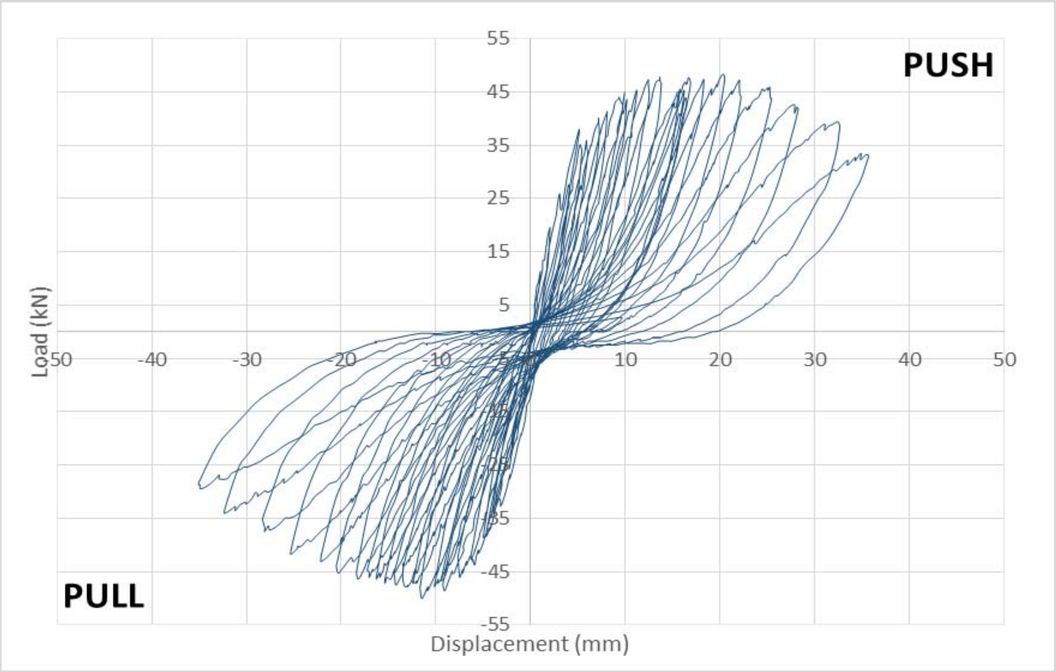

Figure 5-15 Hysteresis curve of specimen SP-5

Figure 5-16 shows the crack pattern observed at initial stages of loading. During third cycle of loading both in push and pull the first crack appeared at the beam-joint interface at a load of 27 kN and 28 kN corresponded to displacement of 3.1 mm and 3.0 mm respectively. The main shear crack in the joint appeared at fifth and fourth cycle of loading during push and pull respectively.

Main diagonal shear cracks appeared at the middle of BCJ but propagated towards the outer edge of the column at a high inclination that is around 75°. With subsequent loading cycles cracks width and length increased and several parallel cracks were observed

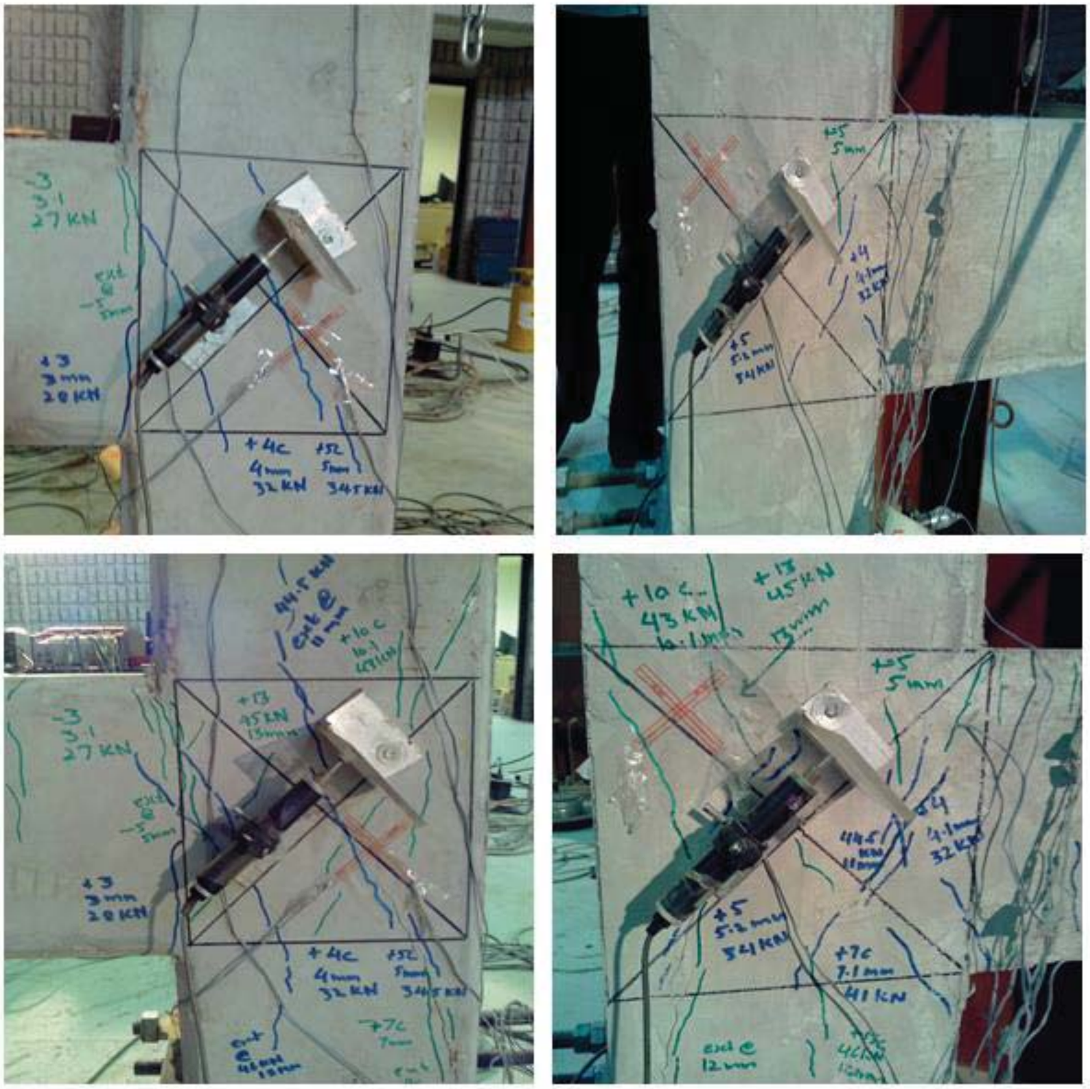

Figure 5-16 Development of cracks in initial loading stage of specimen SP-5

Although specimen SP-5 was subjected to high axial load on column but no crushing of concrete either in column or joint was observed also reinforcement of both beam and column had not yielded thus joint failed in typical joint shear failure mode. The joint failed at peak load of 47.3 kN and 50 kN in push and pull respectively after that cracks in both directions increased in width and propagated towards the column. Vertical cracks at the outer edge of joint were initiated and crack at beam-joint interface also increased excessively at later phases of loading shown in Figure 5-17.

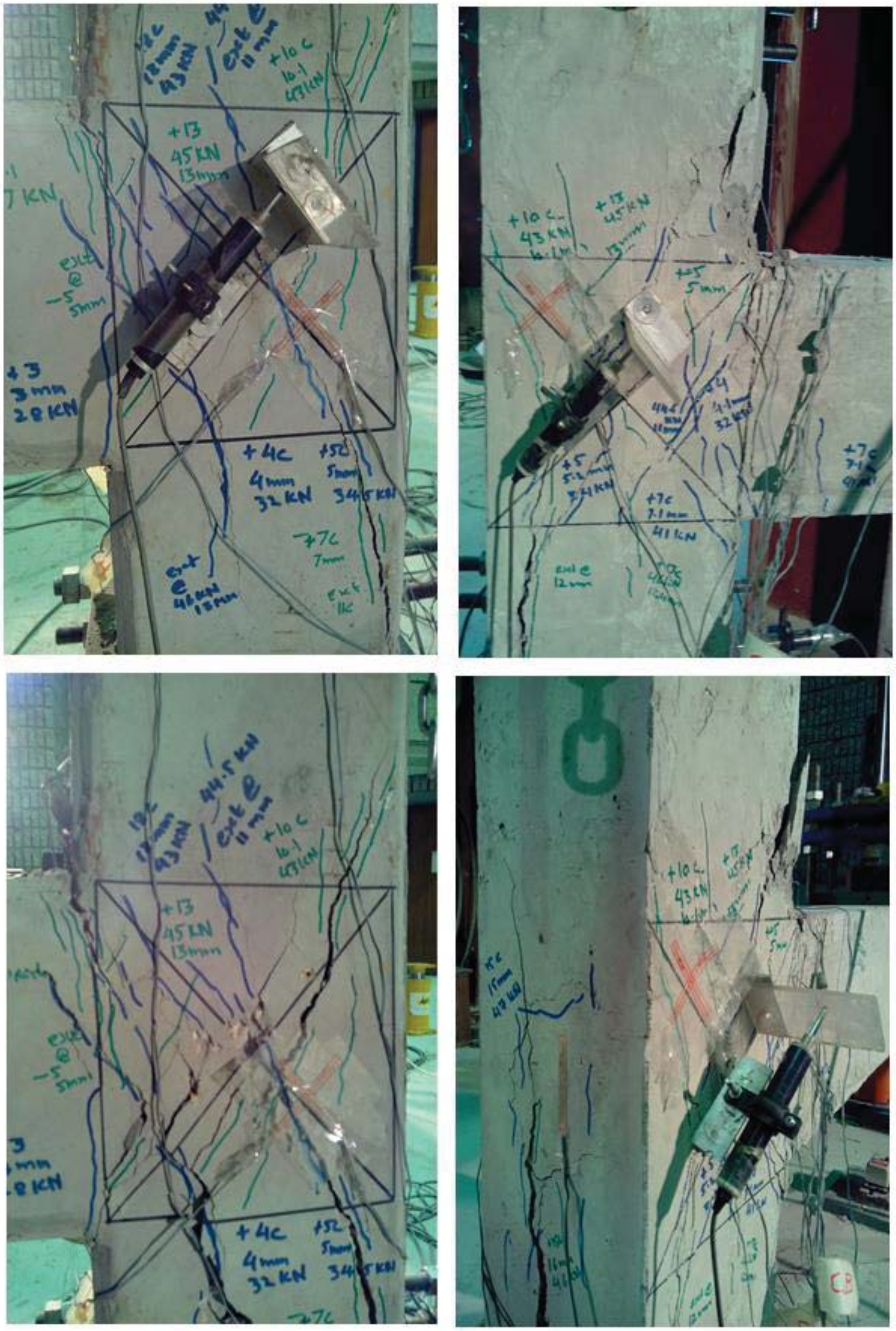

Figure 5-17 Crack pattern at intermediate and final loading stage of specimen SP-5

It can be noticed that pinching effect of hysteresis in this specimen is comparatively less as compared to specimen SP-4 which is because high CAL confined the joint against shear failure and prevent bond-slip behavior to some extend and thus subjected the reinforcement achieve higher strains. The phenomenon of pinching is more pronounced at high displacements due to severe shear damage of joint and bond between concrete and reinforcement.

Figure 5-18 displays the load-displacement envelope curve of SP-5. The maximum load achieved in push and pull was 47.3 kN and 50 kN respectively against 57 kN as obtained in the monotonic counterpart of this specimen. Thus the shear strength obtained is 3.43 MPa and 3.50 MPa in push and pull respectively against 4.23 MPa obtained in specimen SP-3 with monotonic loading due to continuous stiffness degradation in each cycle of loading.

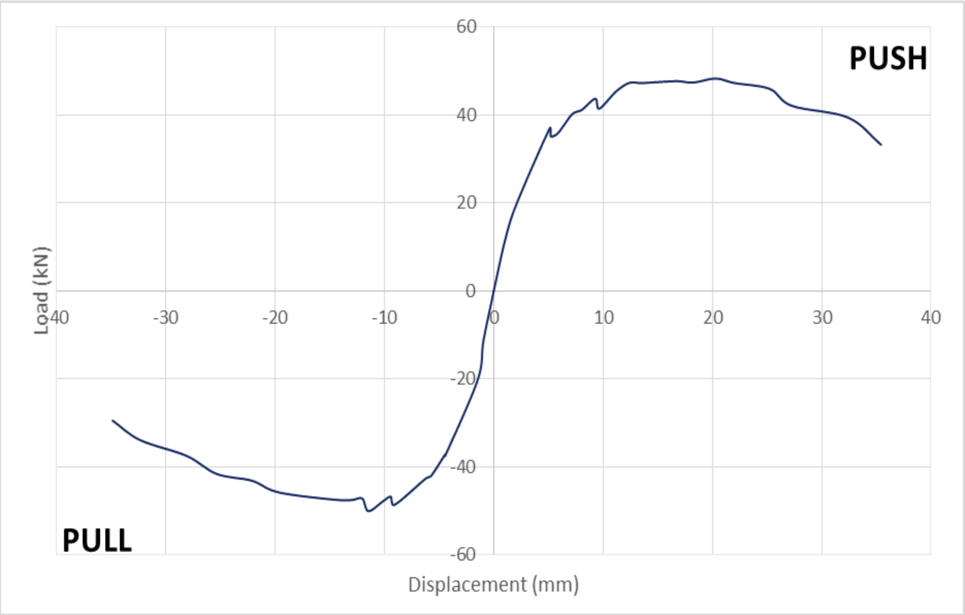

Figure 5-18 Load-displacement envelope curves of test specimen SP-5

Figure 5-19 shows the stiffness degradation curve of specimen SP-5. Stiffness degraded continuously from the first to the last cycle of loading which is calculated as 92 %. In initial stages of loading stiffness degraded more rapidly due to shear cracks in BCJ however in later load cycles degradation is more gradual as large displacements are required for the further propagation and damage to occur.

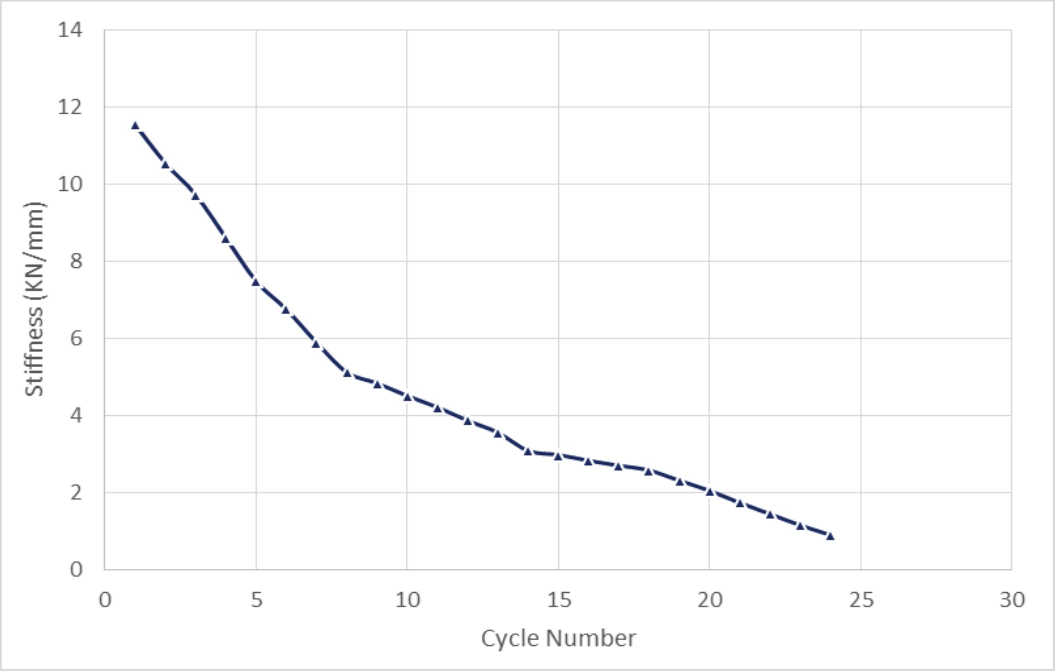

Figure 5-19 Stiffness degradation curve of specimen SP-5

Figure 5-20 shows the cumulative energy dissipation curve of specimen SP-5. Increase in total energy is observed however this increase is not proportional to the applied displacement due to degradation of strength associated with each loading cycle. Thus energy dissipation associated with post-peak loading cycles was considerably higher than that associated with elastic ones.

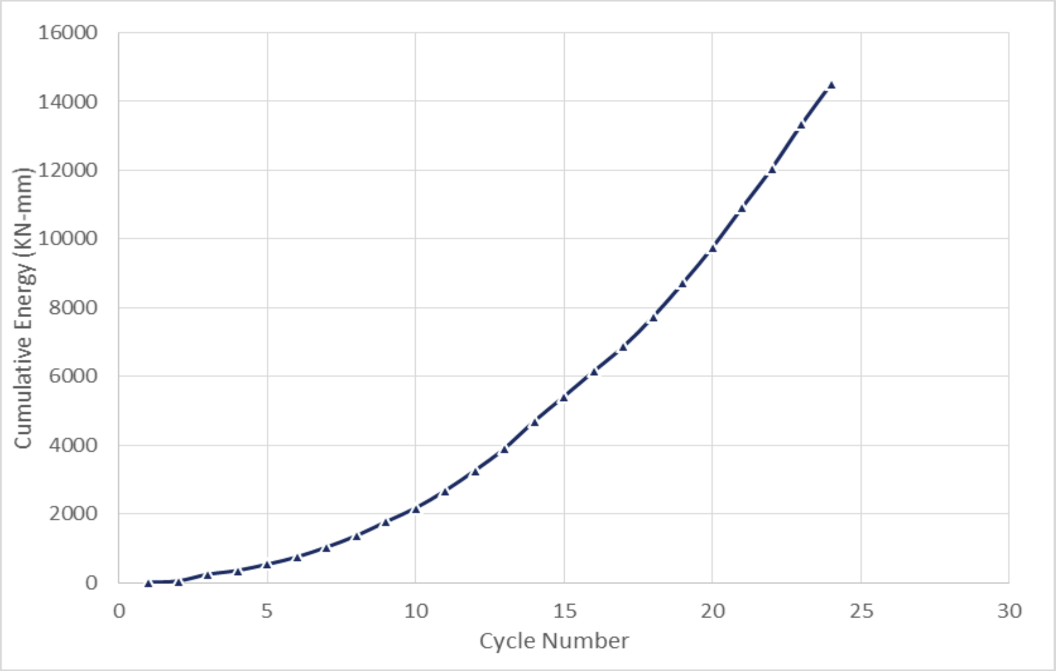

Figure 5-20 Cumulative energy dissipation curve of specimen SP-5

5.3.3. Specimen SP-7

Specimen SP-7 was tested under reverse loading with CAL of 1050 kN (ALR = 0.70 $f'_c A_g$) having a concrete compressive strength of 30 MPa. Figure 5-21 displays the hysteresis response of specimen SP-7 while Figure 5-22 displays the crack pattern and development observed during the test. JF mode was observed in this specimen both in push and pull.

The first diagonal crack seemed in the joint at 51 kN during push and pull corresponded to the eighth positive cycle at a displacement of 7.50 mm. The maximum load in the positive direction reached at 58.9 kN at 9.91 mm giving the shear strength of joint as 4.58 MPa whereas maximum load of 54.0 kN was achieved in the negative direction of loading at displacement of 7.81 mm which corresponded to shear strength of 4.30 MPa.

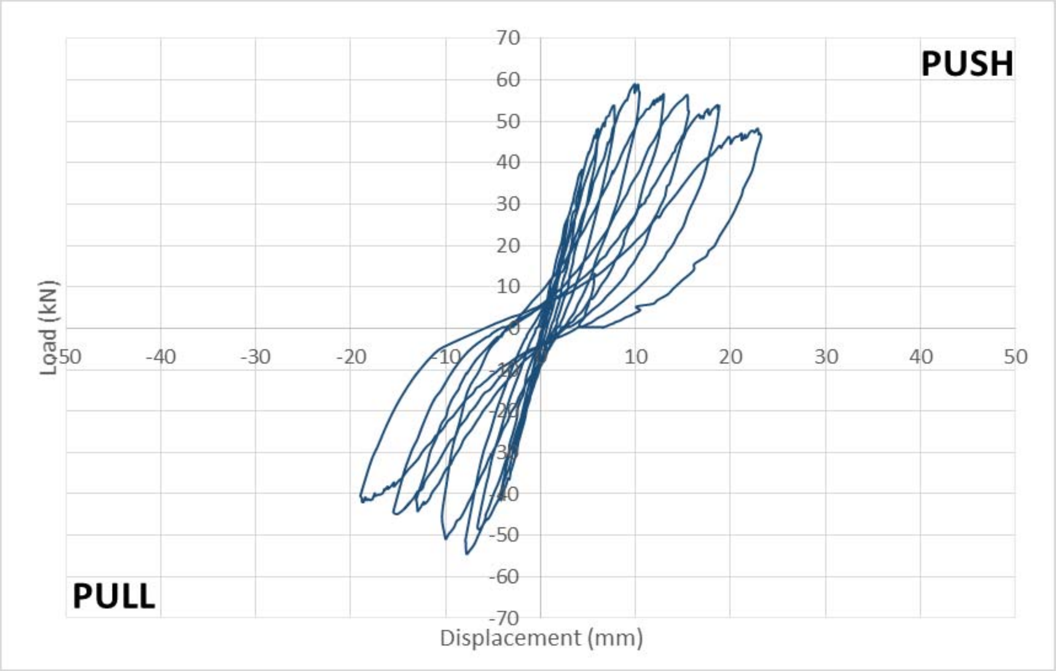

Figure 5-21 Hysteresis curve of specimen SP-7

Figure 5-22 shows propagation of cracks observed throughout the test. Several hair line cracks appeared in the beam in initial loading cycles however the main diagonal shear cracks appeared at the middle of BCJ in both pull and push in eighth cycle and propagated almost vertically towards the column at an angle of around 85°. In ninth cycle of loading cracks became much wider and finally in the tenth cycle of pull joint failed completely.

Although specimen SP-7 failed in joint shear failure mode as reinforcement of both beam and column had not yielded but slight crushing of concrete at the outer edge of joint was also observed at ultimate failure of joint.

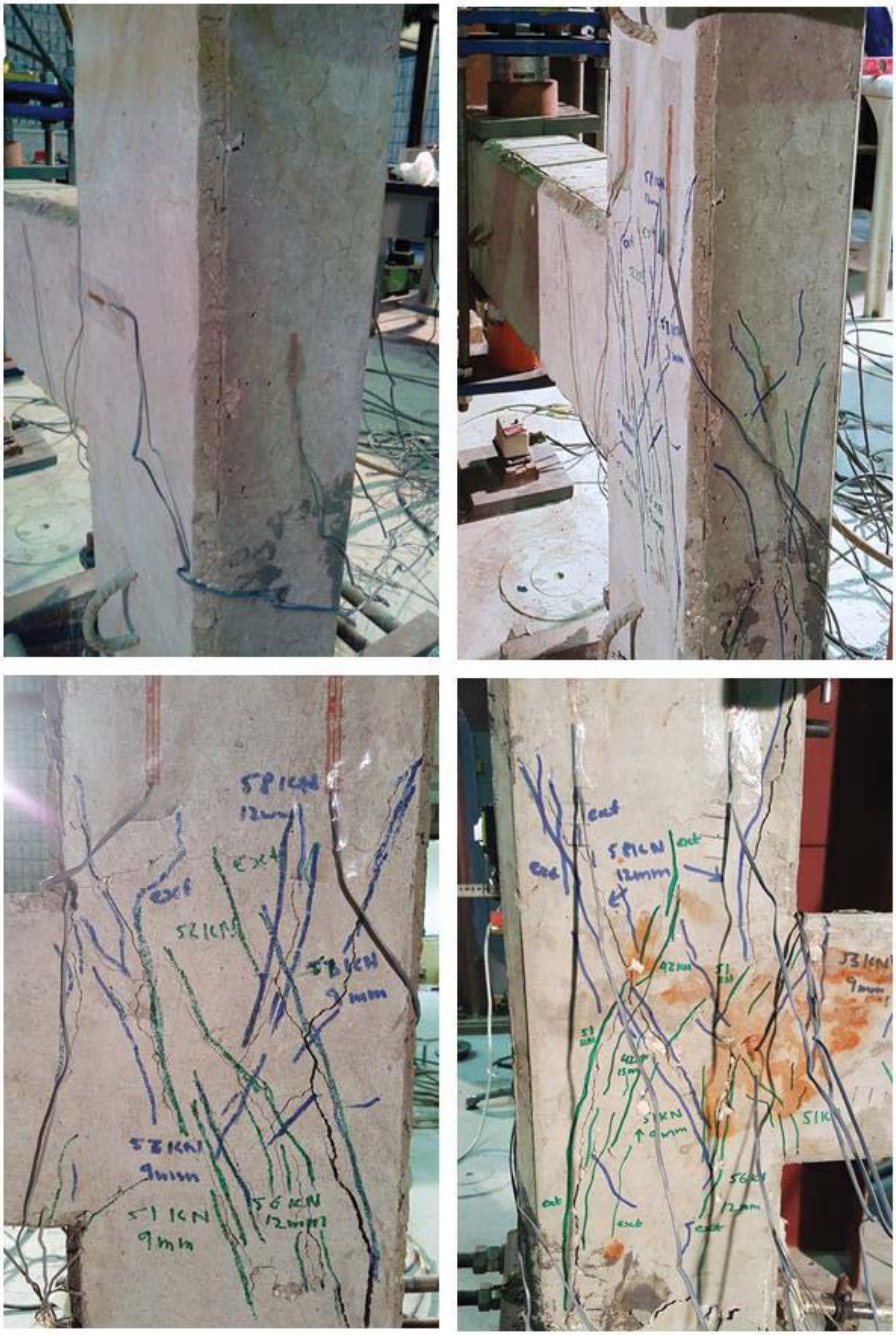

Figure 5-22 Development and propagation of cracks in specimen SP-7

It can be noticed that pinching effect of hysteresis in this specimen is even far less as compared to specimen SP-4 and SP-5 which is due to the fact that very high axial load on this specimen prevent bond-slip failure to considerable extend and subjected the reinforcement to achieve higher strains. This is the reason that excessive fine cracks were observed in beam of specimen SP-7 as compared to the specimen SP-4 and SP-5.

Figure 5-23 displays the load-displacement curve envelope of specimen SP-7. The maximum load achieved in push and pull was 58.9 kN and 54 kN respectively against 66 kN as obtained in the monotonic counterpart of this specimen. Thus the shear strength obtained is 4.58 MPa and 4.30 MPa in push and pull respectively against 5.36 MPa obtained in specimen SP-6 with monotonic loading due to continuous stiffness degradation in each cycle of loading.

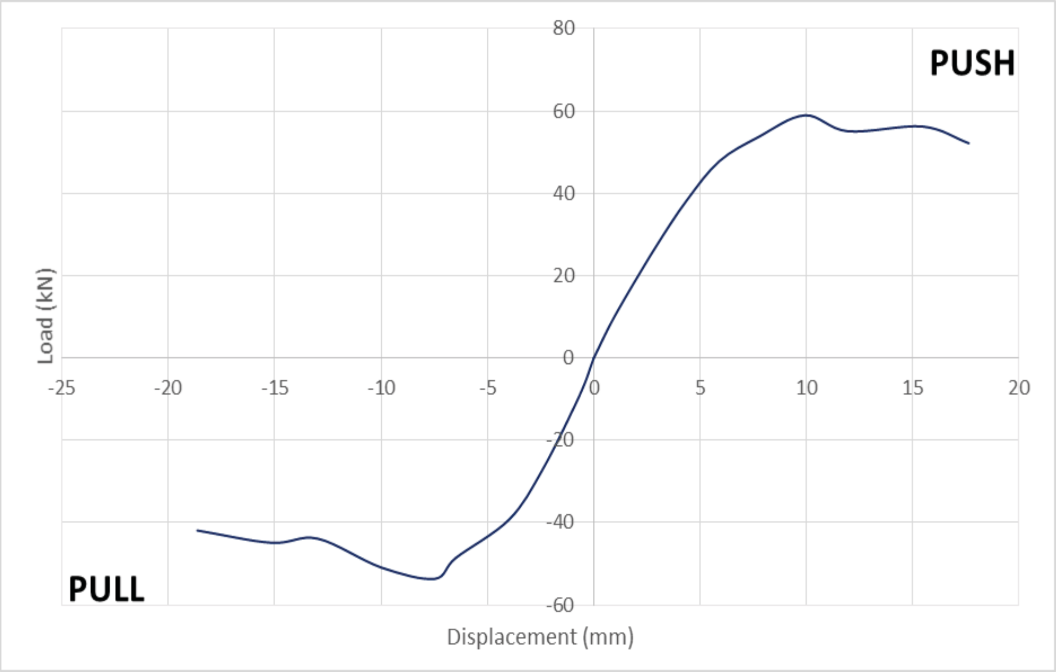

Figure 5-23 Load-displacement envelope curves of test specimen SP-7

Figure 5-24 shows the stiffness degradation curve of specimen SP-7. Stiffness degraded continuously from the first to the last cycle of loading which is calculated as 77 %. Stiffness degraded rapidly due to continuous damage in BCJ due to combined effect of very high CAL and shear forces transferring through beam.

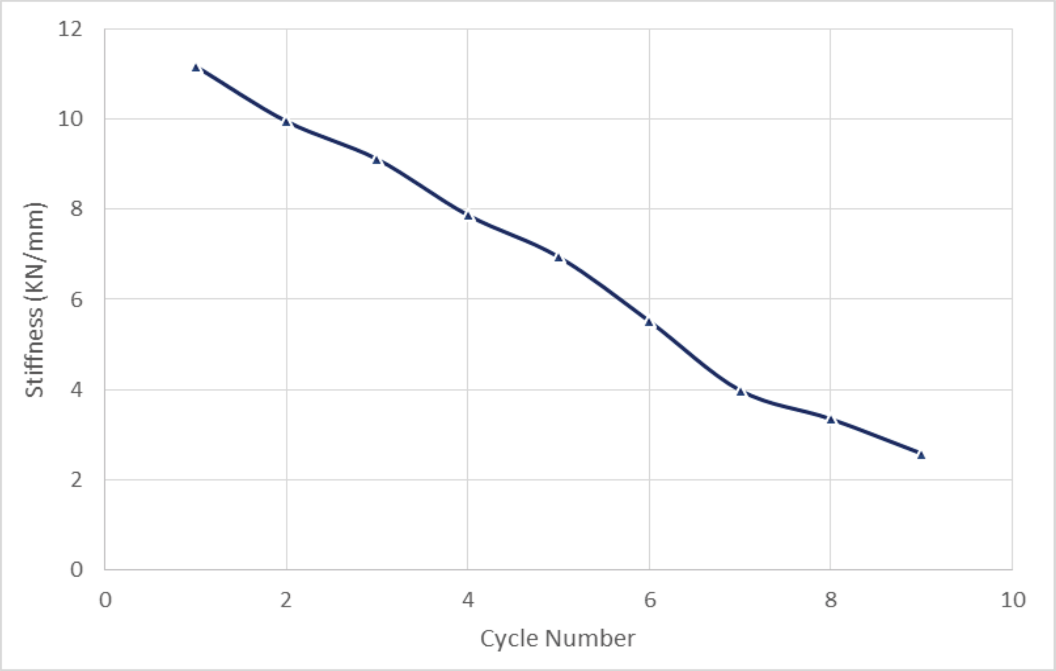

Figure 5-24 Stiffness degradation curve of specimen SP-7

Figure 5-25 shows the cumulative energy dissipation curve of specimen SP-7. Exponential increase in total energy is observed after few cycles of loading due to greater damage caused due to brittle behavior of this specimen caused by high axial load on the column.

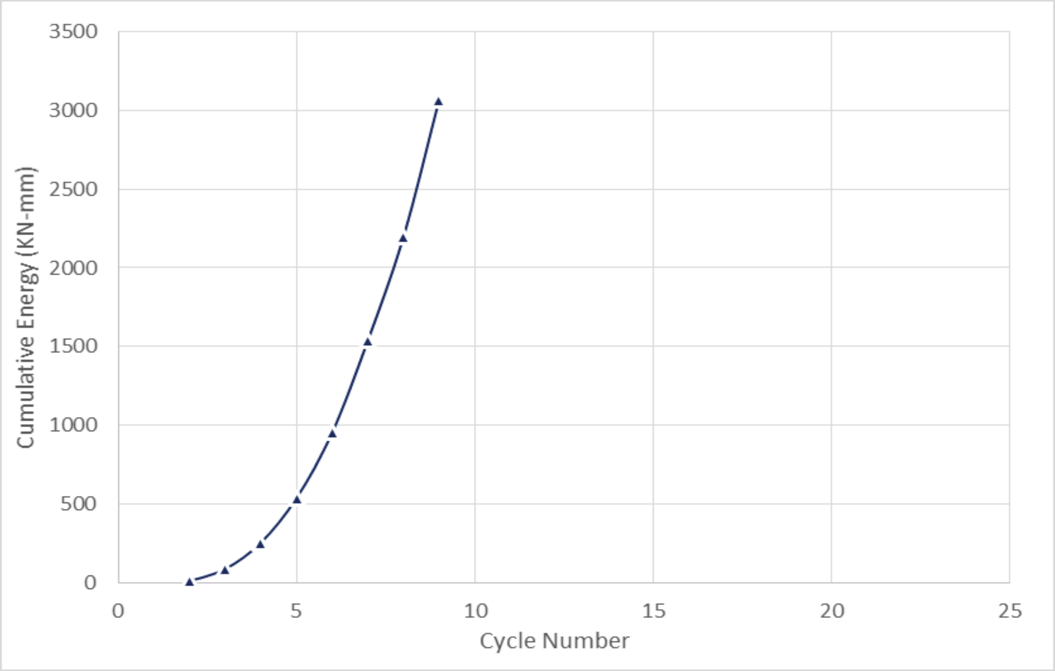

Figure 5-25 Cumulative energy dissipation curve of specimen SP-7

5.4. Effects of Axial Load on Performance Measures of Test Specimens.

5.4.1. Effect on Shear Strength of BCJ

Figure 5-26 shows the load displacement response of experimentally tested BCJs. Specimen SP-1, SP2, SP-3 and SP-6 were tested at ALR of 0.00, 0.19, 0.57 and 0.70 respectively. Continuous increase in failure load is observed with rise of CAL. Increase in failure load is due to two main reason first the higher CAL confines the joint against shear failure. Secondly the high CAL prevent the bond-slip behavior to some extend which enables the beam longitudinal reinforcement to gain higher strains which causes more flexural cracks in beam but increases the joint shear capacity. Another effect of CAL observed is that it delayed the occurrence of first crack at the interface as depicted in Table 5-2.

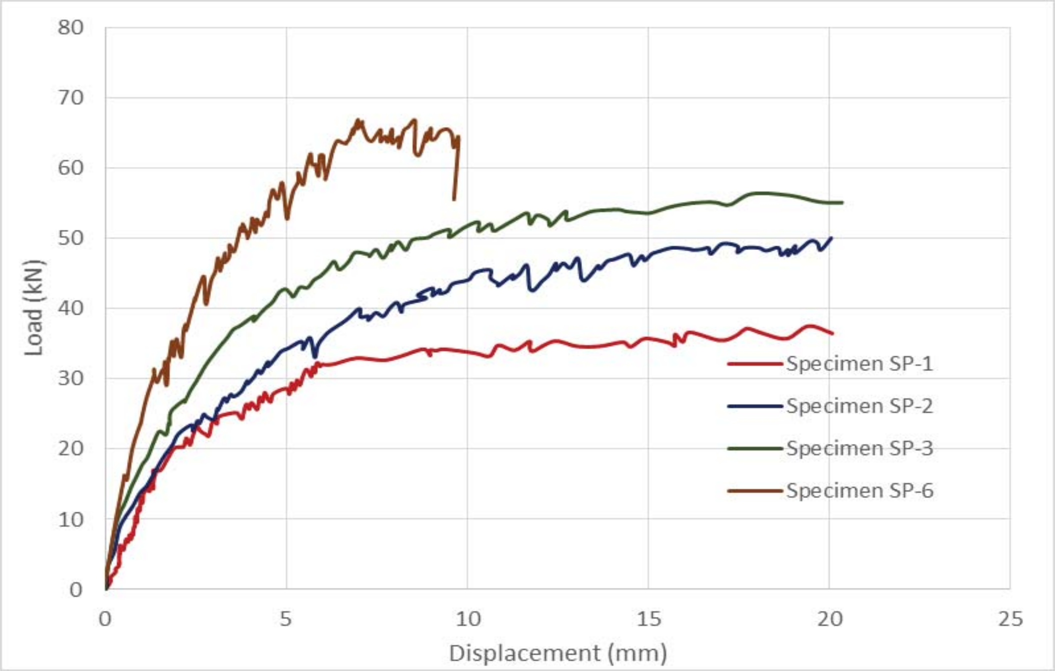

Figure 5-26 Load-displacement response of specimens

Figure 5-27 shows normalized shear strength – ALR interaction curve obtained experimentally.

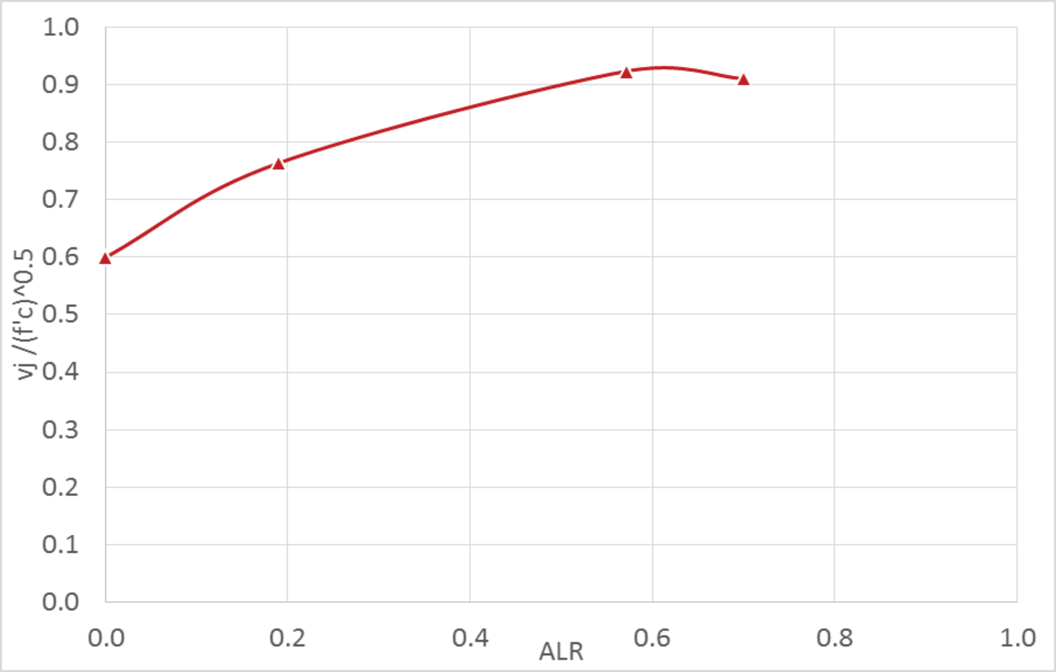

Figure 5-27 Shear strength - axial stress interaction curve of specimens

Figure 5-28 shows the load displacement response of specimen SP-2 and SP-4 which were subjected to monotonic and reverse cyclic loading respectively at an ALR of 0.19. The failure load achieved in case of SP-2 was 51 kN whereas that observed in SP-4 was 40.9 kN and 43 kN in push and pull respectively. The corresponding shear strength achieved in SP-2 was 3.45 MPa while in SP-4 shear strength achieved in push and pull was 2.98 and 3.09 which is 13.6 % and 10.4 % lower due to continuous strength degradation associated with each cycle of loading.

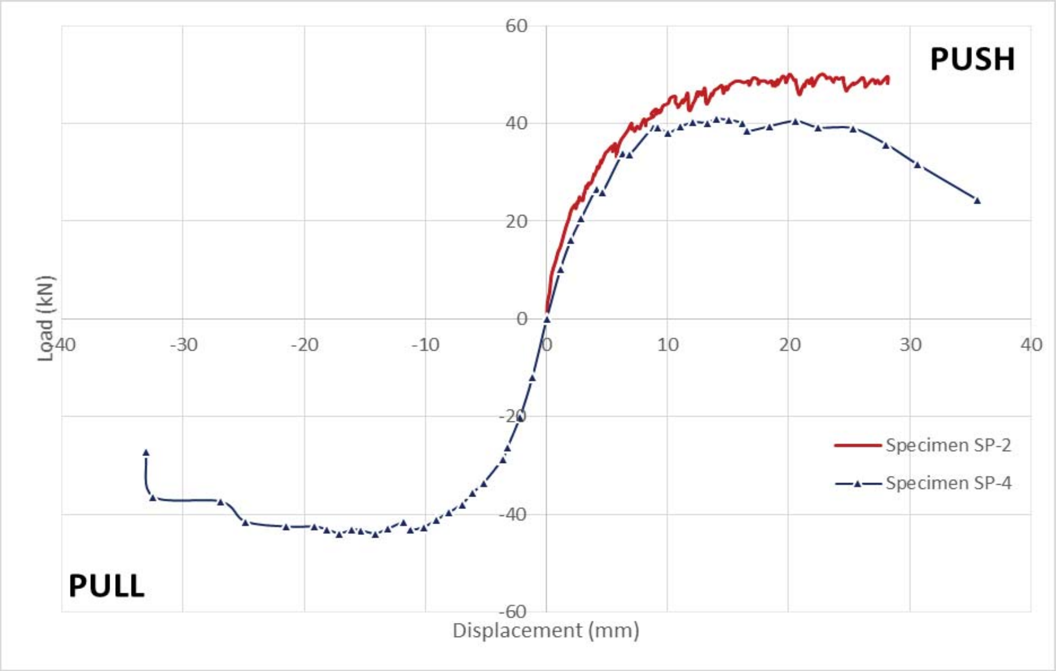

Figure 5-28 Comparison of load-displacement response of specimen SP-2 and SP-4

Load displacement response of specimen SP-3 and SP-5 is shown in Figure 5-29. The failure load achieved in case of SP-3 was 56.87 kN whereas that observed in SP-5 was 47.3 kN and 50 kN in push and pull respectively. The corresponding shear strength achieved in SP-3 was 4.23 MPa while in SP-5 shear strength achieved in push and pull was 3.43 and

3.5 which is 18.9 % and 17.2 % lower due to strength degradation linked with each cycle of loading.

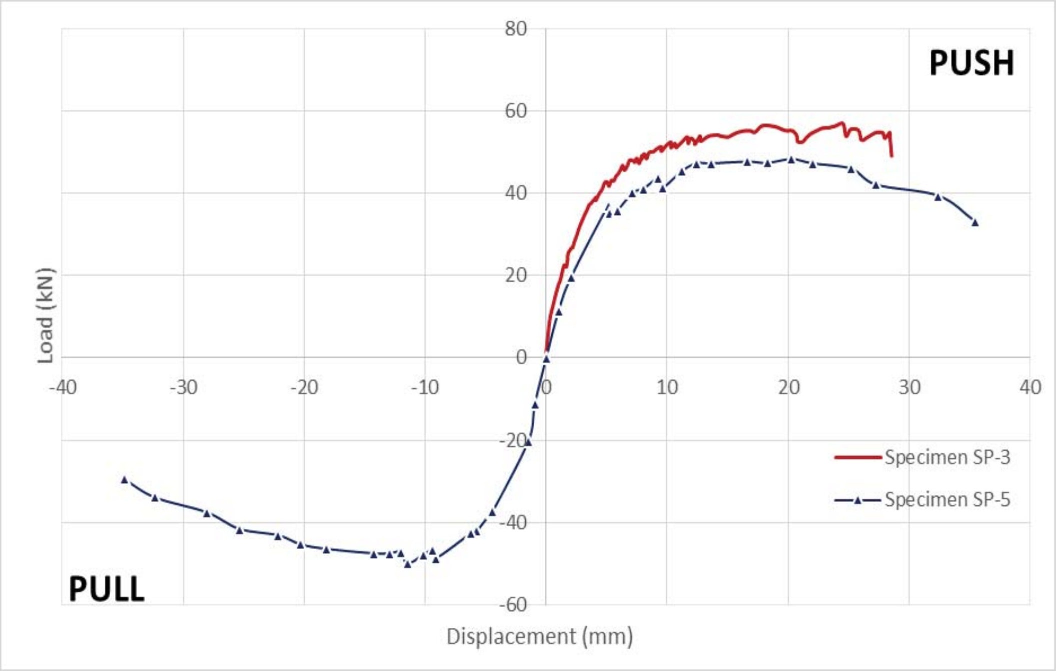

Figure 5-29 Comparison of load-displacement response of specimen SP-3 and SP-5

Figure 5-30 shows the load displacement response of specimen SP-6 and SP-7. The failure load achieved in case of SP-6 was 66.89 kN whereas that observed in SP-7 was 58.9 kN and 54 kN in push and pull respectively. The corresponding shear strength achieved in SP-6 was 5.20 MPa while in SP-7 shear strength achieved in push and pull was 4.58 and 3.97 which is 14.5 % and 25.9 % lower due to continuous strength degradation associated with each cycle of loading.

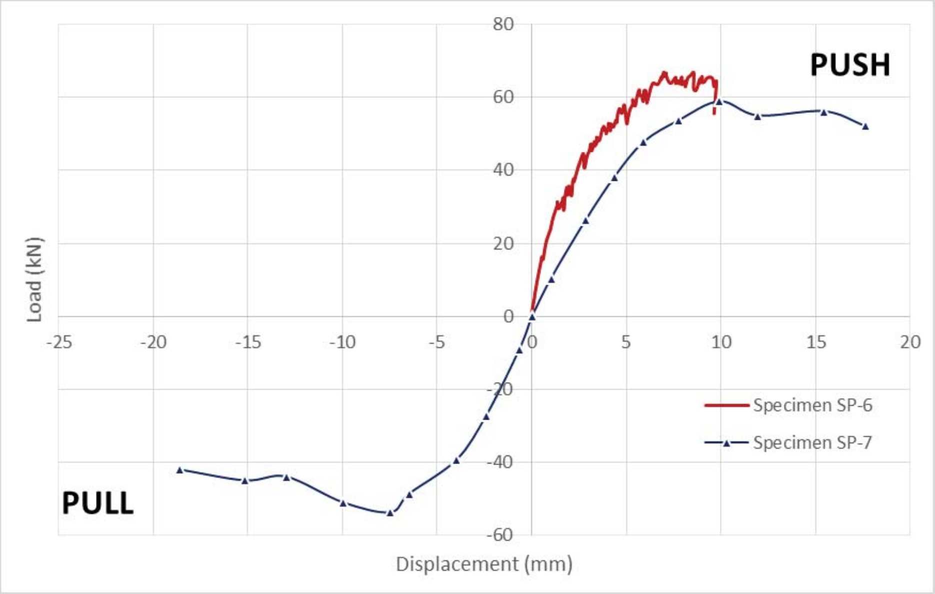

Figure 5-30 Comparison of load-displacement response of specimen SP-6 and SP-7

Figure 5-31 shows normalized shear strength – ALR interaction curves of BCJs exposed to monotonic and reverse cyclic loading. In both the cases enhancement in shear strength of BCJs is observed with increase in ALR. However shear strength of joints subjected to reverse cyclic loading is on average 14 % less as compared to their monotonic counterparts.

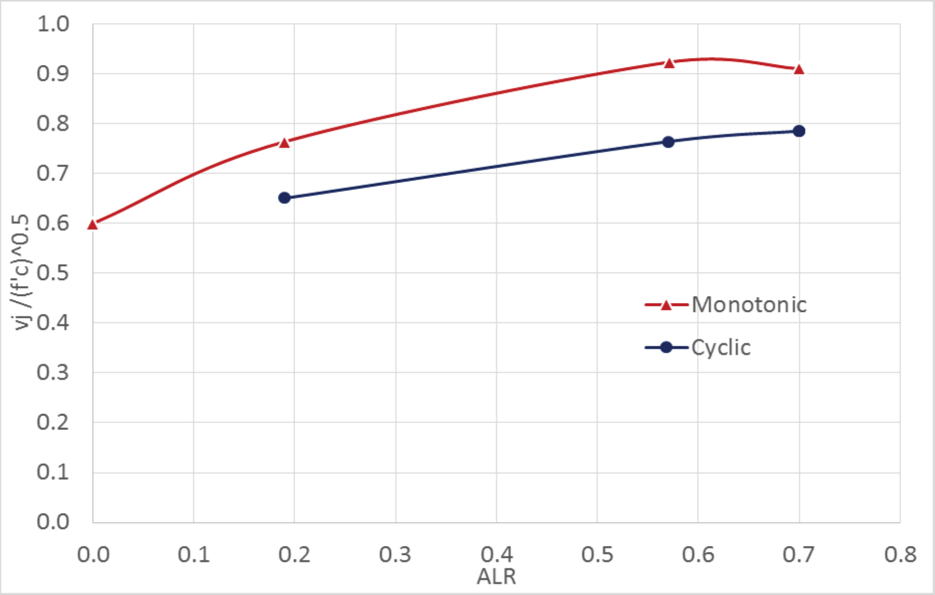

Figure 5-31 Normalized shear strength-ALR interaction curves

5.4.2. Effect on Stiffness Degradation

Figure 5-32 depicts the stiffness degradation curves of specimen SP-4, SP-5 and SP-7. Experimental results dictated that many factors such as shear and flexural cracking, reinforcement slippage and loss of cover effects the stiffness degradation of joint. As depicted in the Figure 5-32 specimen SP-5 has high initial stiffness as compared to the specimen SP-4 owing to high ALR. Although specimen SP-5 maintained its stiffness higher than specimen SP-4 up to the failure load corresponded to the fourteenth cycle of loading but rate of stiffness degradation is found to be more in SP-5. Both specimens showed similar stiffness degradation trend in post peak stage of loading. Specimen SP-7 showed high initial stiffness but the rate of stiffness degradation is highest due to more deterioration caused by local crushing and bond damage especially after shear failure of joint during pull in eighth cycle of loading. Specimen SP-7 showed highly brittle behavior owing to very high axial load as compared to other specimens.

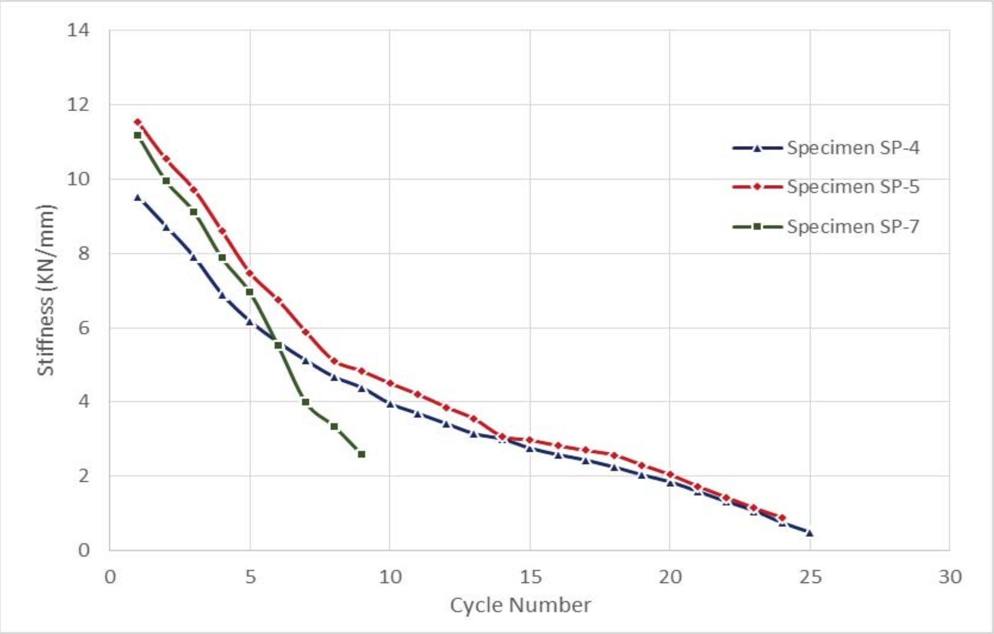

Figure 5-32 Stiffness degradation curves of Specimen SP-4, SP-5 and SP-7

5.4.3. Effect on Energy Dissipation Capacity

Figure 5-33 shows the cumulative energy dissipation curves of specimens SP-4, SP-5 and SP-7. It is observed that SP-4 with higher ALR that is 0.57 showed improved energy dissipation capacity than the specimen with lower ALR that is SP-4 with ALR of 0.19. Similarly, specimen SP-7 showed better energy dissipation capacity initially but after few cycles of loading due to very high ALR that is 0.70 specimen failed without achieving reasonable deformability. Improvement in energy dissipation capacity due to high axial load is due to confinement provided by axial load against joint shear and improved bond-slip behavior of longitudinal reinforcement. However, the same is not true for very high ALR where joint experience local crushing or complete axial failure in such cases high ALR damage the joint in crushing and thus causes severe detrimental effects on shear strength as will be discussed in subsequent chapters.

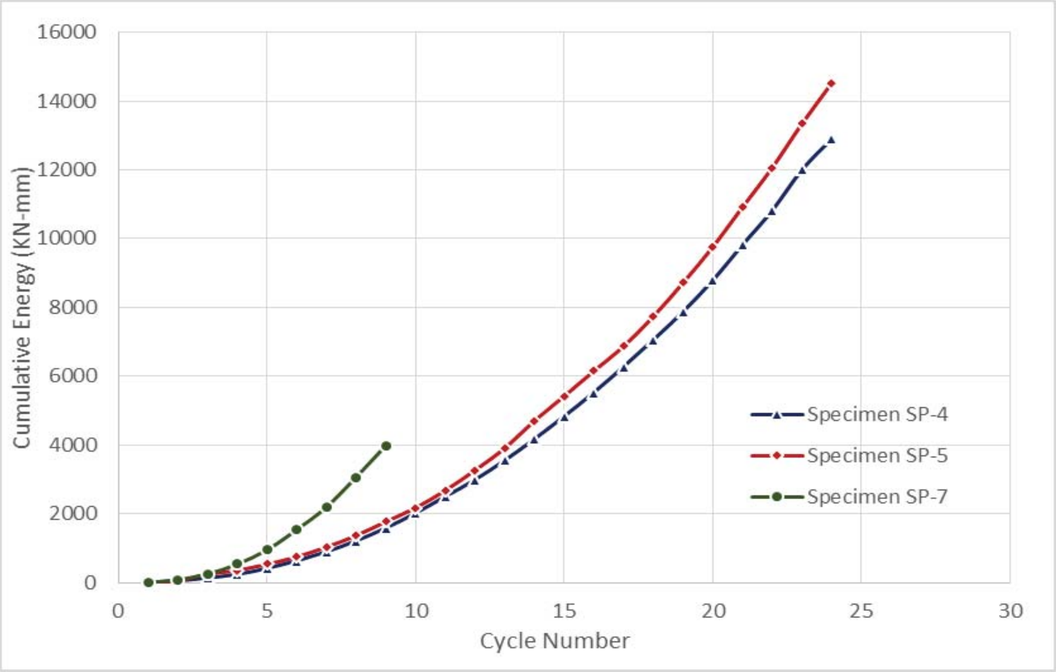

Figure 5-33 Energy dissipation capacity curves of specimen SP-4, SP-5 and SP-7

Table 5-1 tabulates the results of all experimentally tested specimens.

Table 5-1 Experimental results summary

Specimen ID	Loading	σ_N (f'c %)	σ_N (MPa)	P (kN)	T (kN)	$V_{u(col)}$ (kN)	$V_{j(Joint)}$ (kN)	$v_{j(Joint)}$ (MPa)
SP-1	M	0.00	0	37	166	28	137	2.74
SP-2	M	0.19	4	51	212	37	174	3.50
SP-3	M	0.57	12	57	254	43	211	4.23
SP-6	M	0.70	21	66	310	49	260	5.20
SP-4	RC	0.19	4	41/43	182/187	31/32	152/155	2.98/3.09
SP-5	RC	0.57	12	47/50	207/210	35/37	171/172	3.43/3.50
SP-7	RC	0.70	21	59/54	273/255	44/40	228/215	4.58/4.30

Note:

M = Monotonic

RC = Reverse cyclic

Table 5-2 tabulates the summary of cracking loads and joint failure modes of all experimentally tested specimens.

Table 5-2 Summary of cracking loads and failure mode of test specimens

Specimen ID	σ_N (f'c %)	ICL (kN)	JCL (kN)	Joint Failure Mode
SP-1	0.00	16	16	JF
SP-2	0.19	29	29	JF
SP-3	0.57	38	38	JF
SP-6	0.70	45	45	JF
SP-4	0.19	20	21	JF
SP-5	0.57	27	36	JF
SP-7	0.70	51	51	JF

Note:

ICL = Beam-joint interface cracking load

JCL = Joint cracking load

CHAPTER 6

NUMERICAL MODELLING OF BCJS

6.1. Introduction

This chapter presents the numerical modeling of BCJs. First an FE model is presented in which models to simulate cracking in concrete are discussed and appropriate model is adopted which takes in to an account the numerical computational difficulties, convergence and solution degradation problems associated with other concrete models. Modelling of concrete, reinforcing steel and their bond behavior is then discussed. Commercially available non-linear FE software ABAQUS is used to validate the developed FE model with experimental results presented in the previous chapter. Finally, calibrated finite element model is used to extend the research work for different concrete strengths in order to gain further in depth knowledge of effect of different magnitude of axial load on performance of BCJs.

6.2. Finite Element Model

FE model presented below delineates the modelling to simulate concrete followed by modelling of reinforcing steel and its bond behavior with concrete. Dynamic explicit approach is adopted to overcome convergence problems associated with cracking of concrete.

6.2.1. Models to Simulate Damage in Concrete

To simulate quasi-brittle nature of reinforced concrete various conceptual models are available in literature which includes discrete crack model, smeared crack model, inner softening band. Numerical modelling of concrete cracking is mostly carried out using discrete crack model and smeared crack model like by Chen GM [39]. In discrete crack model, opening which arises due to cracks are physically modelled and taken as a geometrical identity. Since cracks are defined along the surfaces of the elements, it creates mesh bias. A lot of researches attempts to resolve this issue by developing finite element codes capable of generating remeshing like Yang ZJ [40]–[42] but the computational difficulties associated with remeshing is still a great challenge as found by De Borst et al. [32]. While in the case of smeared crack model phenomenon known as "strain localization" leads to zero energy utilization during crack opening when element size approaches zero, this results in a non-mesh objective case that causes solution not to converge or to degrade.

In this research, damage plasticity model has been utilized for concrete which is a constitutive model available in non-linear finite element software ABAQUS. In damage plasticity model, compression and tension are two hardening variables that control development of yield surface. A continuum damage mechanics is used to model the damage by stiffness degradation approach which essentially means that elasticity is degraded in the concrete where it cracks.

6.2.2. Modelling of Concrete

To model a concrete material in ABAQUS "concrete damaged plasticity" is used which requires the following material functions:

1. Uniaxial stress-strain relation of concrete under compressive and tensile loading.
2. Damage parameters dc and dt for compressive and tensile load respectively.

Model Code of fib for Concrete Structures [43] has been adopted as this model has advanced parameters to control ascending as well as post-peak behavior of stress-strain curve for concrete. The compressive stress-strain relationship is as follow:

$$\frac{\sigma_c}{f_{cm}} = -\left(\frac{k\,.\,\eta-\eta^2}{1+(k-2)\,.\eta}\right) \tag{6.1}$$

where:

$$\eta = \in_c/\in_{c1}\,; \tag{6.2}$$

$$k = E_{ci}/E_{c1}\,; \tag{6.3}$$

f_{cm} is the concrete compressive strength; $\in_c$ is the concrete compressive strain; $\in_{c1}$ is the strain at maximum compressive stress; E_{ci} is the modulus of elasticity at 28 days; E_{c1} is the secant modulus and k is the plasticity number

Figure 6-1 shows the stress-strain relationship with related parameters.

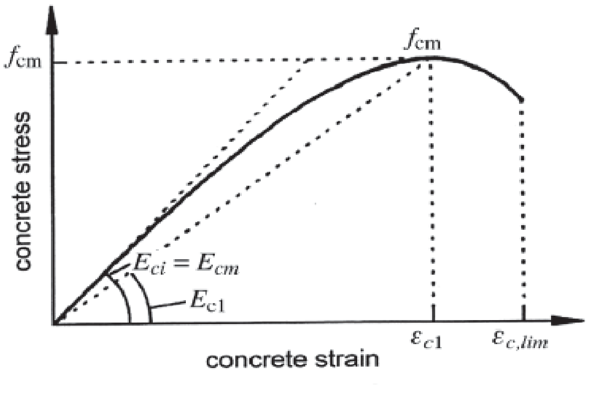

Figure 6-1 Compressive stress-strain relationship for concrete modelling [43]

Following bilinear stress strain relationship is used for tensile behavior of concrete:

$$\sigma_{ct} = E_{ci} \in_{ct} \quad for\ \sigma_{ct} \le 0.9\, f_{ctm} \tag{6.4}$$

$$\frac{\sigma_{ct}}{f_{ctm}} = \left(1 - 0.1\frac{0.00015 - \in_{ct}}{0.00015 - 0.9\, f_{ctm}/E_{ci}}\right) for\ 0.9\, f_{ctm} \le \sigma_{ct} \le f_{ctm} \tag{6.5}$$

where $\in_{ct}$ is the tensile strain; σ_{ct} is the tensile strain and f_{ctm} is the tensile strength

Figure 6-2 shows the tensile stress-strain relationship with related parameters.

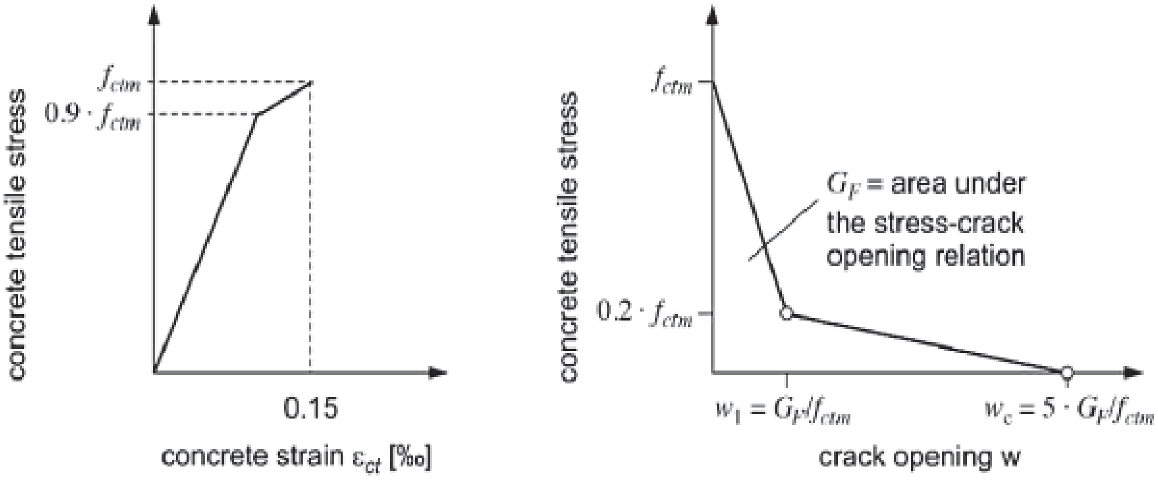

Figure 6-2 Stress-strain and stress-crack opening relation for concrete in tension [43]

Concrete compression damage parameters that is used in model are given as [44]:

$$d_c = 1 - \frac{\sigma_c E_c^{-1}}{\epsilon_c^{pl}\left(\frac{1}{b_c} - 1\right) + \sigma_c E_c^{-1}} \tag{6.6}$$

where:

d_c = Concrete tension damage parameter; σ_c = Compressive Stress; E_c = Modulus of elasticity of concrete; ϵ_c^{pl} = Plastic strain corresponding to compressive strength; b_c = Constant ranges $0 < b_c < 1$

Figure 6-3 shows the physical interpretation of compression damage parameter in defining stiffness after damage in non-linear part of stress-strain curve of concrete in uniaxial compression.

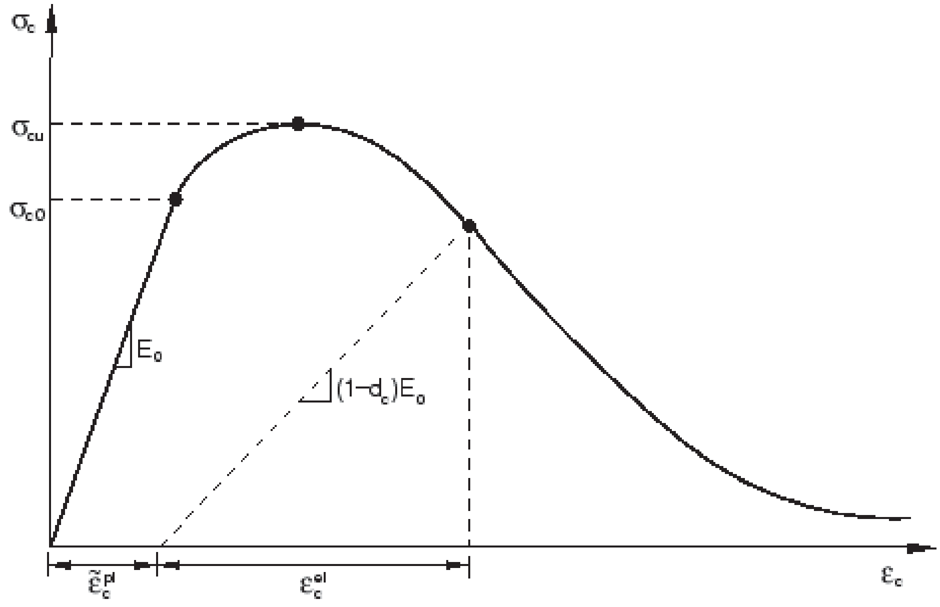

Figure 6-3 Damage parameter for uniaxial compression [45]

Whereas concrete tension damage parameter that is used in model is given as [44]:

$$d_t = 1 - \frac{\sigma_t E_c^{-1}}{\epsilon_t^{pl}\left(\frac{1}{b_t} - 1\right) + \sigma_t E_c^{-1}} \tag{6.7}$$

where:

d_t = Concrete tension damage parameter; σ_t = Tensile Stress; E_c = Modulus of elasticity of concrete; ϵ_t^{pl} = Plastic strain corresponding to tensile strength; b_t = Constant ranges $0 < b_t < 1$

Figure 6-4 shows the physical interpretation of tension damage parameter in defining stiffness after damage in softening part of stress-strain curve of concrete in uniaxial tension.

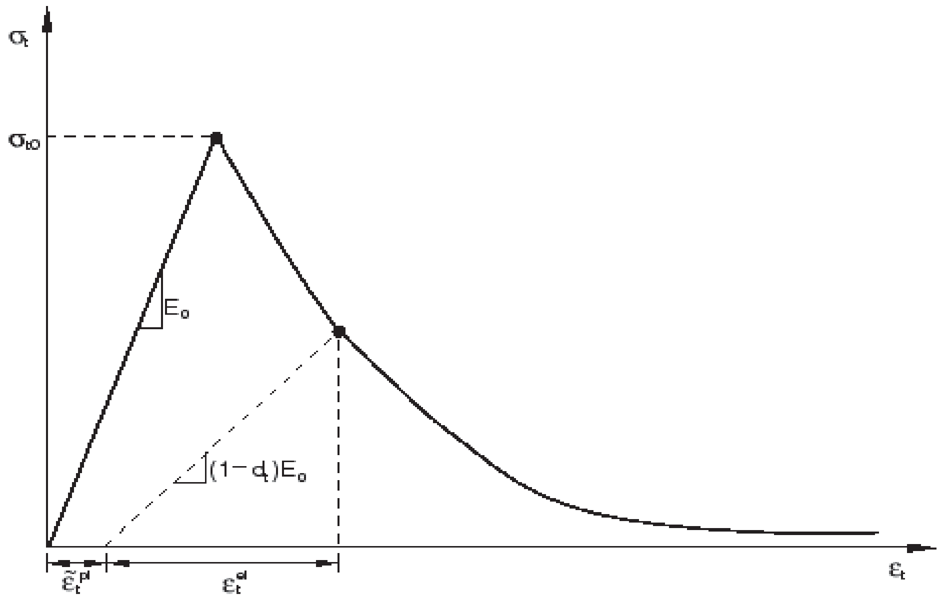

Figure 6-4 Damage parameter for uniaxial tension [45]

The concrete parameters used in the plastic damage model are shown in the Table 6-1.

Table 6-1 Concrete parameters used in the plastic damage model

Concrete Strength (MPa)	Mass Density (tonne/mm3)	E (MPa)	Poisson’s Ratio	Dilation Angle ψ (Degrees)	Eccentricity ϵ	f_{bo}/f_{co}	b_c/b_t
Varies	2.4E-009	Varies	0.19/0.20	36	0.1	1.16	0.7/0.85

6.2.3. Modelling of Reinforcing Steel and its Bond with Concrete

Reinforcing steel has been modelled using truss element in ABAQUS. The stress-strain curve adopted for steel is shown in Figure 4-17 and Figure 4-18. The other parameters used to define reinforcing steel is shown in Table 6-2.

Table 6-2 Parameters used to define reinforcing steel

Elastic Modulus (MPa)	193600 / 195161
Poisson's ratio	0.3
Mass Density (tonne/mm3)	7.85E-009
Yield Stress (MPa)	580/605

Steel reinforcement is bonded with concrete as an embedded element in ABAQUS. Embedment technique successfully used by many researchers is a very powerful finite element tool which allows number of elements to be embedded inside another element known as host element. One of the significant utilization of embedment technique is that modelling of interaction surface between the embedded and the host element is not required which eradicates numerically costly iterations linked with surface formulations.

6.3. Validation of FE Model

The proposed FE model described above has been validated with experimental results presented in chapter 5. A comparison of experimental results and finite element model prediction is presented next to validate the competency of FEM to envisage the failure load, mode of failure and overall behavior of BCJs.

6.3.1. Specimen SP-1

Load displacement response predicted by FEM for specimen SP-1 is shown in Figure 6-5 along with experimentally obtained curve. Maximum load at beam predicted by FEM is 36.11 kN at displacement of 18.34 mm against experimental value of 37.55 kN at displacement of 19.44 mm. Overall FEM prediction of load displacement response is in perfect match with that of experiment.

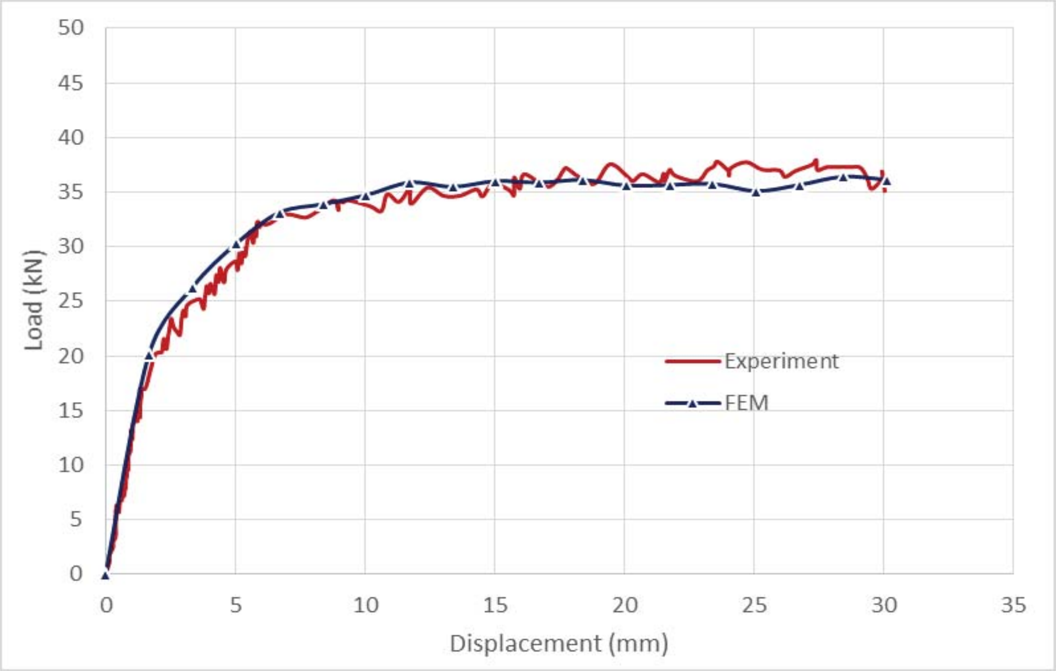

Figure 6-5 Load vs. displacement response of specimen SP-1

The predicted failure mode of specimen SP-1 is joint failure mode as expected from the results of experiment. The crack pattern of the experiment and FE prediction is also well matched as shown in Figure 6-6.

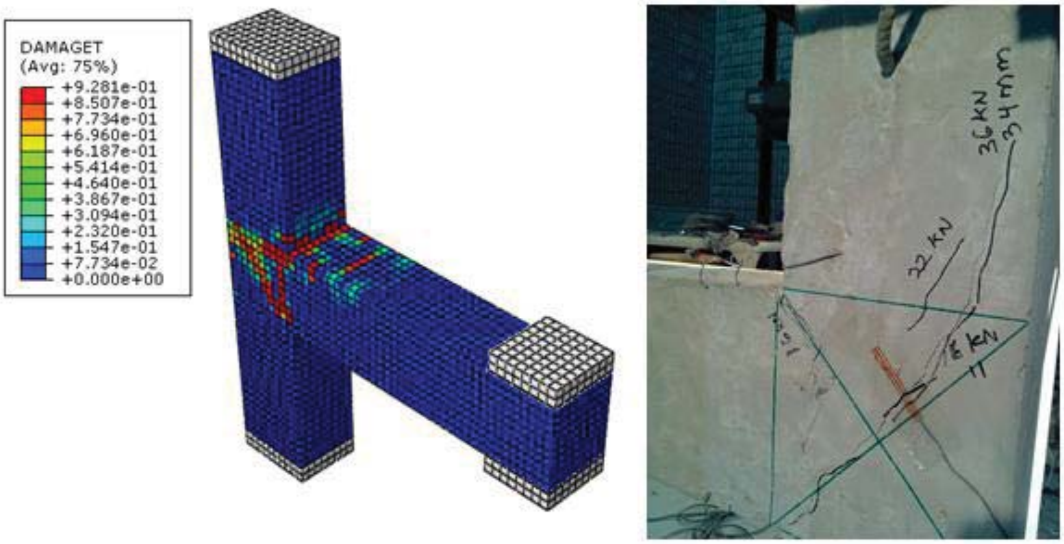

Figure 6-6 FEM and experimental crack pattern of specimen SP-1

Figure 6-7 shows the steel stresses at failure load of specimen SP-1. The maximum stress obtained is 145 MPa which is far less than the yield stress of reinforcement.

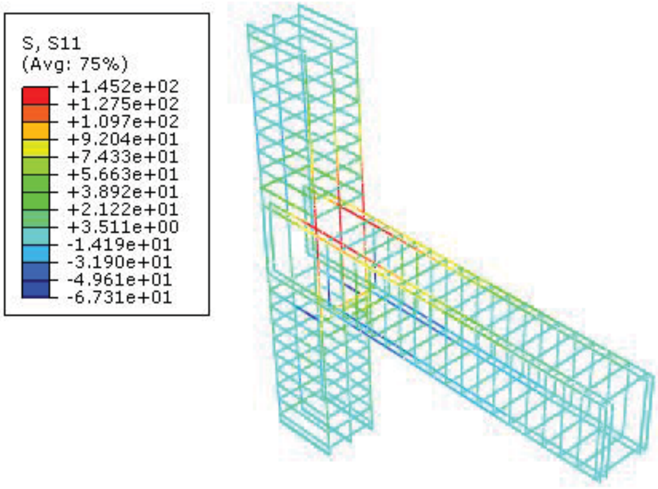

Figure 6-7 Steel stresses at failure load of specimen SP-1

Figure 6-8 shows the steel strains at failure load of specimen SP-1. The average maximum strain in beam's top longitudinal bars is obtained as 0.000687 mm/mm which is in good agreement with the experimental value of 0.00066 mm/mm. The shear stress calculated with FEM results is 2.77 MPa against 2.74 MPa as obtained experimentally.

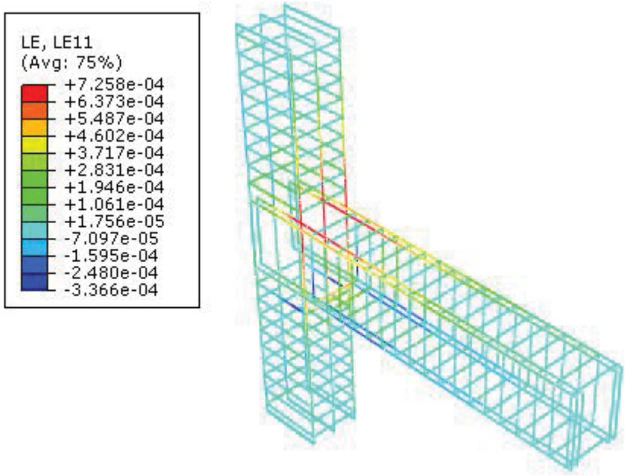

Figure 6-8 Steel strains at failure load of specimen SP-1

6.3.2. Specimen SP-2

Figure 6-9 displays the load-displacement response of specimen SP-2 obtained experimentally and as predicted by FEM. Failure load predicted by FEM is 50.13 kN corresponding to displacement of 16.75 mm against experimental value of 50.08 kN at 19.48 mm. In general, the load displacement curve predicted by FEM is in good agreement with that of experiment.

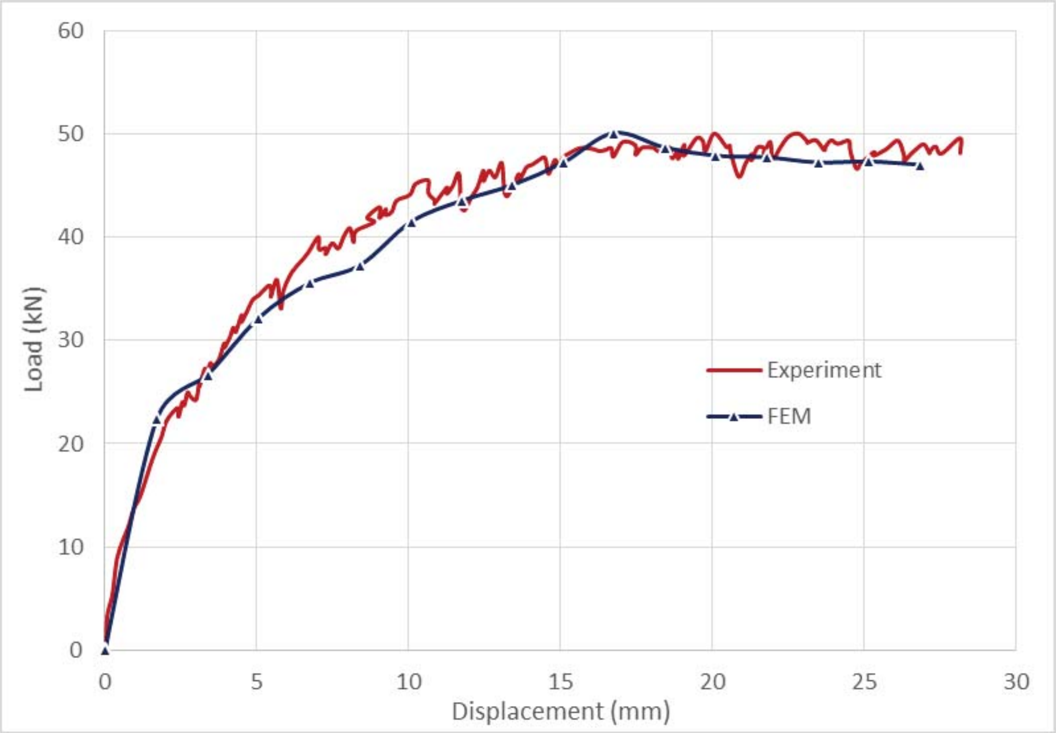

Figure 6-9 Load vs. displacement response of specimen SP-2

The predicted failure mode of SP-2 is joint failure mode as expected from the experimental results. The crack pattern of the experiment and FE prediction is also well matched as shown in Figure 6-10.

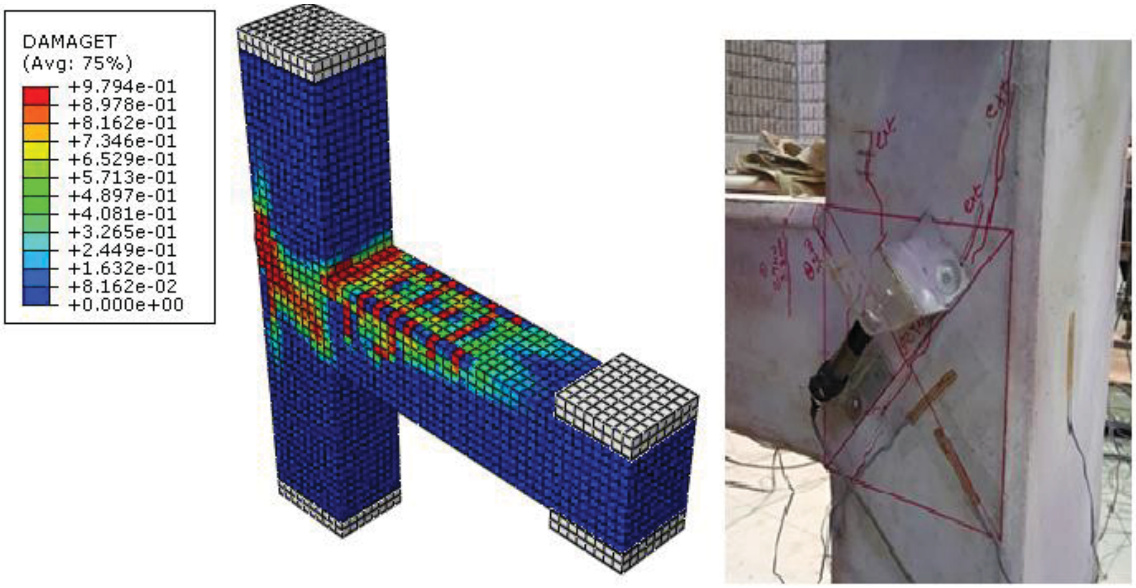

Figure 6-10 FEM and experimental crack pattern of specimen SP-2

Figure 6-11 shows the steel stresses at failure load of specimen SP-2. The maximum stress obtained in beam longitudinal reinforcement is 186 MPa which is much less than the yield stress of reinforcement.

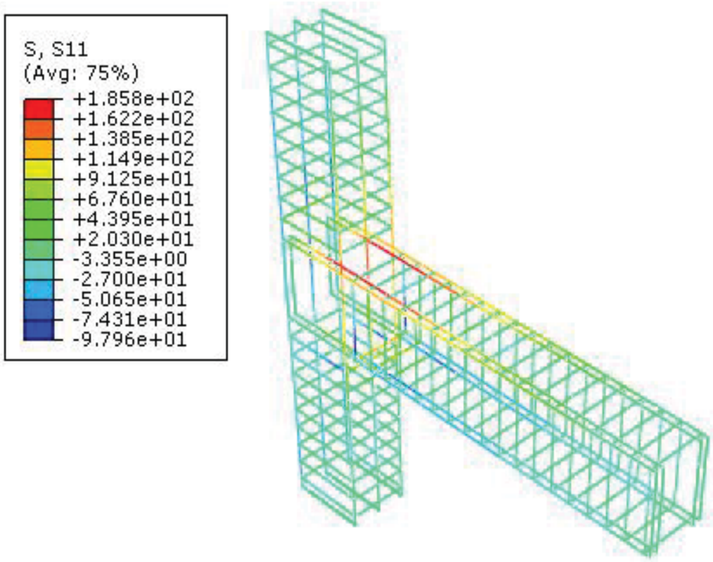

Figure 6-11 Steel stresses at failure load of specimen SP-2

Figure 6-12 shows the steel strains at failure load of specimen SP-2. The average maximum strain in beam's top bars is obtained as 0.00096 mm/mm against experimental value of 0.00088 mm/mm. The shear stress calculated with FEM results is 3.71 MPa against 3.45 MPa as obtained experimentally.

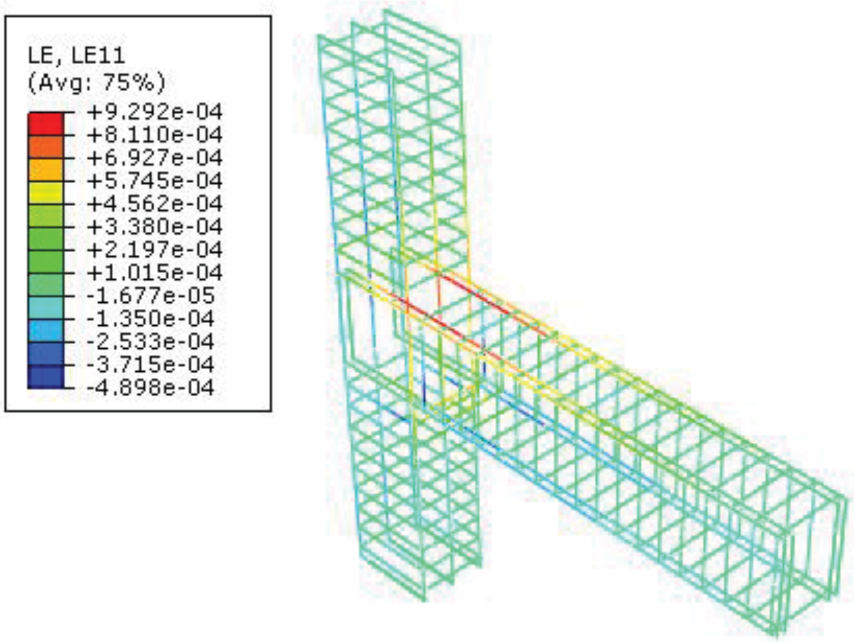

Figure 6-12 Steel strains at failure load of specimen SP-2

6.3.3. Specimen SP-3

Figure 6-13 shows the load-displacement response of SP-3 obtained experimentally and as predicted by FEM. Failure load predicted by FEM is 58.78 kN at 18.23 mm against experimental value of 56.87 kN at a displacement of 17.86 mm. In general, the load displacement curve predicted by FEM is in good agreement with that of experiment.

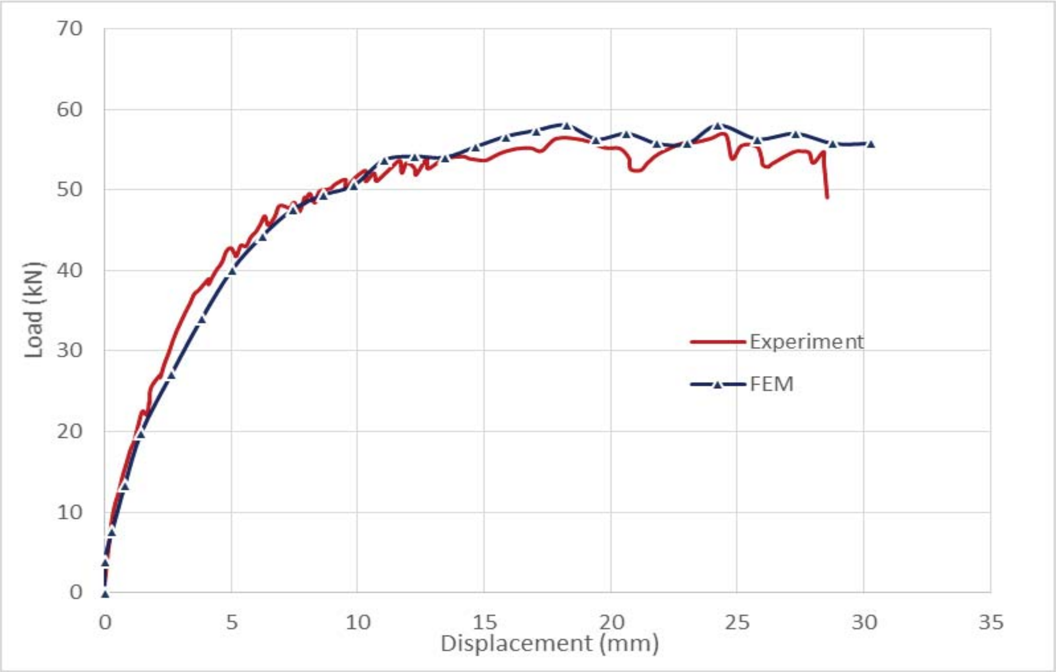

Figure 6-13 Load vs. displacement response of specimen SP-3

The predicted failure mode of specimen SP-3 is joint failure mode as expected from the experimental results. The crack pattern of the experiment and FE prediction is shown in Figure 6-14 where cracks are at more inclination than the previous two case.

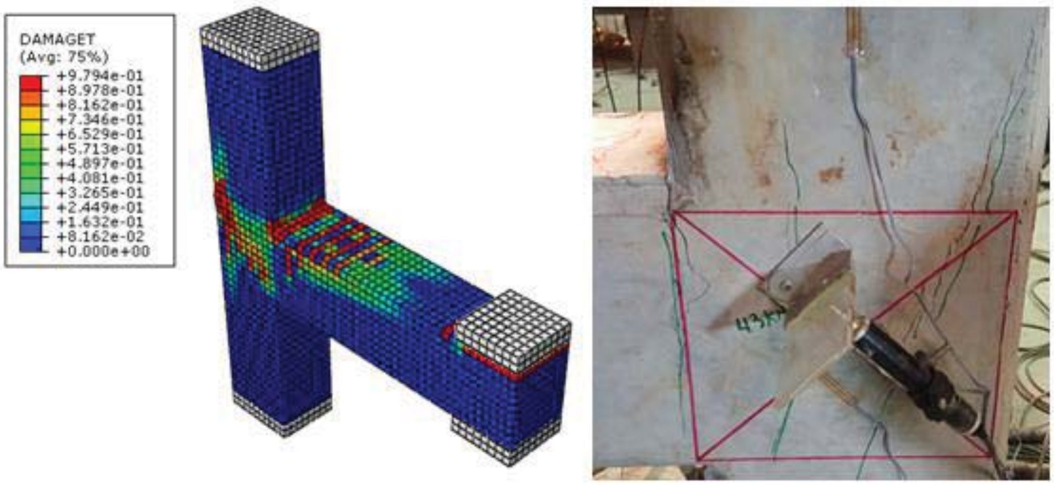

Figure 6-14 FEM and experimental crack pattern of specimen SP-3

Figure 6-15 shows the steel stresses at failure load of specimen SP-3. The maximum stress obtained in beam longitudinal reinforcement is 249 MPa which is less than yield stress.

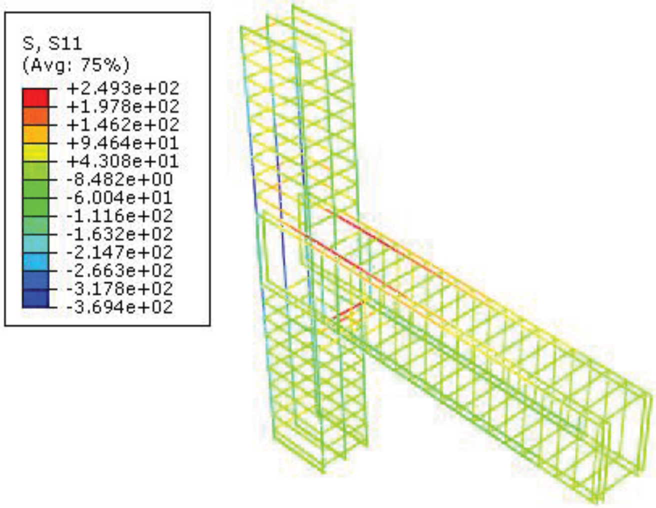

Figure 6-15 Steel stresses at failure load of specimen SP-3

Figure 6-16 shows the steel strains at failure load of specimen SP-3. The average maximum strain in beam's top bars is obtained as 0.00106 mm/mm against experimental value of 0.00098 mm/mm. The shear stress calculated with FEM results is 4.43 MPa against 4.23 MPa as obtained experimentally.

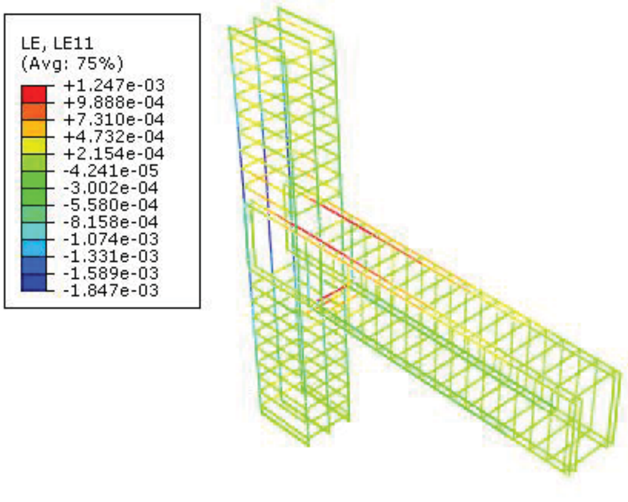

Figure 6-16 Steel strains at failure load of specimen SP-3

6.3.4. Specimen SP-6

Figure 6-17 shows the load-displacement response of specimen SP-4 obtained experimentally and as predicted by FEM. Failure load predicted by FEM is 68.66 kN at 5.81 mm against experimental value of 66.94 kN at a displacement of 6.98 mm. In general, the load displacement curve predicted by FEM is in close agreement with that of experiment.

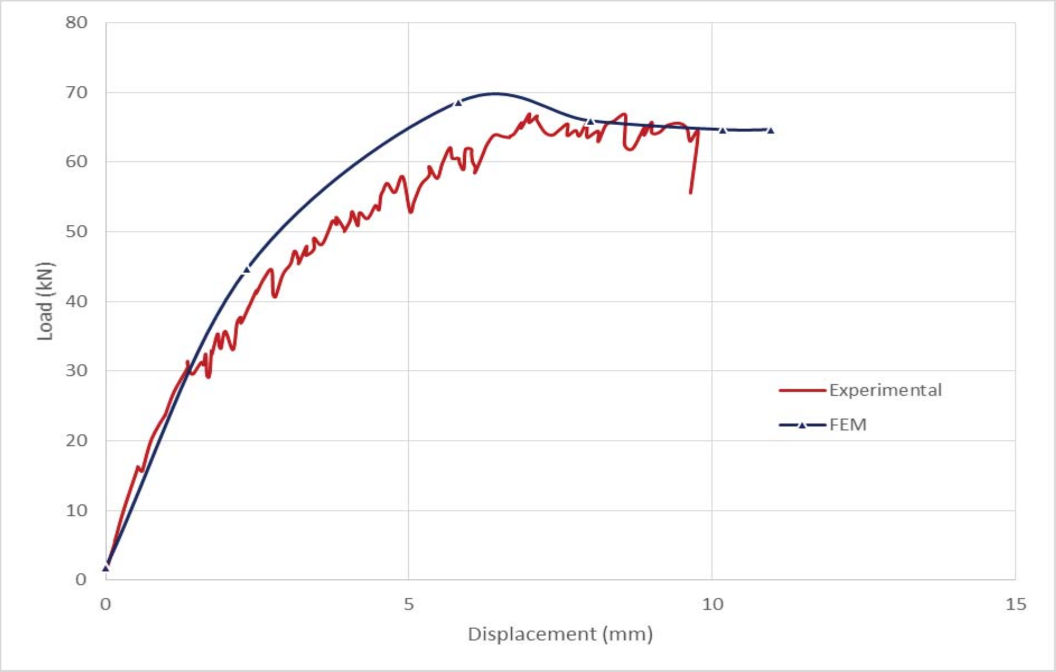

Figure 6-17 Load vs. displacement response of specimen SP-6

The predicted failure mode of specimen SP-6 is joint failure mode as expected from the experimental results. The crack pattern of the experiment and FE prediction is shown in Figure 6-18 where cracks are almost vertical.

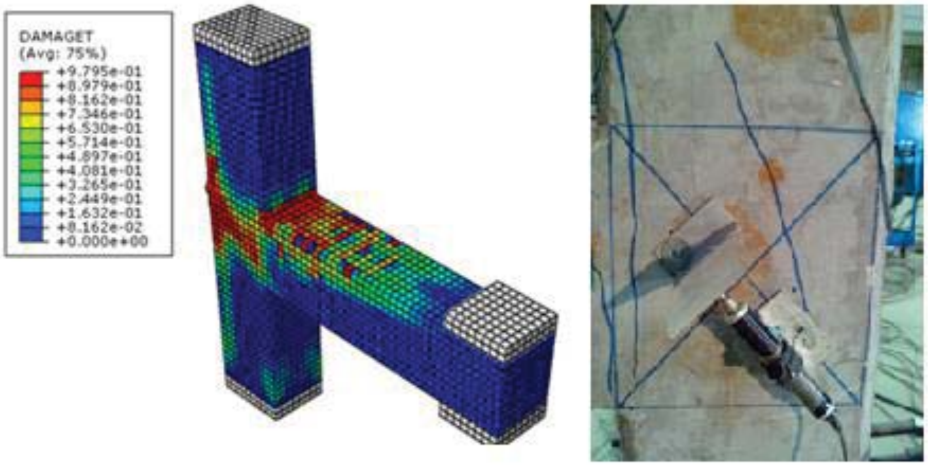

Figure 6-18 FEM and experimental crack pattern of specimen SP-6

Figure 6-19 shows the steel stresses at failure load of specimen SP-6. The maximum stress obtained in beam longitudinal reinforcement is 251 MPa which is again less than the yield stress of reinforcement.

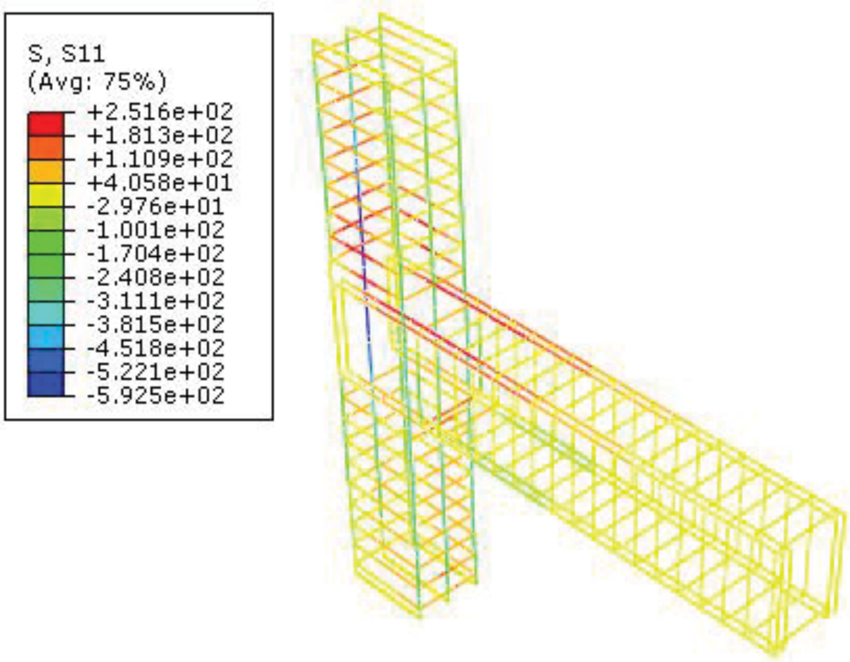

Figure 6-19 Steel stresses at failure load of specimen SP-6

Figure 6-20 shows the steel strains at failure load of specimen SP-6. The average maximum strain in beam's top longitudinal bars is obtained as 0.00127 mm/mm which is in close match with the experimental value of 0.00119 mm/mm. The shear stress calculated with FEM results is 5.36 MPa against 5.06 MPa as obtained experimentally.

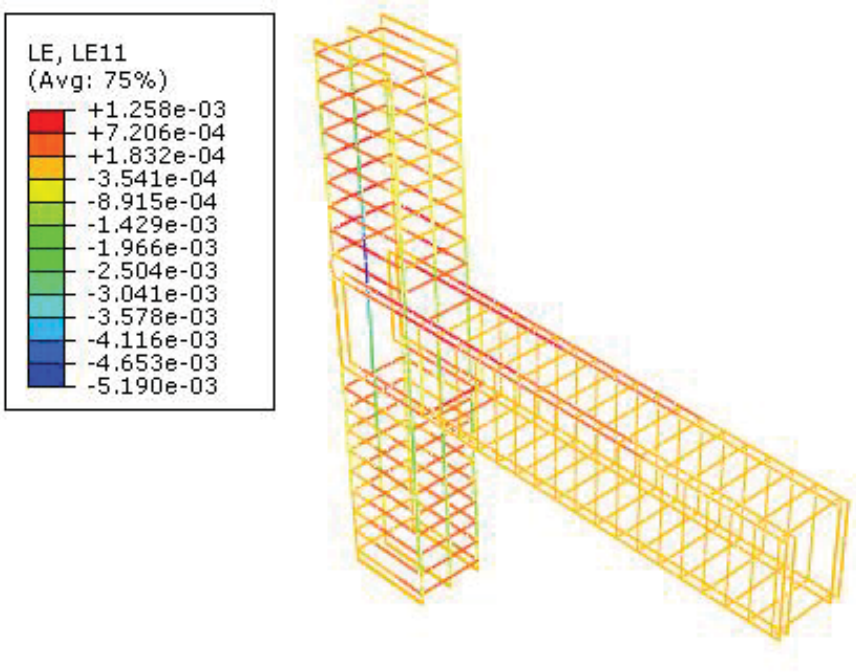

Figure 6-20 Steel strains at failure load of specimen SP-6

6.4. Extension of Research Using Finite Element Modelling

Based on validation of finite element model using experimental results as discussed in the previous section, calibrated FE model is used to extend the research work for different concrete strengths in order to gain further in depth knowledge of the effect of different magnitude of axial load on performance of BCJs. Table 6-3 shows the layout of finite element models.

Table 6-3 Layout of finite element models

Group	M-21	M-30	M-36	M-50	M-65
f'c / ALR	21	30	36	50	65
0.00	M-21-00	M-30-00	M-36-00	M-50-00	M-65-00
0.10	-	M-30-10	M-36-10	M-50-10	M-65-10
0.20	M-21-19	M-30-20	M-36-20	M-50-20	M-65-20
0.30	-	M-30-30	M-36-30	M-50-30	M-65-30
0.40	-	M-30-40	M-36-40	M-50-40	M-65-40
0.50	-	M-30-50	M-36-50	M-50-50	M-65-50
0.60	M-21-57	M-30-60	M-36-60	M-50-60	M-65-60
0.70	-	M-30-70	M-36-70	M-50-70	M-65-70
0.80	M-21-80	M-30-80	M-36-80	M-50-80	M-65-80
0.90	-	M-30-90	M-36-90	M-50-90	M-65-90
1.00	-	M-30-100	M-36-100	M-50-100	-
1.05	-	-	-	-	M-65-AC
1.08	-	-	-	M-50-AC	-
1.10	M-21-AC	M-30-AC	M-36-110	-	-
1.13	-	-	M-36-AC	-	-

Note:

1) Axial load ratio (ALR) = $\frac{N}{A_g f'_c}$

2) f'_c = Concrete compressive strength (MPa)

6.4.1. Group M-21

Figure 6-21 shows the load-displacement response of group M-21. The first three models that are M-21-00, M-21-19 and M-21-57 has been validated with experimental results as presented in the previous section. Calibrated model is then used to develop M-21-80 to understand the behavior of BCJ at very high axial load. Failure load increased with rise of ALR to 0.57 however, with further increase in an axial load on column the failure load decreased from 59 kN as in case of ALR of 0.57 to 42 kN at ALR of 0.80 with reduced ductility. Model M-21-AC is done primarily to see the ultimate axial capacity of the joint which is achieved at ALR of 1.10. Thus the shear strength of joint increased from 2.77 MPa to 4.43 MPa at ALR from 0.00 to 0.57 and then decreased to 4.09 MPa at ALR of 0.80. Finally, the pure axial failure of joint occurred at ALR of 1.10.

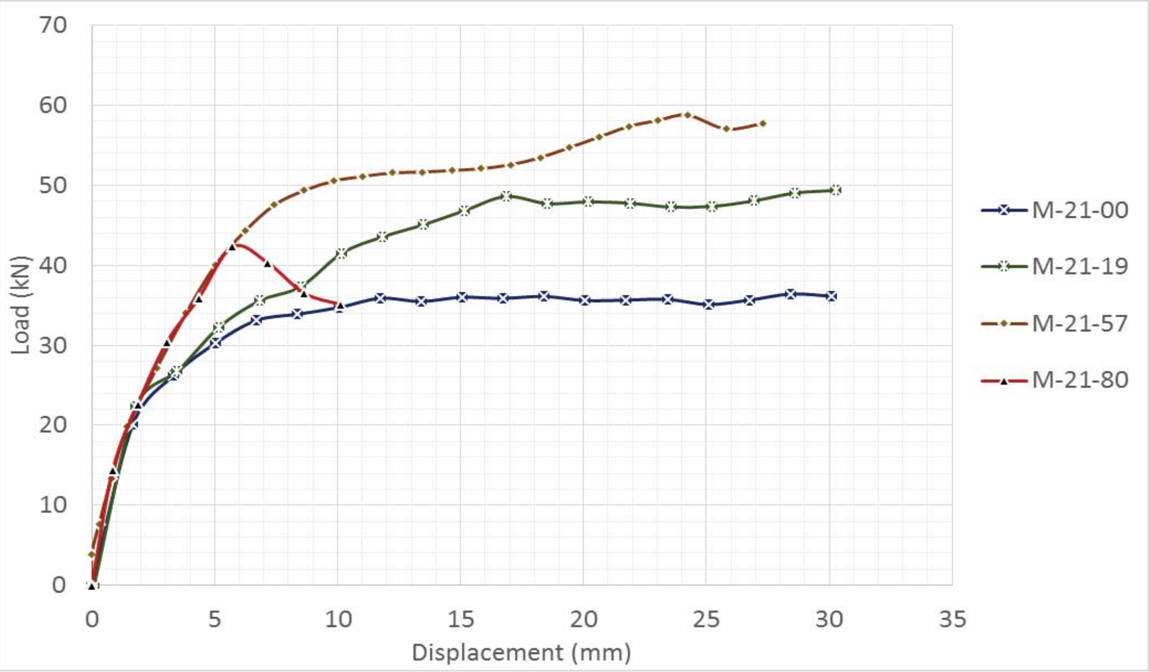

Figure 6-21 Load displacement response of group M-21

In Figure 6-22 it can be observed that when no CAL as in case of M-21-00 the main diagonal shear crack appeared in the joint is inclined at 45° with very few flexural cracks in the beam, However, with increase in axial load as depicted in M-21-19 and M-21-57 at ALR of 0.19 and 0.57 respectively the inclination of crack increased with excessive flexural cracks in the beam.

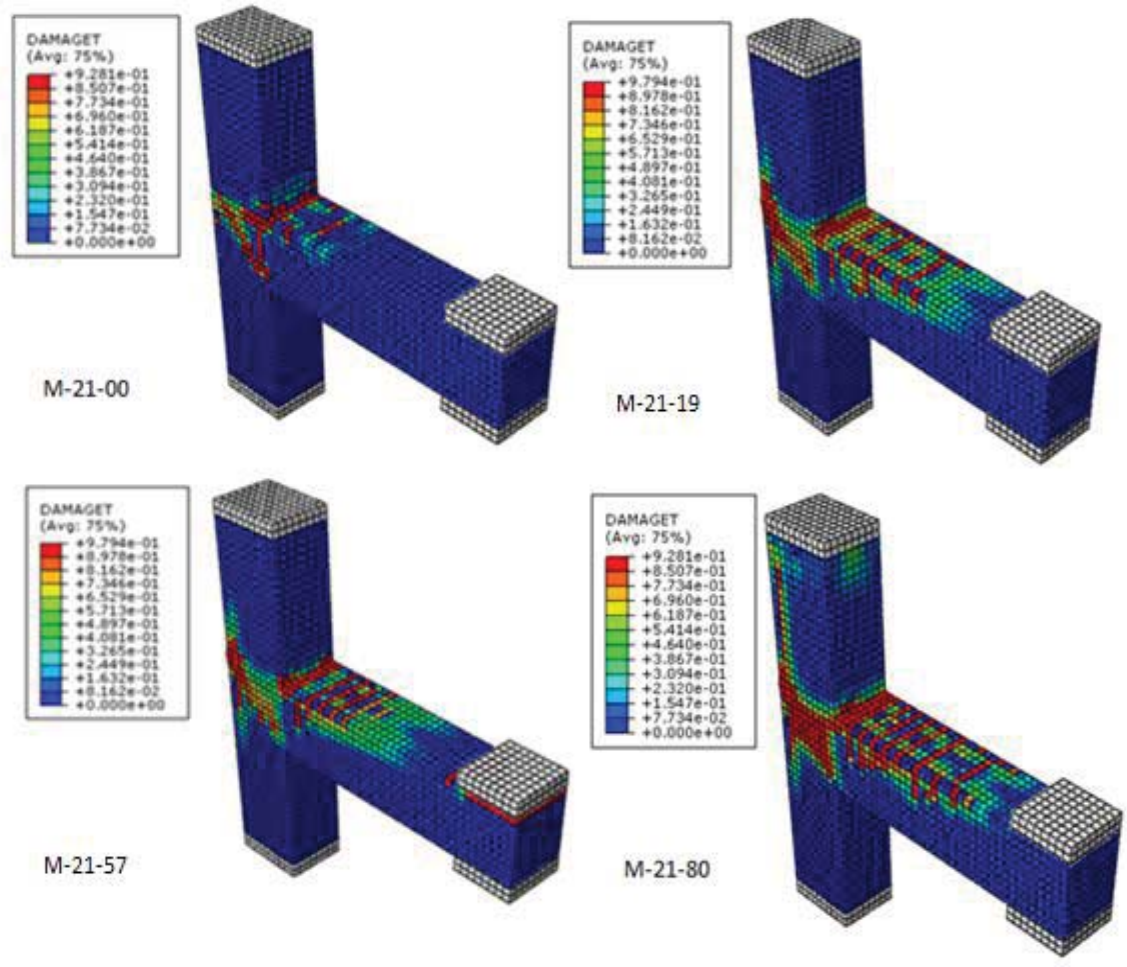

Figure 6-22 Crack pattern at failure load of group M-21

Failure mechanism observed up to an ALR of 0.57 is joint failure mode as no yielding of reinforcement either in column or beam is observed. M-21-80 at ALR of 0.80 although failed primarily in joint failure mode but local crushing is also observed at outer face of joint where joint experienced a strain of 0.0147 mm/mm. However, the average axial strain in the joint is 0.0022 mm/mm which is lower than a threshold limit of 0.0040 mm/mm. Joint in M-21-AC failed in pure axial failure with maximum strain of 0.0059 mm/mm.

Table 6-4 shows the finite element results of group M-21 models whereas Figure 6-23 shows the interaction curve between the shear strength and axial stress on the column.

Table 6-4 Summary of FEM results – group M-21

Model ID	σ_N (f'c %)	σ_N (MPa)	P (kN)	T (kN)	$V_{u(col)}$ (kN)	$V_{j(Joint)}$ (kN)	$v_{j(Joint)}$ (MPa)	Joint Failure Mode
M-21-00	0.00	0	36	166	27	139	2.77	JF
M-21-19	0.19	4	50	223	38	186	3.71	JF
M-21-57	0.57	12	59	266	44	222	4.43	JF
M-21-80	0.80	17	42	236	32	205	4.09	JF
M-21-AC	1.10	23	-	-	-	0	0	JAF

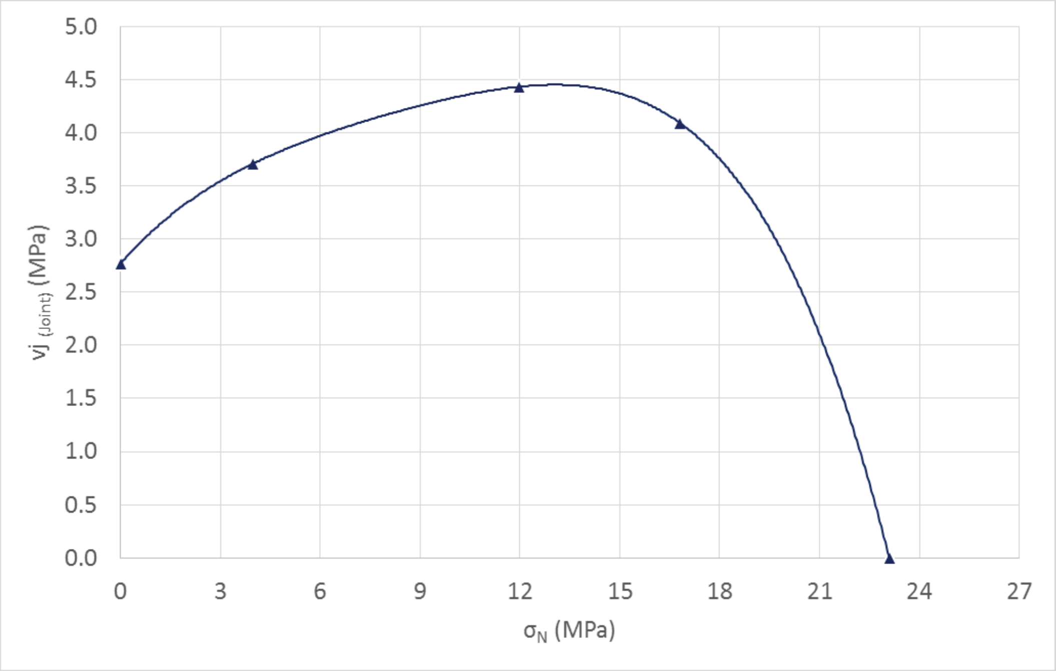

Figure 6-23 Shear strength - axial stress interaction curve of group M-21

6.4.2. Group M-30

Figure 6-24 shows the load-displacement response of group M-30. In this case the failure load at ALR of 0.00 is achieved at 54 kN corresponding to shear strength value of 3.40 MPa. Continuous increase in failure load and corresponding shear strength is observed as ALR is increased from 0.00 to 0.70. The maximum shear strength of joint achieved is 5.36 MPa at ALR of 0.70. With further increase in ALR the failure load decreased gradually to a minimum level of 45 kN corresponding to shear strength of 2.28 MPa as in case of M-30-100. The ultimate axial capacity of joint is found to be 1650 kN as in case of M-30-AC corresponding to ALR of 1.10. It is also evident from Figure 6-24 that with increase in ALR from 0.00 to 0.70 ductility reduced gradually whereas beyond ALR of 0.70 it decreased drastically.

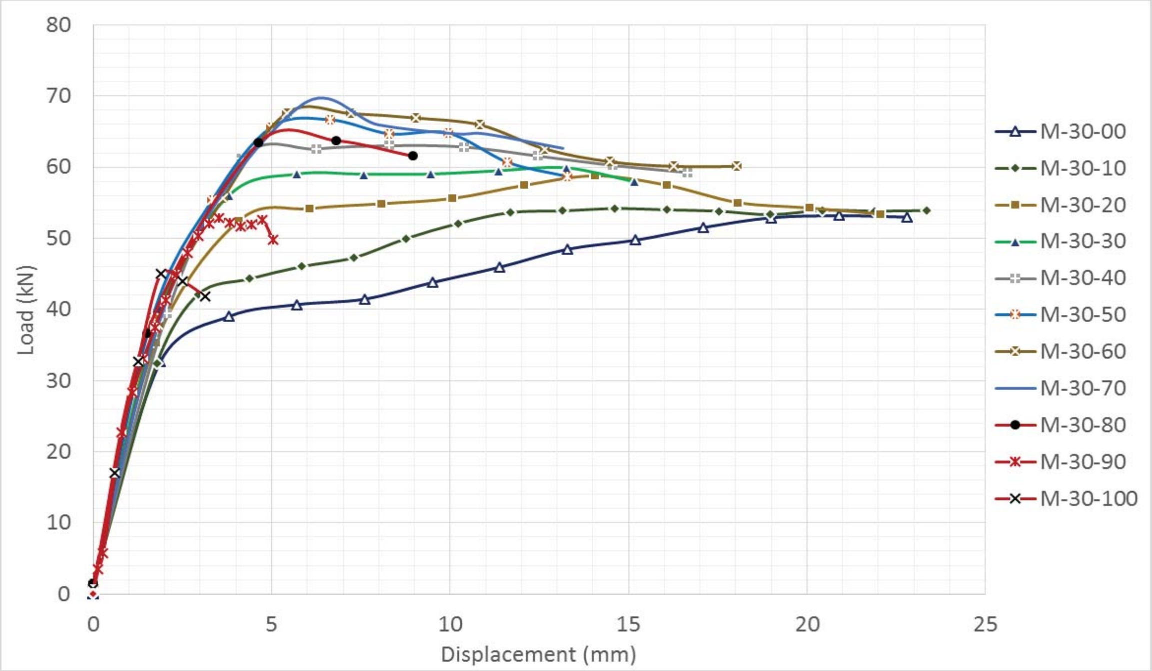

Figure 6-24 Load displacement response of group M-30

Figure 6-25 and Figure 6-26 shows the crack pattern at failure load of group M-30. It can be observed that cracks at low ALR are inclined at 45° but with increase in ALR inclination is increased until the joint failed absolutely in an axial failure mode.

Failure mechanism observed up to an ALR of 0.70 is joint failure mode as no yielding of reinforcement either in column or beam is observed. M-30-80 at ALR of 0.80 failed in axial failure mode where average joint strain reached at 0.0054 mm/mm which is above a threshold limit of 0.0040 mm/mm. M-30-90, M-30-100 and M-30-AC also failed in joint axial failure mode where joint strain reached at 0.00685 mm/mm, 0.00691 mm/mm and 0.00689 mm/mm respectively. Also yielding of one column longitudinal bar at outer face of joint is also observed in cases where joint failed in axial failure mode.

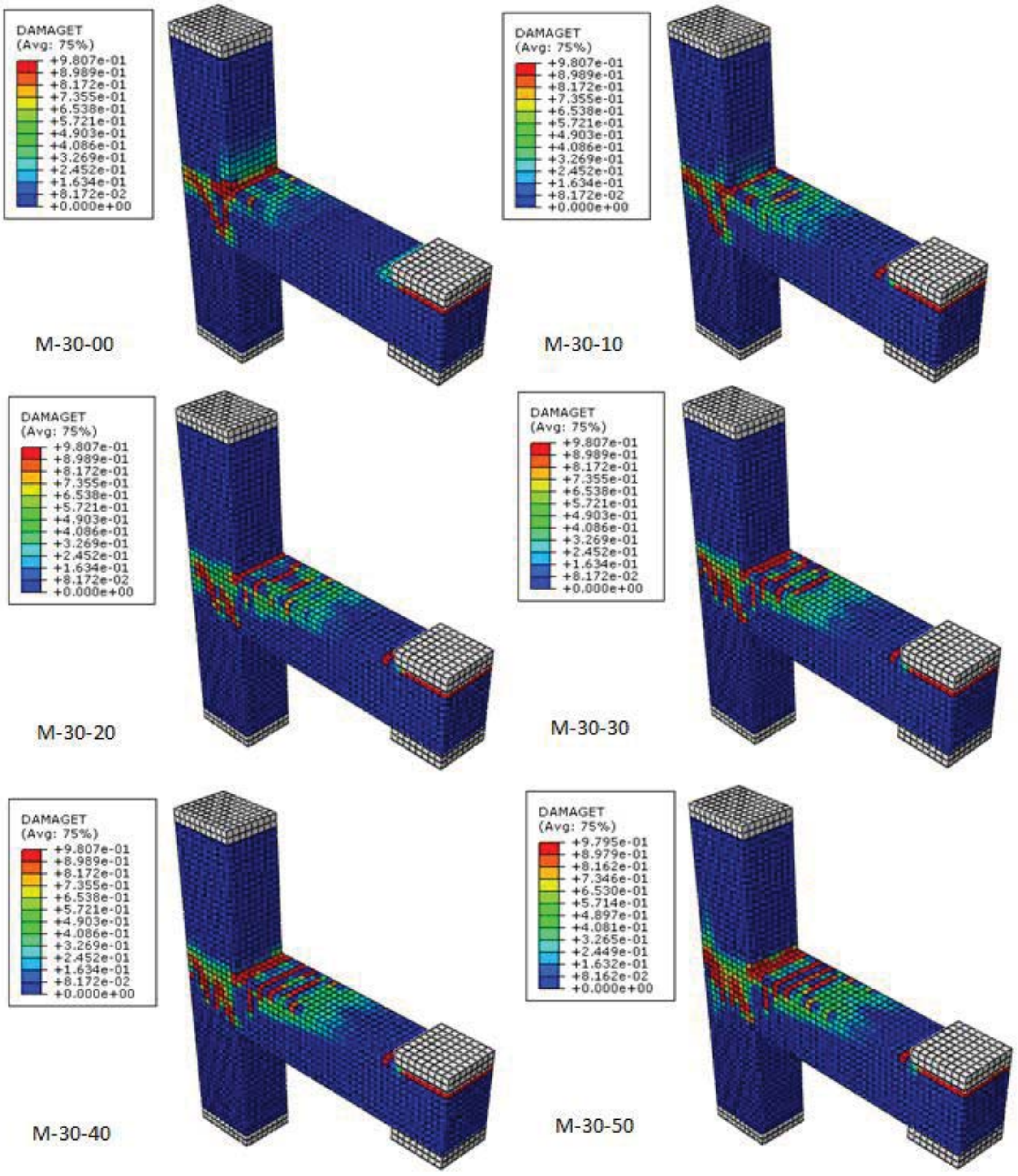
M-30-00
M-30-10
M-30-20
M-30-30
M-30-40
M-30-50

Figure 6-25 Crack pattern at failure load of group M-30

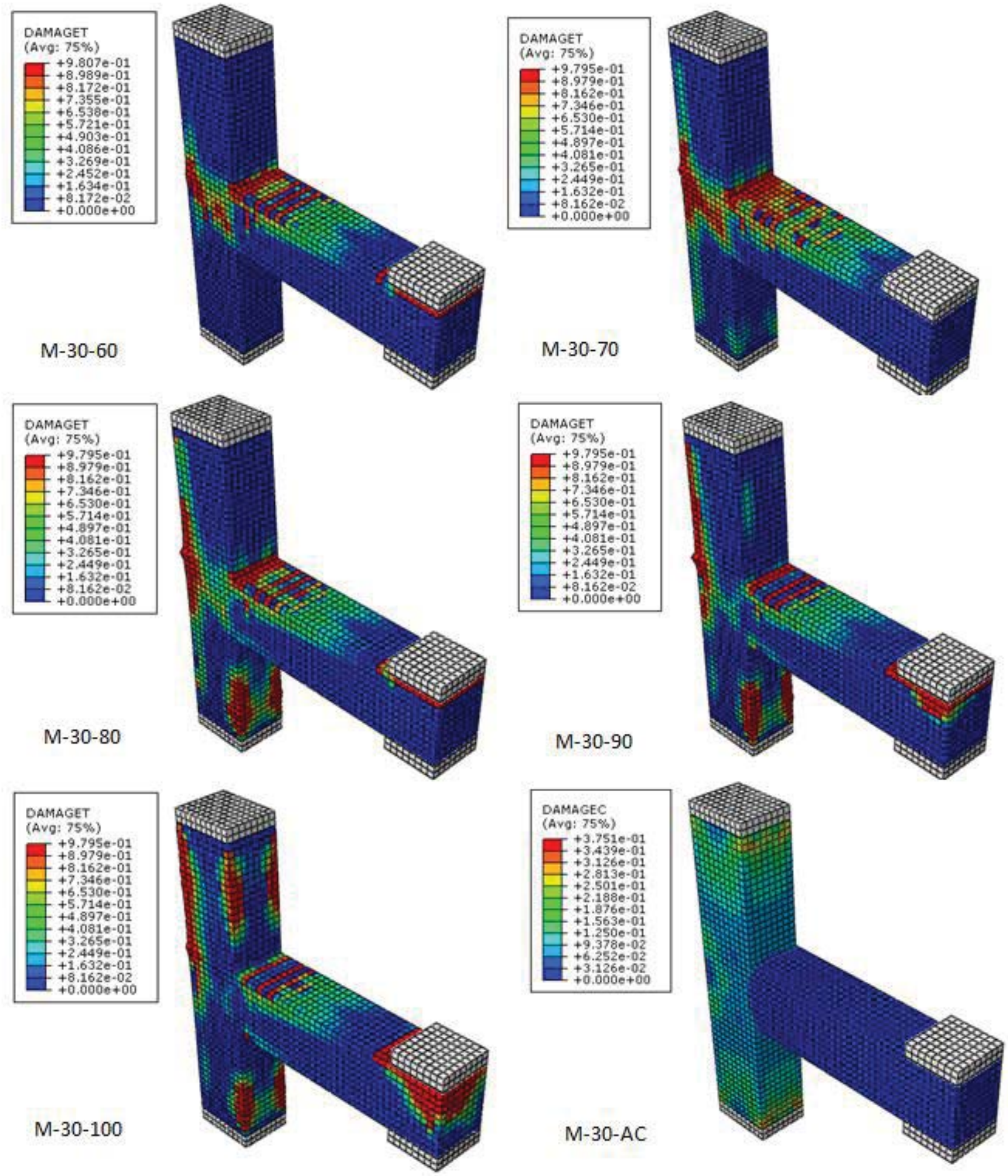

Figure 6-26 (Continued) Crack pattern at failure load of group M-30

Table 6-5 summarize the finite element results of group M-30 whereas Figure 6-27 shows the interaction curve between the shear strength and axial stress on the column.

Table 6-5 Summary of FEM results – group M-30

Model ID	σ_N (f'c %)	σ_N (MPa)	P (kN)	T (kN)	$V_{u(col)}$ (kN)	$V_{j(Joint)}$ (kN)	$V_{j(Joint)}$ (MPa)	Joint Failure Mode
M-30-00	0.00	0	54	210	40	170	3.40	JF
M-30-10	0.10	3	54	239	41	198	3.97	JF
M-30-20	0.20	6	59	273	44	229	4.58	JF
M-30-30	0.30	9	60	283	45	238	4.76	JF
M-30-40	0.40	12	63	297	47	250	5.00	JF
M-30-50	0.50	15	67	309	50	259	5.18	JF
M-30-60	0.60	18	68	318	51	268	5.35	JF
M-30-70	0.70	21	69	320	51	268	5.36	JF
M-30-80	0.80	24	64	284	48	236	4.72	JAF
M-30-90	0.90	27	53	215	40	176	3.52	JAF
M-30-100	1.00	30	45	148	34	114	2.28	JAF
M-30-AC	1.10	33	-	-	-	0	0	JAF

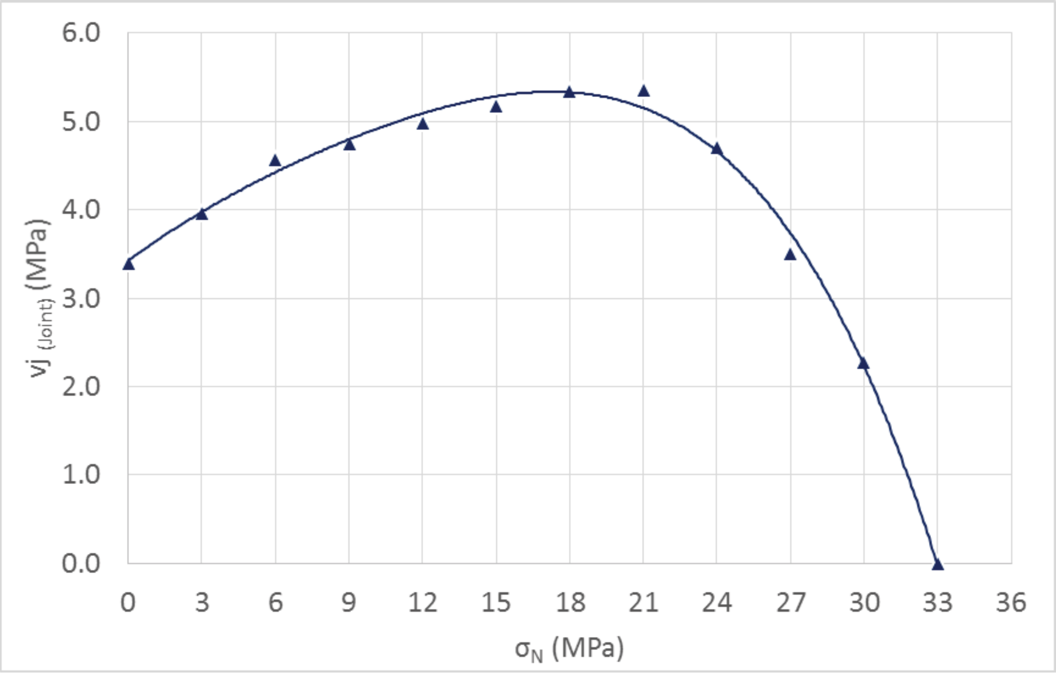

Figure 6-27 Shear strength - axial stress interaction curve of group M-30

6.4.3. Group M-36

Figure 6-28 shows the load-displacement response of group M-36. In this case the failure load at ALR of 0.00 is achieved at 57 kN corresponding to shear strength value of 4.12 MPa. Continuous increase in failure load and corresponding shear strength is observed as ALR is increased from 0.00 to 0.70. The maximum shear strength of joint achieved is 6.08 MPa at ALR of 0.70. With further increase in ALR the failure load decreased gradually to a minimum level of 24 kN corresponding to shear strength of 1.16 MPa as in case of M-36-110. The ultimate axial capacity of joint is found to be 2050 kN as in case of M-36-AC corresponding to ALR of 1.13. Gradual reduction in ductility is observed with increase in ALR for 0.00 to 0.70 as evident from the Figure 6-28 whereas ductility reduced drastically beyond the ALR of 0.70. The effect of CAL on ductility is somewhat more prominent than the previous cases.

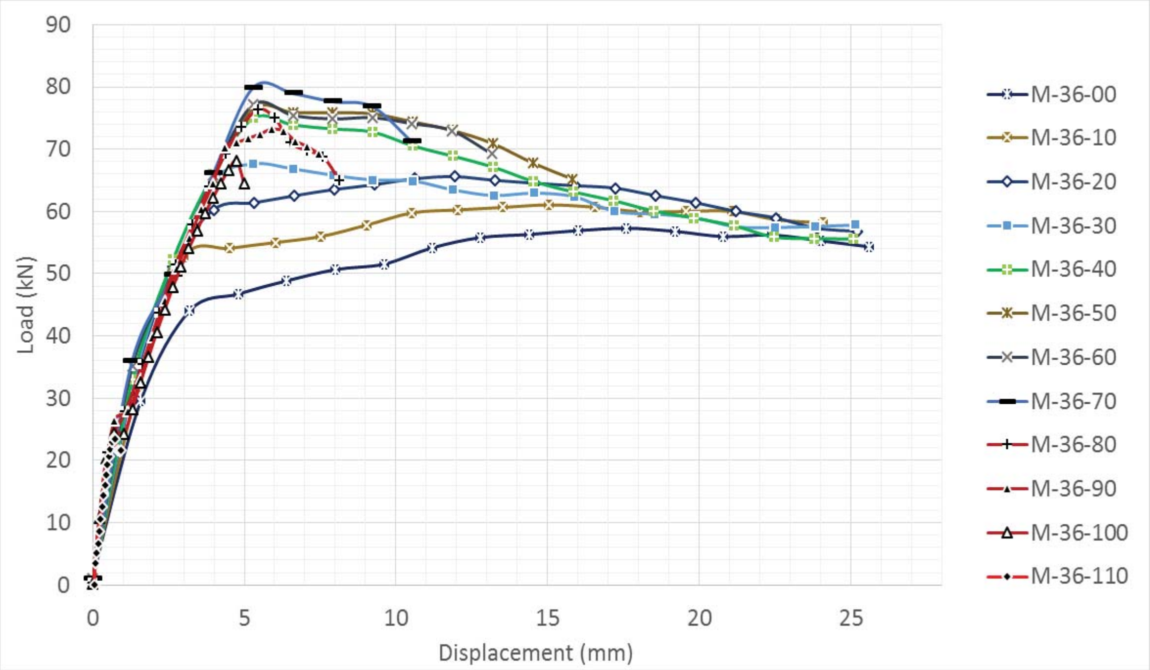

Figure 6-28 Load displacement response of group M-36

Figure 6-29 and Figure 6-30 displays the crack pattern at failure load of M-36. It can be observed that inclination of diagonal cracks is increased with increase in ALR until the axial failure of joint.

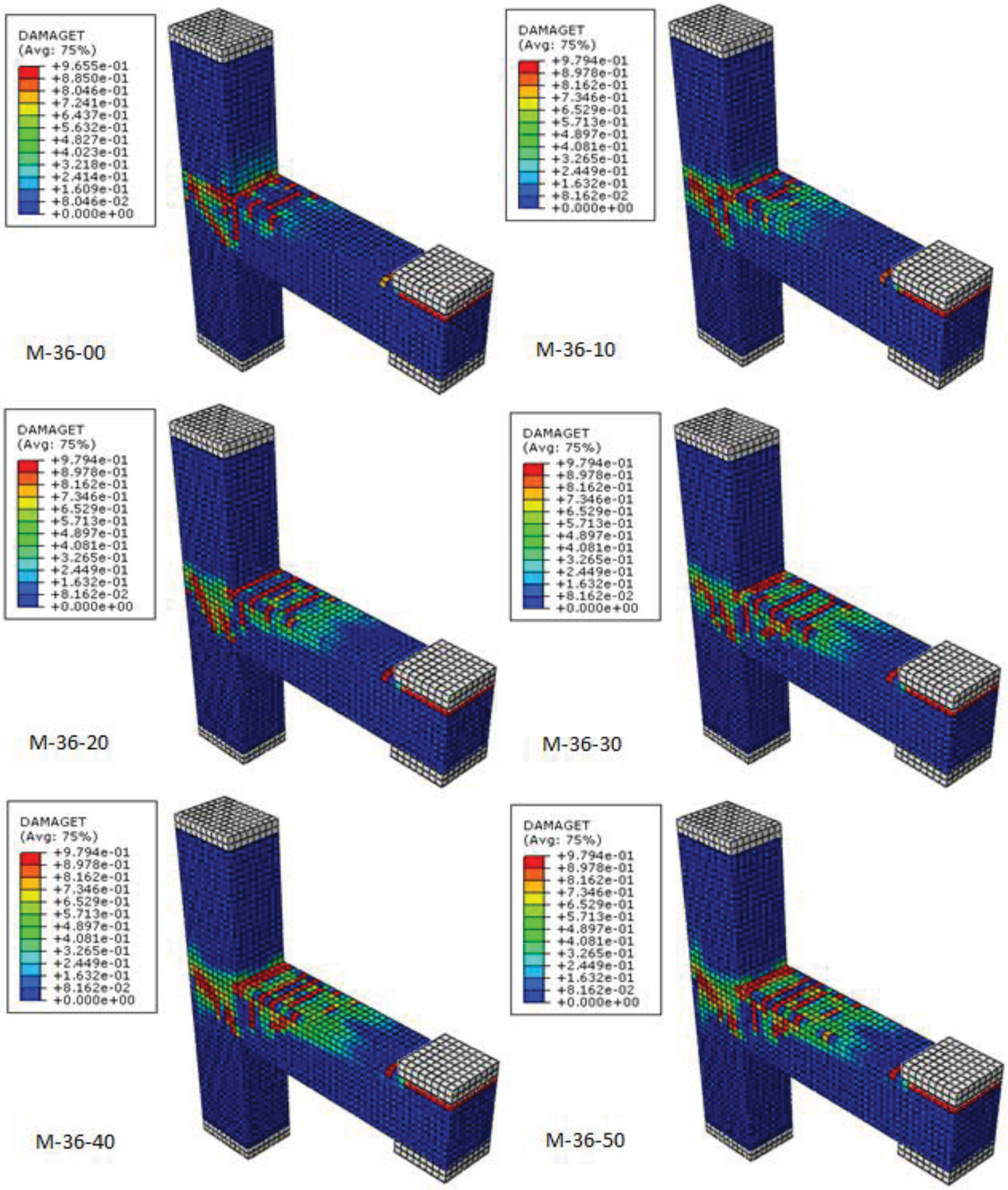

Figure 6-29 Crack pattern at failure load of group M-36

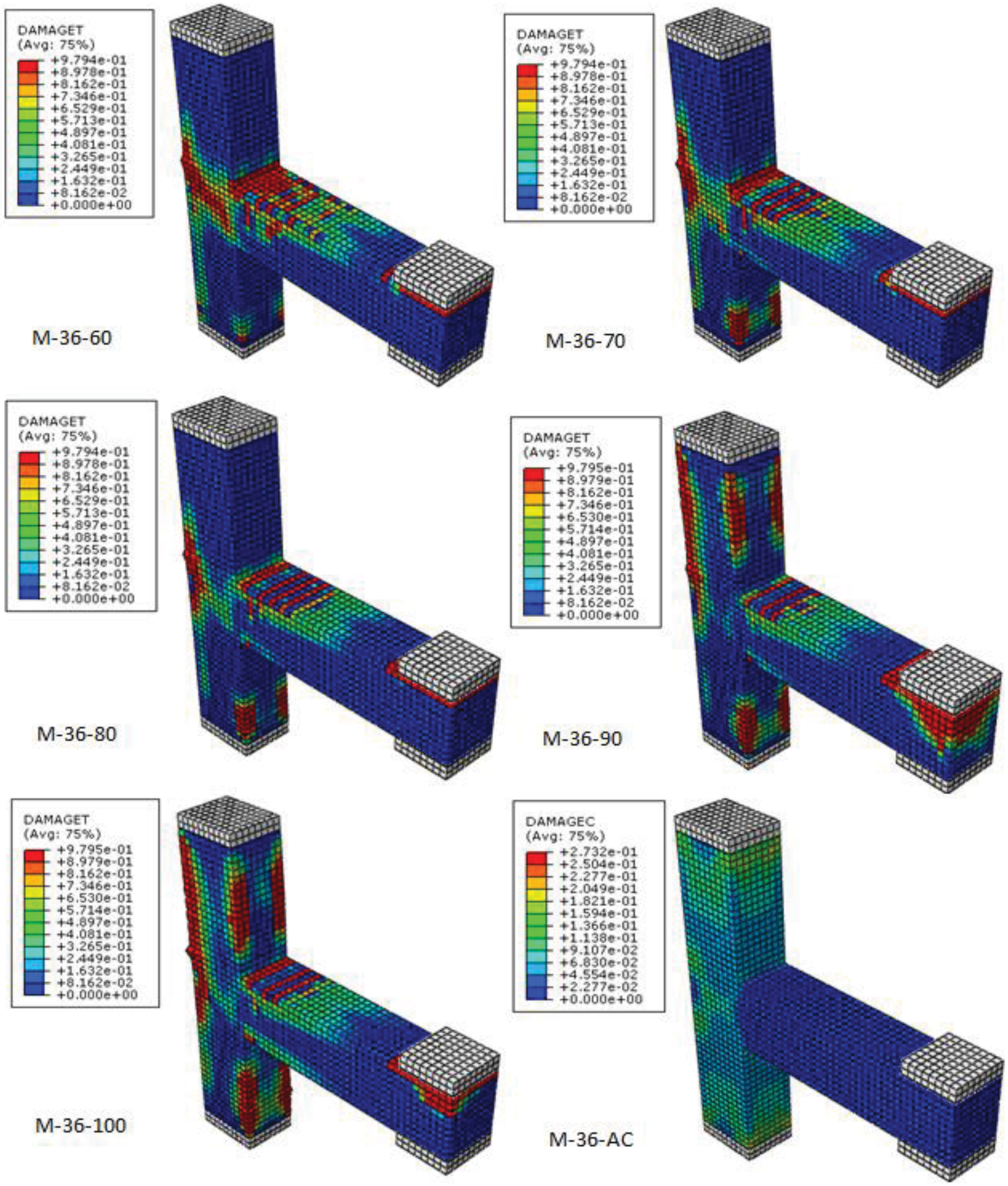

Figure 6-30 (Continued) Crack pattern at failure load of group M-36

Failure mechanism observed up to an ALR of 0.70 is joint failure mode as no yielding of reinforcement either in column or beam is observed. M-36-80 at ALR of 0.80 failed first in axial failure mode where average joint strain reached at 0.00661 mm/mm which is above a threshold limit of 0.0040 mm/mm yielding of middle column bar at outer face of joint is also observed. M-36-90, M-36-100. M-36-110 and M-36-AC also failed in joint axial failure mode where joint axial strain reached at 0.00673 mm/mm, 0.00742 mm/mm, 0.00685 mm/mm and 0.00681 mm/mm respectively. Table 6-6 summarize the finite element results of group M-36 whereas Figure 6-31 shows the interaction curve between the shear strength and axial stress on the column.

Table 6-6 Summary of FEM results – group M-36

Model ID	σ_N (f'c %)	σ_N (MPa)	P (kN)	T (kN)	$V_{u(col)}$ (kN)	$V_{j(Joint)}$ (kN)	$V_{j(Joint)}$ (MPa)	Joint Failure Mode
M-36-00	0.00	0	57	249	43	206	4.12	JF
M-36-10	0.10	4	61	287	46	242	4.83	JF
M-36-20	0.20	7	66	312	49	262	5.25	JF
M-36-30	0.30	11	68	329	51	278	5.56	JF
M-36-40	0.40	14	75	345	56	289	5.77	JF
M-36-50	0.50	18	76	353	57	295	5.91	JF
M-36-60	0.60	22	77	359	58	302	6.03	JF
M-36-70	0.70	25	80	364	60	304	6.08	JF
M-36-80	0.80	29	76	346	57	288	5.77	JAF
M-36-90	0.90	32	73	312	55	258	5.15	JAF
M-36-100	1.00	36	68	212	51	161	3.21	JAF
M-36-110	1.10	40	24	76	18	58	1.16	JAF
M-36-AC	1.13	41	-	-	-	0	0	JAF

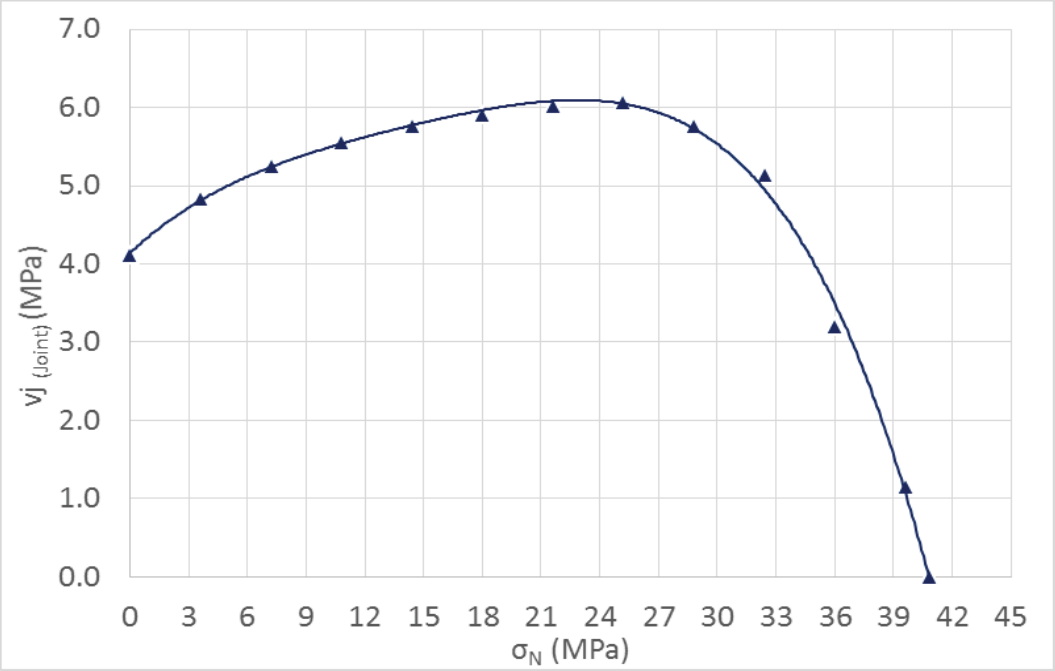

Figure 6-31 Shear strength - axial stress interaction curve of group M-36

6.4.4. Group M-50

Figure 6-32 shows the load-displacement response of group M-50. In this case the failure load at ALR of 0.00 is achieved at 70 kN corresponding to shear strength value of 5.25 MPa. The maximum shear strength of joint achieved is 7.75 MPa at ALR of 0.60 and 0.70. With further increase in ALR the failure load decreased gradually to a minimum level of 58 kN corresponding to shear strength of 2.45 MPa as in case of M-50-100. The ultimate axial capacity of joint is found to be 2700 kN as in case of M-50-AC corresponding to ALR of 1.08. Gradual reduction in ductility is observed with increase in ALR for 0.00 to 0.50 as obvious from the Figure 6-32 whereas ductility reduced drastically beyond the ALR of 0.50. The effect of CAL on ductility is more prominent than the previous cases owing to higher strength of concrete.

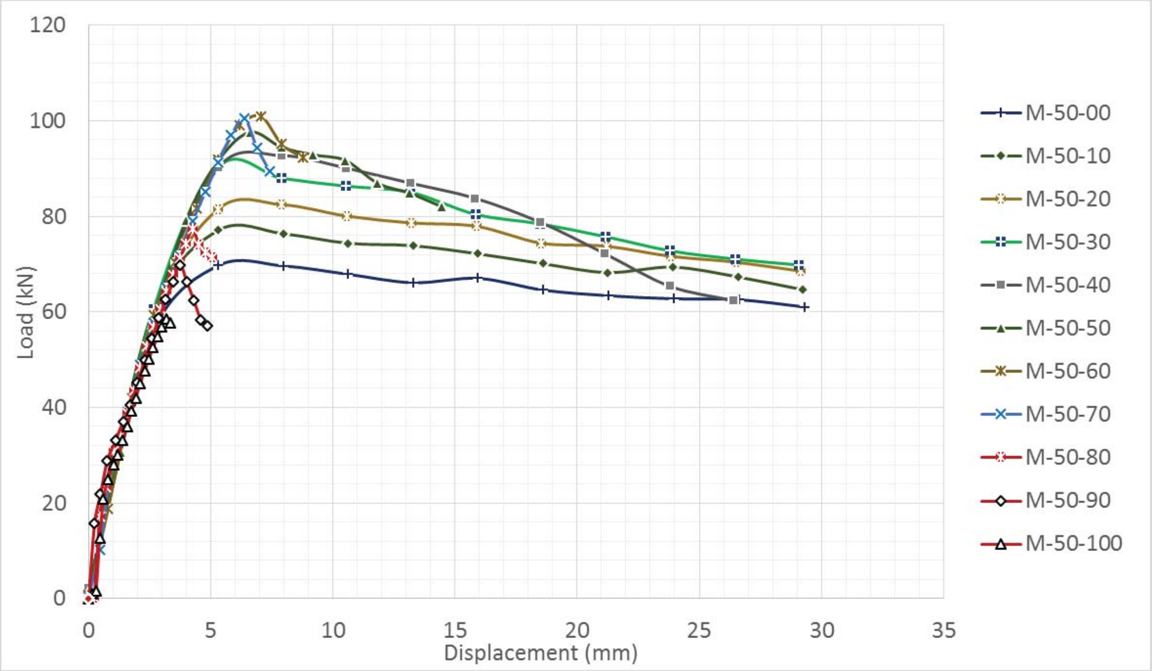

Figure 6-32 Load displacement response of group M-50

Figure 6-33 and Figure 6-34 shows the crack pattern at failure load of group M-50. Increase in inclination of cracks is observed with increase in ALR until axial failure of joint as observed in previous cases.

Failure mechanism observed up to an ALR of 0.60 is joint failure mode as no yielding of reinforcement either in column or beam is observed with axial strains below the threshold value. Joint axial failure mode is first observed in M-50-70 at ALR of 0.70 where average joint strain reached at 0.00440 mm/mm which is slightly above a threshold limit of 0.00400 mm/mm. Rest of the models with ALR greater than 0.70 experienced joint axial failure owing to axial strain greater than threshold value along with yielding of middle column bar at outer face of the joint.

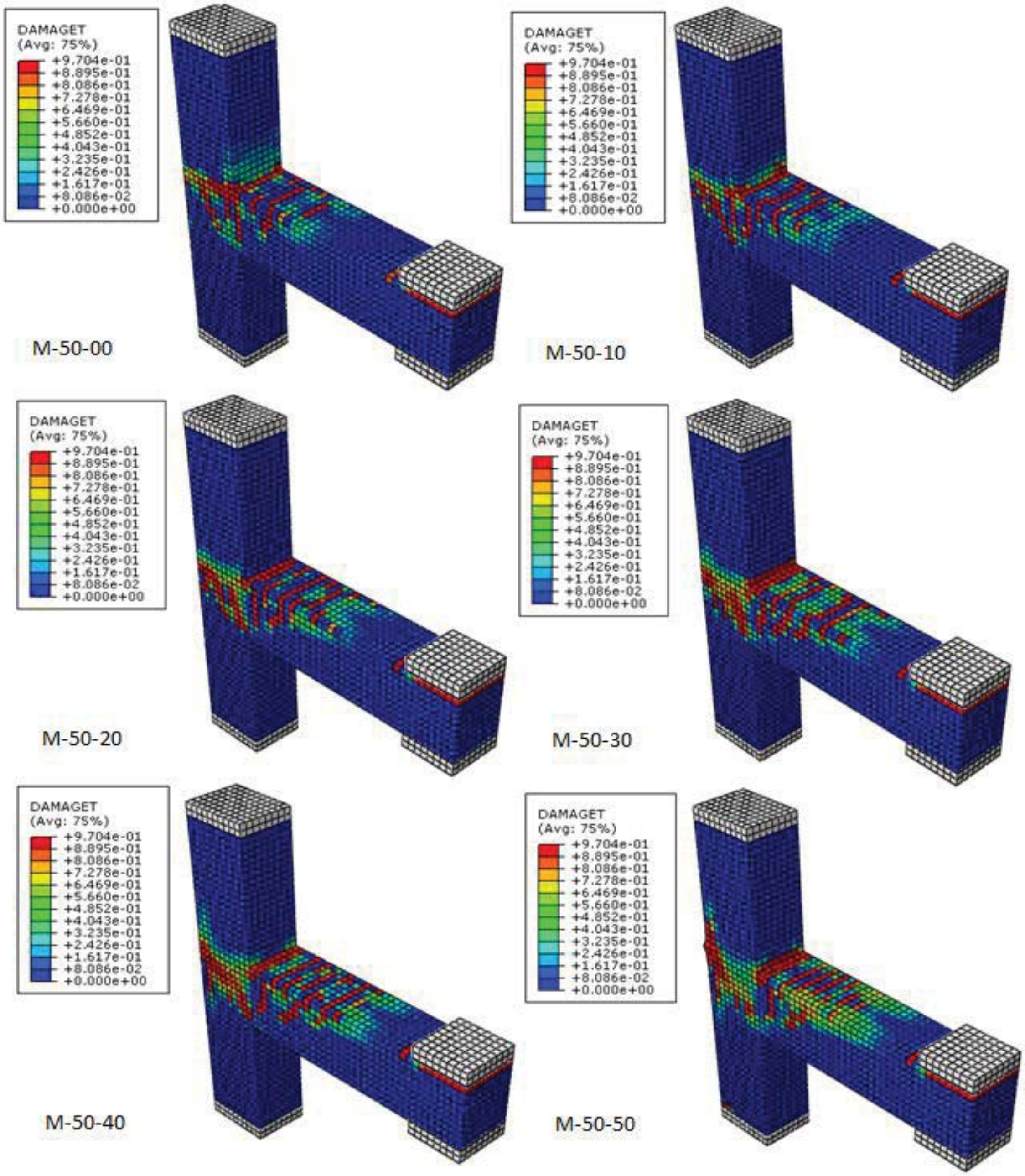

Figure 6-33 Crack pattern at failure load of group M-50

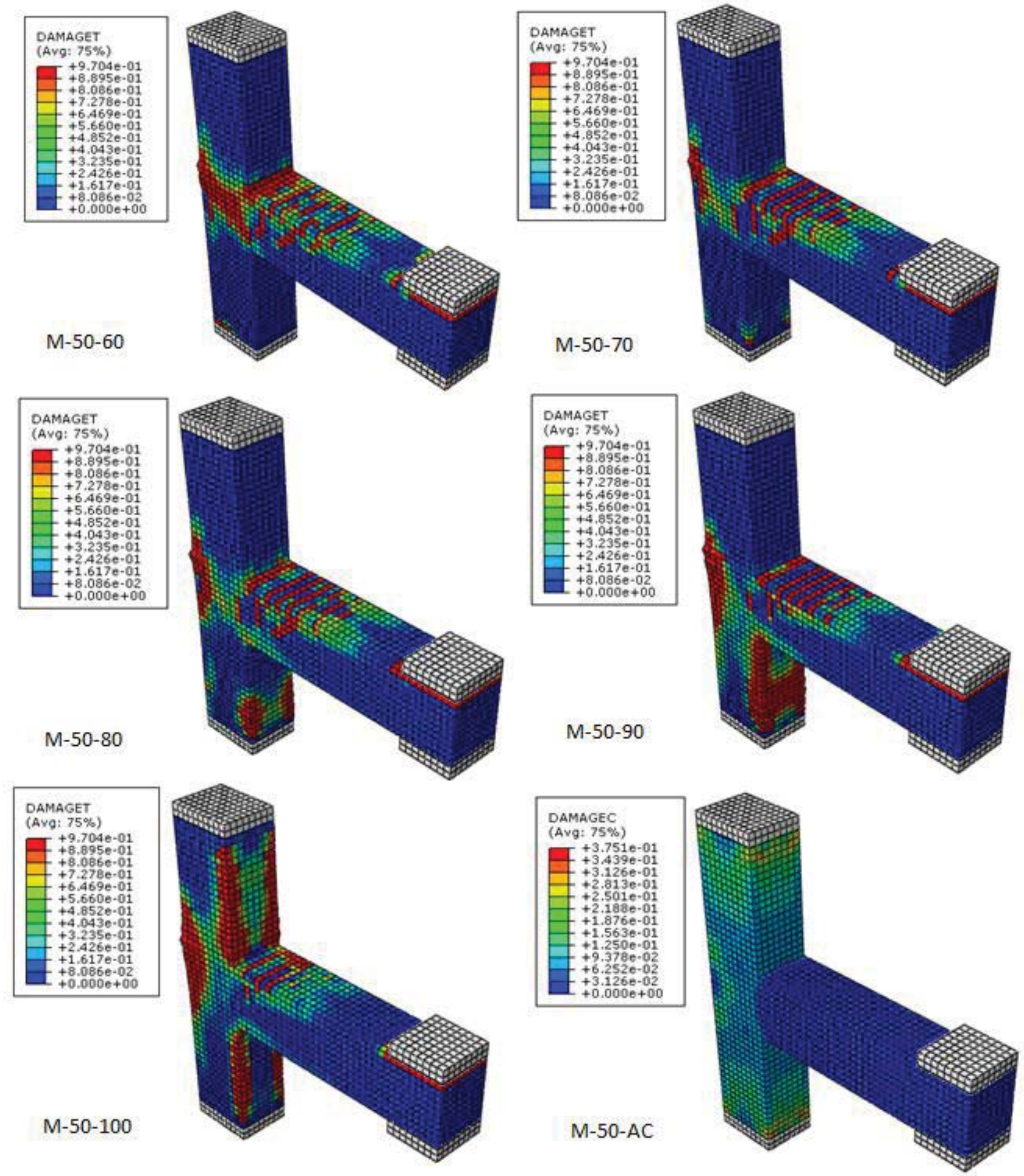

Figure 6-34 (Continued) Crack pattern at failure load of group M-50

Table 6-7 summarize the finite element results of group M-50 whereas Figure 6-35 shows the interaction curve between the shear strength and axial stress on the column.

Table 6-7 Summary of FEM results – group M-50

Model ID	σ_N (f'c %)	σ_N (MPa)	P (kN)	T (kN)	$V_{u(col)}$ (kN)	$V_{j(Joint)}$ (kN)	$V_{j(Joint)}$ (MPa)	Joint Failure Mode
M-50-00	0.00	0	70	314	52	262	5.24	JF
M-50-10	0.10	5	77	352	58	295	5.89	JF
M-50-20	0.20	10	82	398	62	336	6.73	JF
M-50-30	0.30	15	90	419	68	351	7.02	JF
M-50-40	0.40	20	93	439	70	370	7.40	JF
M-50-50	0.50	25	98	449	73	376	7.53	JF
M-50-60	0.60	30	101	463	76	387	7.75	JF
M-50-70	0.70	35	101	463	75	388	7.75	JAF
M-50-80	0.80	40	77	371	58	313	6.26	JAF
M-50-90	0.90	45	70	273	52	221	4.42	JAF
M-50-100	1.00	50	58	166	44	122	2.45	JAF
M-50-AC	1.08	54	-	-	-	0	0	JAF

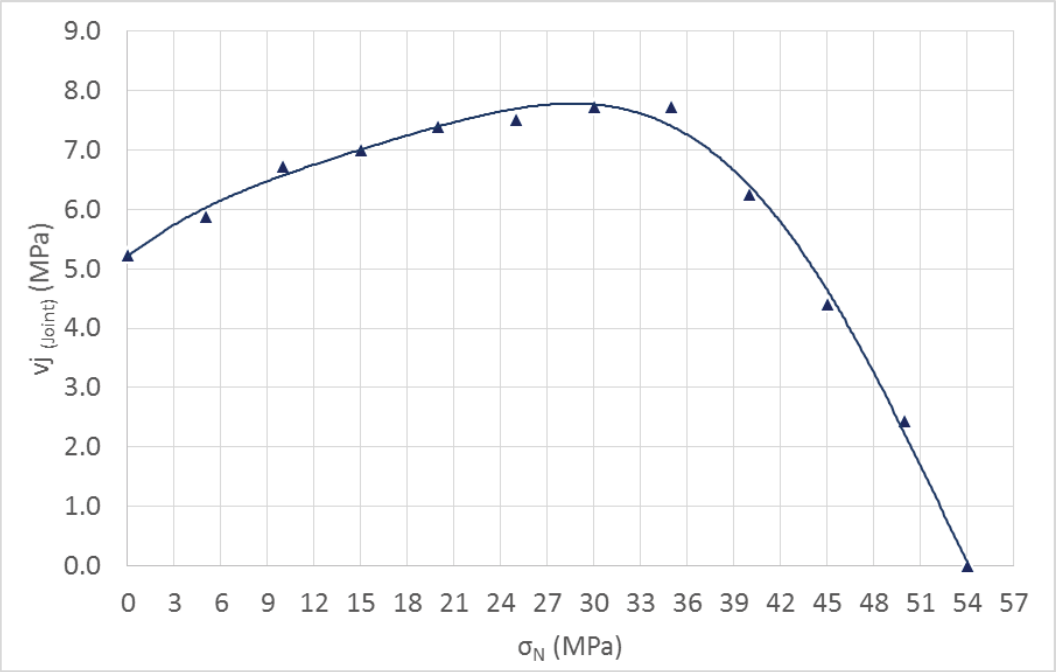

Figure 6-35 Shear strength - axial stress interaction curve of group M-50

6.4.5. Group M-65

Figure 6-36 shows the load-displacement response of group M-65. In this case the failure load at ALR of 0.00 is achieved at 82 kN corresponding to shear strength value of 6.31 MPa. The maximum shear strength of joint achieved is 9.12 MPa at ALR of 0.60. With further increase in ALR the failure load decreased gradually to a minimum level of 79 kN corresponding to shear strength of 5.86 MPa as in case of M-65-90. The ultimate axial capacity of joint is found to be 3400 kN as in case of M-65-AC corresponding to ALR of 1.05. Gradual reduction in ductility is observed with increase in ALR for 0.00 to 0.50 as obvious from the Figure 6-36 whereas ductility reduced drastically beyond the ALR of 0.50. The effect of CAL on ductility is even more prominent than the previous case.

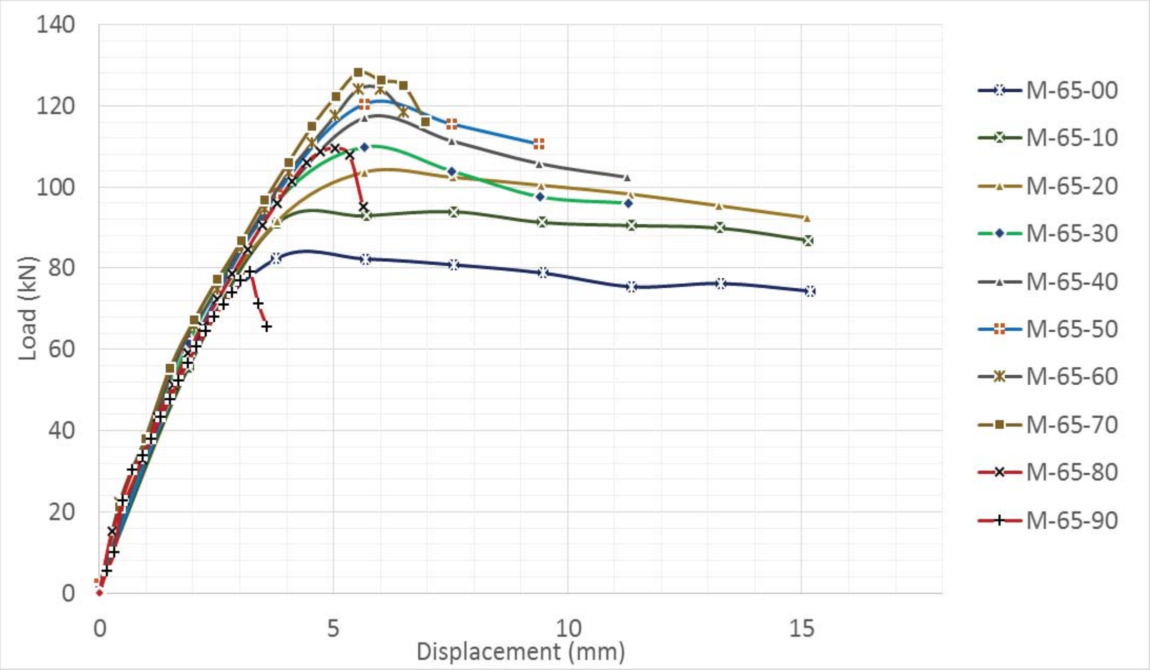

Figure 6-36 Load displacement response of group M-65

Figure 6-37and Figure 6-38 shows the crack pattern at failure load of group M-65. Increase in inclination of cracks is observed with increase in ALR until axial failure of joint as observed in previous cases.

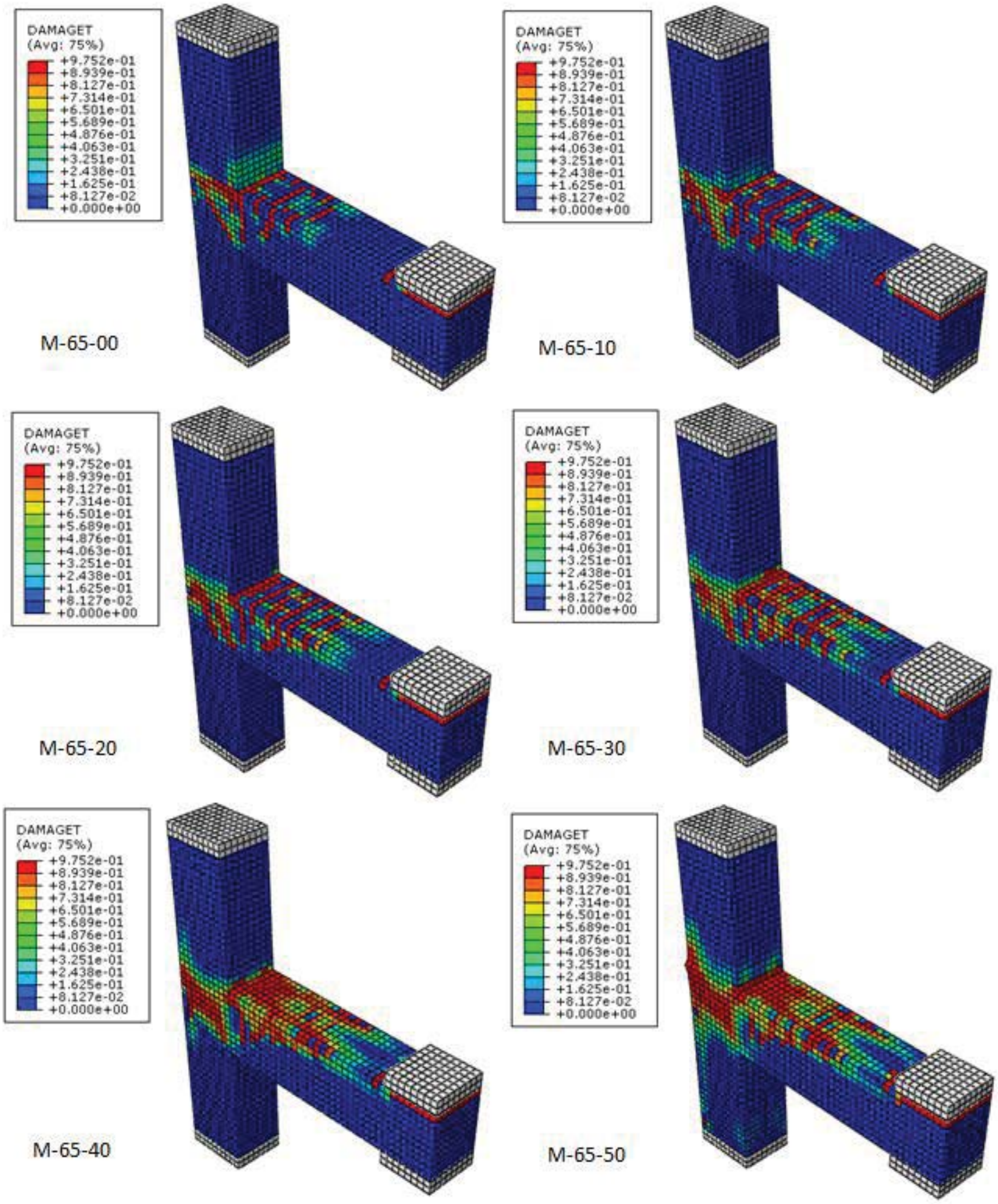

Figure 6-37 Crack pattern at failure load of group M-65

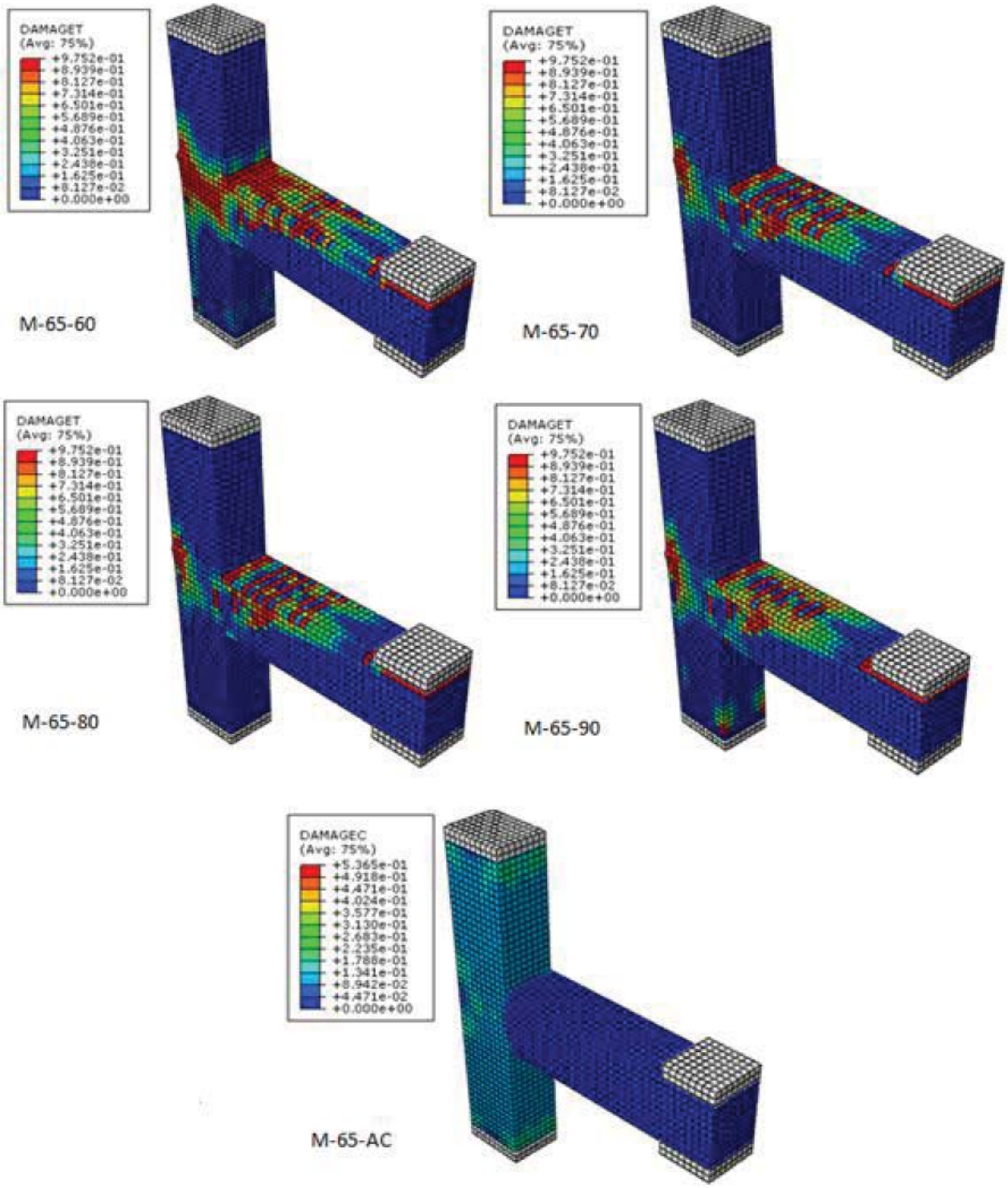

Figure 6-38 (Continued) Crack pattern at failure load of group M-65

Failure mechanism observed up to an ALR of 0.60 is joint failure mode as no yielding of reinforcement either in column or beam is observed with axial strains below the threshold value. Joint axial failure mode is first observed in M-65-70 at ALR of 0.70 where average joint strain reached at 0.00732 mm/mm which is slightly above a threshold limit of 0.00400 mm/mm. Models with ALR greater than 0.70 experienced joint axial failure owing to axial strain greater than threshold value along with yielding of middle column bar at outer face of the joint.

Table 6-8 summarize the finite element results of group M-65 whereas Figure 6-39 shows the interaction curve between the shear strength and axial stress on the column.

Table 6-8 Summary of FEM results – group M-65

Model ID	σ_N (f'c %)	σ_N (MPa)	P (kN)	T (kN)	$V_{u(col)}$ (kN)	$V_{j(Joint)}$ (kN)	$v_{j(Joint)}$ (MPa)	Joint Failure Mode
M-65-00	0.00	0	82	377	62	316	6.31	JF
M-65-10	0.10	7	94	440	70	370	7.39	JF
M-65-20	0.20	13	104	483	78	406	8.11	JF
M-65-30	0.30	20	110	506	82	423	8.46	JF
M-65-40	0.40	26	117	519	88	431	8.62	JF
M-65-50	0.50	33	120	535	90	445	8.90	JF
M-65-60	0.60	39	124	549	93	456	9.12	JF
M-65-70	0.70	46	128	549	96	453	9.06	JAF
M-65-80	0.80	52	110	449	82	367	7.34	JAF
M-65-90	0.90	59	79	352	59	293	5.86	JAF
M-65-AC	1.05	68	-	-	-	0	0	JAF

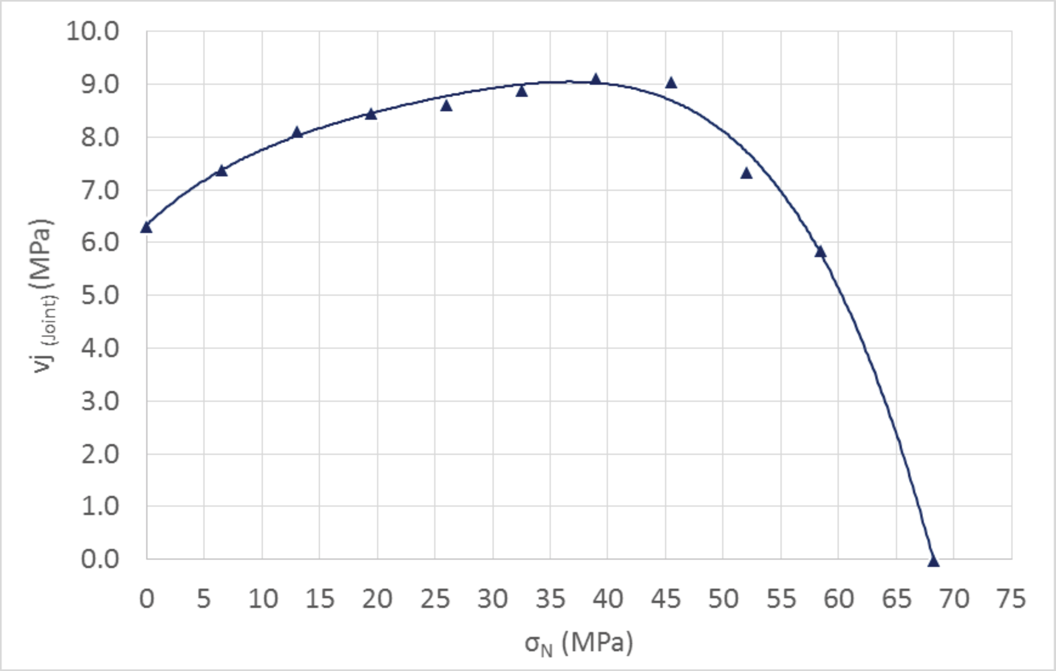

Figure 6-39 Shear strength - axial stress interaction curve of group M-65

6.5. Summary of Effect of Axial Load on Shear Strength of BCJ

BCJs with five different concrete strengths have been examined for the consequence of CAL on shear strength. Almost similar trend is noticed in all the groups where shear strength increases up to ALR of 0.60 to 0.70 due to confinement provided by axial load to BCJ against shear and bond slip failure. At ALR of 0.60-0.70 small crushing in joint is observed at failure load but primarily joint failed in joint failure mode up to this ALR level as no reinforcement yielding is observed either in beam or in column. However, above ALR of 0.60-0.70 decrease in shear strength is observed in all the groups where joint failed in shear followed by axial failure mode because of exceeding the threshold limit of joint axial strain that is 0.00400 mm/mm along with crushing of concrete in BCJ. In all the cases decrease in ductility is observed with increase in axial load on the column. Figure 6-40 summarizes the shear strength- axial stress relation of all the groups discussed above.

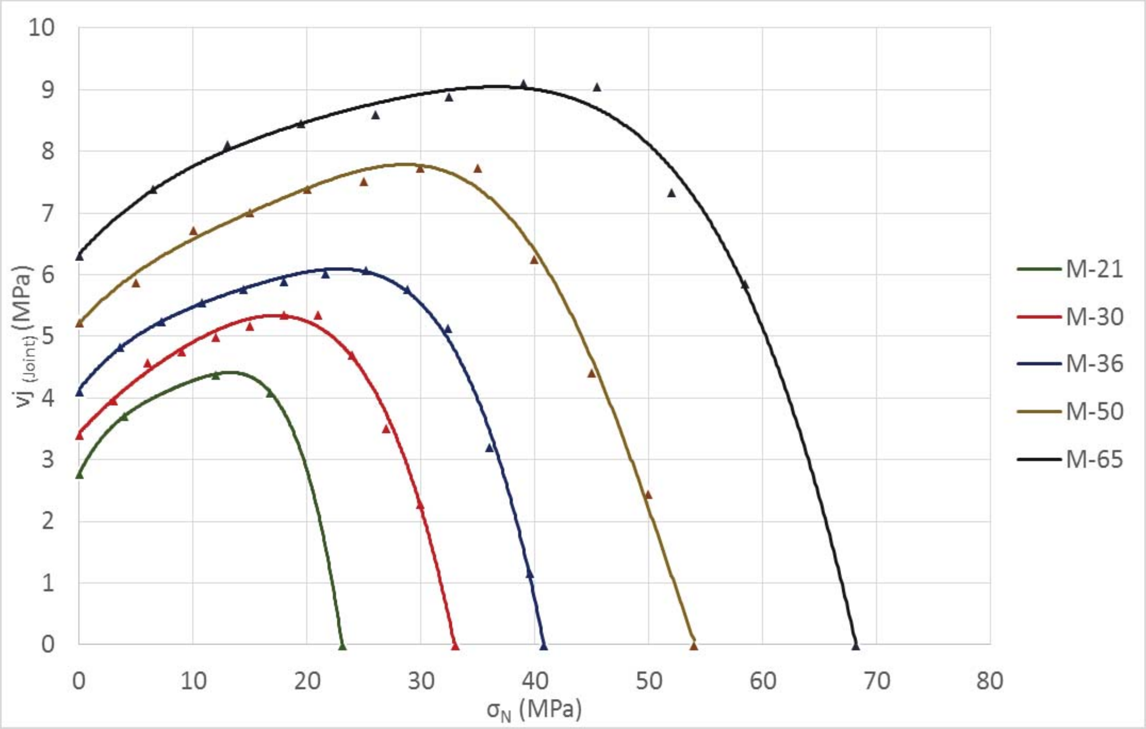

Figure 6-40 Shear strength - axial stress interaction curves

CHAPTER 7

SHEAR STRENGTH EQUATION FOR BCJS

7.1. Introduction

Several empirical and analytical shear strength equations are available to estimate the shear strength of BCJs. However, in most of researches variation of ALR is not more than approximately 0.15 and maximum axial load considered and well documented in form of shear strength equation is 0.42 f'_c $A_{g.}$ In this chapter a new equation is proposed to predict shear strength of BCJs incorporating effect of axial load over a complete range of ALR. Apart from axial load proposed equation takes in to an account an effect of other important parameters like aspect ratio of BCJ and beam reinforcement ratio. Proposed equation is then validated with previous published experimental results and showed good agreement.

7.2. Development of Shear Strength Equation

Figure 7-1 shows the comparison of mechanistic model prediction for shear strength of BCJs with results obtained from experiment and FE modelling. It can be noticed that mechanistic model reasonably predicts the overall trend of shear strength over complete range of ALR. However due to contribution of beam reinforcement in arresting shear crack development in the joint actual shear strength values are found to be higher over entire range of ALR. Also after a certain percentage of axial load unconfined joints become experiences mixed state of failure that is shear failure and local crushing so called axial failure, mechanistic model gives the maximum shear strength due to increase in ALR at around 0.45 to 0.50 however in practice presence of column reinforcement increases the axial capacity of joint which delays this type of failure. This is the reason that difference in actual shear strength values and that predicted by mechanistic model is more pronounced in range of 0.50 to 0.70

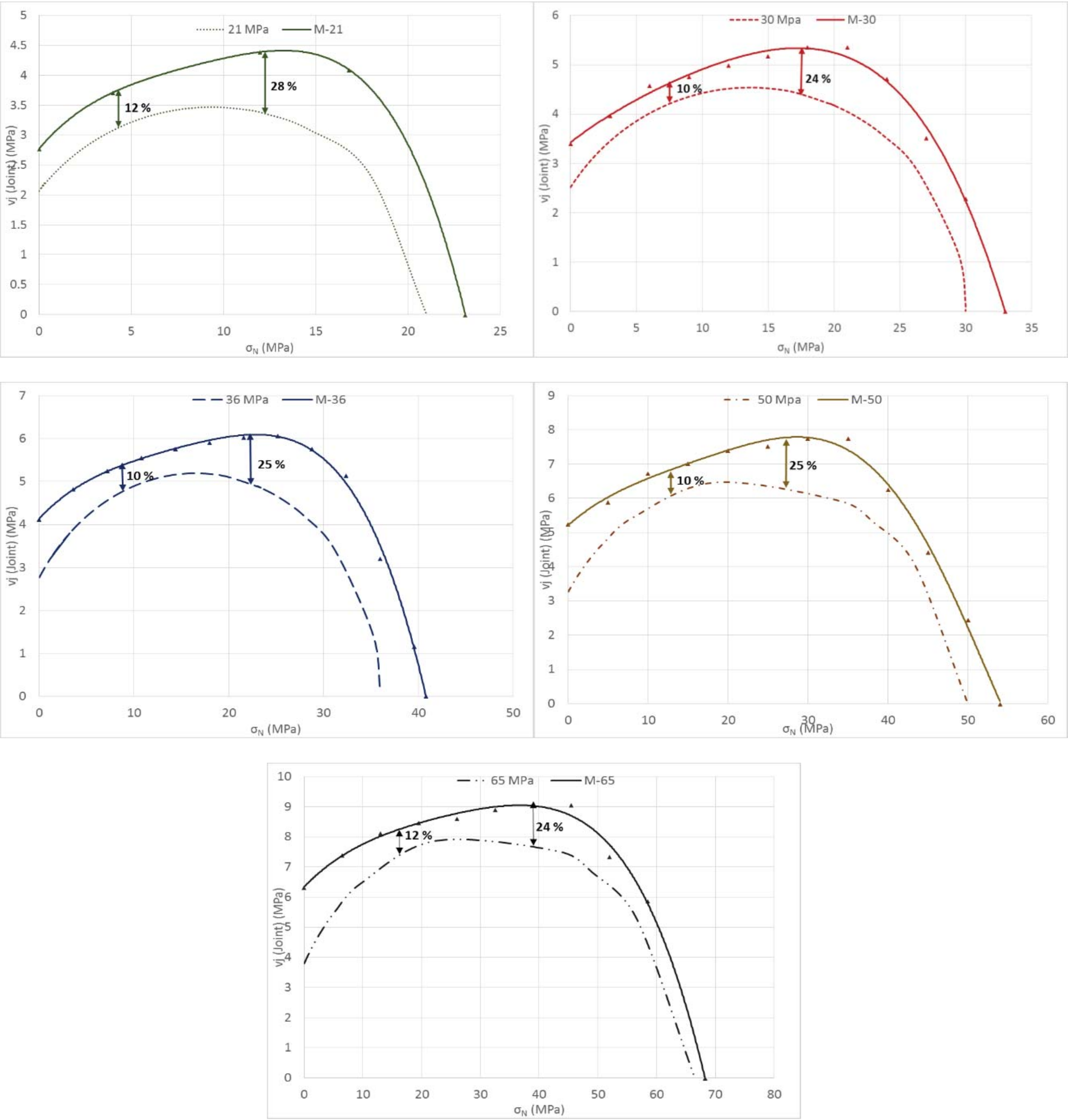

Figure 7-1 Comparison of mechanistic model with FEM and experimental results

Therefore, due practical consideration interactions between axial stress on column and corresponding shear strength of BCJs obtained from experimental and FE modelling is used to develop shear strength equations. Effects of CAL, concrete strength, aspect ratio and beam reinforcement are evaluated independently. The basic steps involved in development of shear strength equation are as follow:

7.2.1. Effect of Axial Load and Concrete Compressive Strength

BCJs with five different concrete strengths have been evaluated for the consequence of CAL on shear strength. Almost similar trend is detected in all the groups. Increasing axial load on column from 0.00 f'c Ag to 0.60 f'c Ag enhances the shear strength of BCJ up to 42 %. However, above ALR of 0.60-0.70 decrease in shear strength is observed in all the groups where joint failed in shear followed by axial failure mode because of exceeding the threshold limit of joint axial strain that is 0.00400 mm/mm along with crushing of concrete in the joint. The interaction between shear strength of joint and axial load on column for various concrete strengths are shown in Figure 7-2.

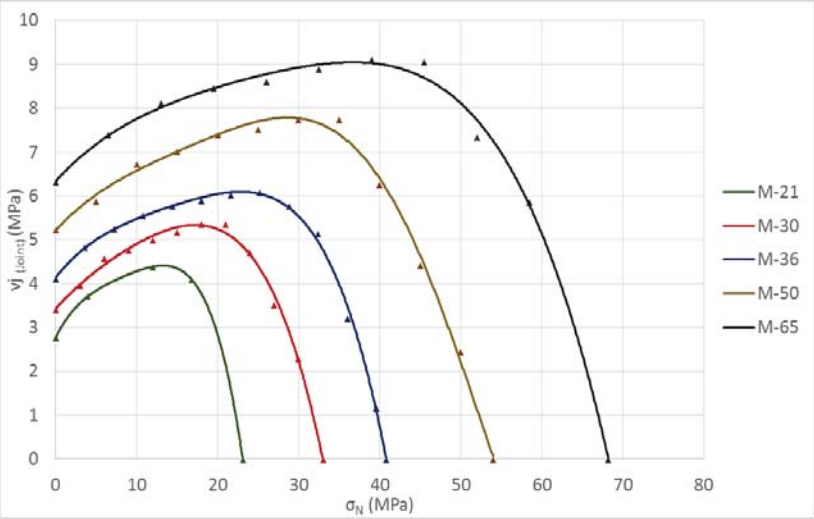

Figure 7-2 Relation between axial stress and shear strength of BCJs

7.2.2. Effect of Beam Reinforcement Ratio

It is evident from the experiment that beam reinforcement in the joint region enhances its shear capacity as it arrests the development of shear cracks. To evaluate the possible effect of different beam reinforcement ratio experimental test results of Hakuto [3], Ghobarah and Said [15], Clyde et al. [16] and Pantelides et al. [20] are investigated. Only those experimental tests are considered in which aspect ratio and CAL was almost similar to reduce the interaction of these parameters. Experimental shear strength was then normalized with $\sqrt{f'_c}$ and plotted against respective beam reinforcement ratio as displayed in Figure 7-3. The following relation between beam reinforcement ratio ρ_b and shear strength is derived from the trend:

$$\frac{v_j}{\sqrt{f'_c}} = 0.7675\ \rho_b^{0.261} \tag{7.1}$$

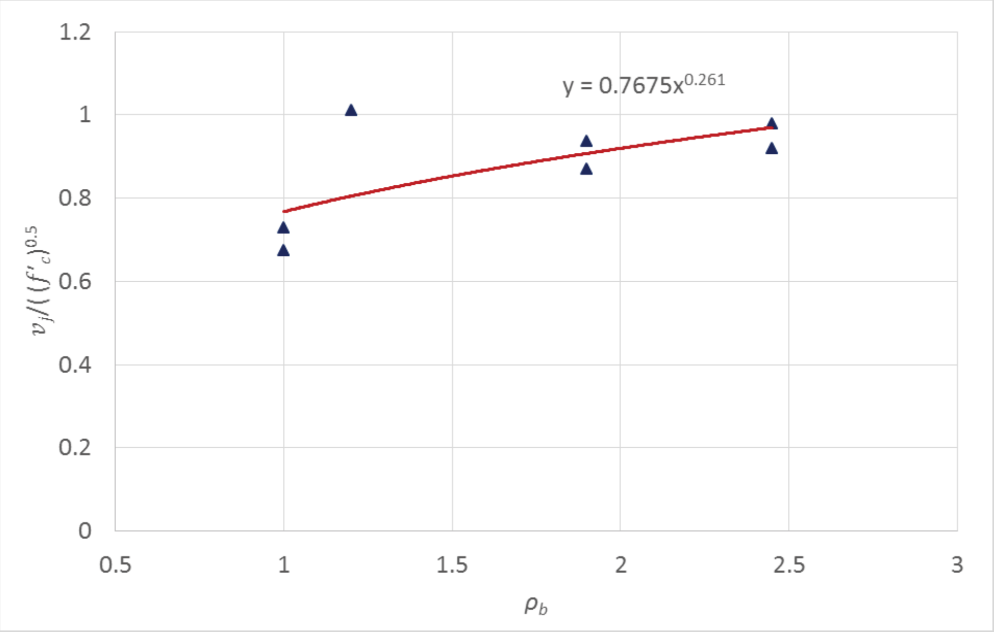

Figure 7-3 Effect of beam reinforcement ratio on shear strength of BCJs

7.2.3. Effect of BCJ Aspect Ratio

To evaluate an effect of aspect ratio on shear strength of BCJ experimental results of Wong [18], Antonopoulos and Triantafillou [19], Pantelides [20] are investigated to cover a range of aspect ratio from 1 to 2. Those experimental results are only considered in which axial load ratio was almost similar. Shear strength was then normalized with $\sqrt{f'_c}$ and effect of beam longitudinal reinforcement that is $\rho_b^{0.261}$ Normalized shear strength is then plotted against respective values of aspect ratio as displayed in Figure 7-4. The following relation between aspect ratio of BCJ (h_b /h_c) and shear strength is derived from the trend:

$$\frac{v_j}{\sqrt{f'_c}\,\rho_b^{0.261}} = 0.7543\left(\frac{h_b}{h_c}\right)^{-0.279} \tag{7.2}$$

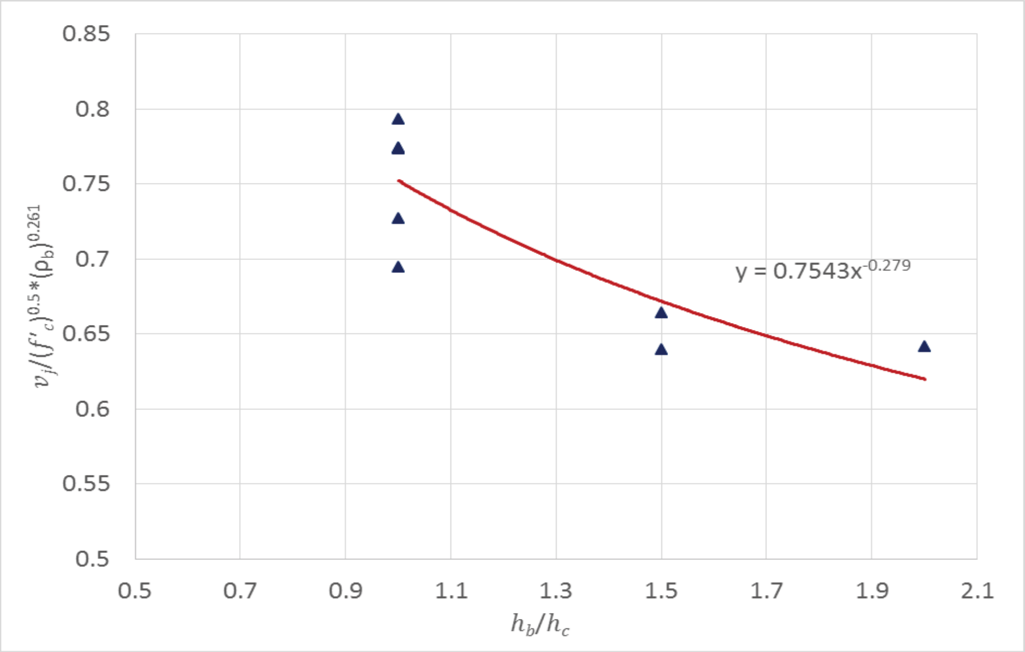

Figure 7-4 Effect of aspect ratio on shear strength of BCJs

7.2.4. Proposed Shear Strength Equation for BCJs

Effect of all the parameters effecting shear strength of unconfined joints with joint failure mode that are axial load on column, concrete strength, beam reinforcement ratio and BCJ aspect ratio are lumped in to following Equation [7.3].

$$V_n = 0.58\sqrt{f'_c}\left(\alpha + \beta\frac{N}{A_g}\right)^{\gamma}\left(\frac{A_{sb}}{b_b\,d}\right)^{0.261}\left(\frac{h_b}{h_c}\right)^{-0.279}\left(\frac{b_b+b_c}{2}\right)h_c \tag{7.3}$$

where V_c is the shear strength of joint without stirrups in newton (N); α, β and γ are shear co-efficient tabulated in Table 7-1 for various ranges of ALR. N is the CAL (N); A_g is the cross-sectional area of column at the joint (mm^2); A_{sb} is area of beam reinforcement (mm^2); b_b, d and h_b are the width, depth and section depth of the beam respectively (mm); b_c and h_c are the column section width and depth respectively (mm). f'_c is the concrete cylinder strength of concrete (MPa).

Table 7-1 Values of joint shear co-efficient

Axial Load Ratio $\frac{N}{A_g f'_c}$	Shear co-efficient		
	α	β	γ
$0.00 < \text{ALR} \le 0.50$	351	100	0.21
$0.50 < \text{ALR} \le 0.70$	4	0.03	1
$0.70 < \text{ALR} \le 0.90$	425	-5	0.25

7.3. Validation of shear strength equation

Database utilized to validate proposed shear strength equation is based on experimental results available in literature. In these experiments BCJs were unconfined, longitudinal reinforcement has standard 90° hook and failure mechanism is joint failure mode. The maximum ALR considered in data base is 0.25 due to unavailability of test results for unconfined joints with joint shear failure mode above this range also the maximum concrete compressive strength considered is 46.2 MPa. Table 7-2 tabulates the validation of proposed shear strength equation.

Table 7-2 Validation of proposed shear strength equation

Researchers	Specimens	Joint Type	Joint aspect ratio	f'_c MPa	Beam			Axial load ratio (ALR)	V_{Test} (MPa)
					ρ_{bb} (%)	ρ_{tb} (%)	f_{yb} MPa		
Hakuto [3]	06	Exterior	1.1	31	0.66	1	308	0	3.75
	07	Exterior	1.1	31	0.66	1	308	0	4.05
Clyde et al. [16]	SP 2	Exterior	0.89	46.2	2.45	2.45	454	0.10	6.26
	SP 6	Exterior	0.89	40.9	2.45	2.45	454	0.10	6.26
	SP 4	Exterior	0.89	37.0	2.45	2.45	454	0.25	7.07
	SP 5	Exterior	0.89	40.1	2.45	2.45	454	0.25	6.83
Pantelides et al. [20]	SP 1	Exterior	1.00	33.0	1.90	1.90	459	0.10	5.39
	SP 2	Exterior	1.00	33.0	1.90	1.90	459	0.25	5.24
	SP 3	Exterior	1.00	34.0	1.90	1.90	459	0.10	5.08
	SP 4	Exterior	1.00	34.0	1.90	1.90	459	0.25	5.66
	SP 5	Exterior	1.00	31.6	1.90	1.90	459	0.10	5.46
	SP 6	Exterior	1.00	31.6	1.90	1.90	459	0.25	5.46

Researchers	Specimens	Joint Type	Joint aspect ratio	f'_c MPa	Beam			Axial load ratio (ALR)	V_{Test} (MPa)
					ρ_{bb} (%)	ρ_{tb} (%)	f_{yb} MPa		
Wong [18]	BS-L	Exterior	1.50	30.8	0.94	0.94	520	0.15	4.05
	BS-U	Exterior	1.50	30.9	0.94	0.94	520	0.15	4.06
	BS-LL	Exterior	1.50	42.1	0.94	0.94	520	0.15	5.39
	BS-L-LS	Exterior	1.50	31.6	0.94	0.94	520	0.15	5.06
	BS-V2T10	Exterior	1.50	32.6	0.94	0.94	520	0.15	3.19
	BS-V4T10	Exterior	1.50	28.3	0.94	0.94	520	0.15	4.76
	BS-L600	Exterior	2.00	36.4	0.68	0.68	520	0.15	3.38
Ghobarah and Said [15]	T 1	Exterior	1.00	30.9	1.20	1.20	425	0.19	5.58
	T 2	Exterior	1.00	30.9	1.20	1.20	425	0.10	5.63
Antonopoulos and Triantafillou [19]	C1	Exterior	1.50	19.4	0.77	0.77	585	0.05	2.57
	C2	Exterior	1.50	23.7	0.77	0.77	585	0.05	2.95
									Standard

Note: V_{Test} = Shear strength from experiment; $V_{Predicted}$ = Shear strength predicted by proposed equation.

7.4. Discussion on Proposed and Previous Shear Strength Equations

Several shear strength equations available in literature including present design guidelines are deficient in predicting shear strength of unconfined joints in one or another way. For example Vollum and Newman [21] model considered the effect of aspect ratio and f'_cbut did not account for the important influencing parameters such as CAL and beam reinforcement ratio. Bakir and Boduroglu considered the effect of beam reinforcement ratio, aspect ratio and f'_c but did not account for the CAL which is a key influencing parameter in determining joint shear strength also effect of beam reinforcement is included without establishing distinction between the mode of failure as in BJ failure mode beam reinforcement does not contributes toward the joint shear strength owing to its yielding at the interface. Sarsam and Phillips [23] considered the effect of aspect ratio of joint, column reinforcement ratio and axial load on column up to ALR of 0.42 but did not include the effect of beam reinforcement ratio. Current design guidelines of ACI-ASCE Committee 352 [25] at first assumes that tension steel yield secondly these guidelines does not take in to an account key parameters like aspect ratio, beam reinforcement ratio and column axial load in estimating shear strength of joint. The proposed shear strength equation considers all the effects like CAL, f'_c, joint aspect ratio and beam reinforcement ratio is validated with experimental database of unconfined joints giving average of $V_{Predicted}/V_{Test}$ equals 0.88 and standard deviation of 0.10. Thus it is concluded that proposed shear strength equation gives more representative and conservative estimates of joint shear strength.

CHAPTER 8

CONCLUSIONS AND RECOMMENDATIONS

8.1. Conclusions

Based on investigation of important parameters effecting seismic performance of BCJ's through review and results obtained and documented in this research work, following important conclusions are derived.

8.1.1. Assessment of Seismic Deficiencies in Reinforced Concrete Buildings

1. Strength of a structure, its ductility or deformability and energy dissipation capacity are prime building blocks of an advanced seismic design.
2. Most of the buildings in the world designed before 1970's are deficient both in strength and deformability capacity.
3. Absence of adequate hoop reinforcement with in a joint, inadequate development length of beam longitudinal bars, deficient splice lengths of column longitudinal reinforcement and use of plain steel bars are most common deficiencies in the BCJs of deficient buildings.
4. To understand the behavior of BCJs it is very imperative to consider the key parameters influencing the behavior of BCJs in order to advance studies not only in successful retrofitting schemes but to reinforce new design concepts.

5. Axial load on the column which is a key influencing parameter in predicting shear strength of BCJ is not considered explicitly so far and due to its complex effects on the shear strength of the joint this parameter is not well understood.
6. In most of the researches variation of ALR is not more than approximately 0.15 and maximum axial load considered and well documented in form of shear strength equation is 0.42 $f'_c A_g$.

8.1.2. Effect of Axial Load on Performance of BCJs

Different magnitude of CAL effects the performance of BCJs in the following ways:

1. Increasing ALR from 0.00 to 0.60 enhances the shear strength of BCJ up to 42 %.
2. Shear strength of joint in range of ALR 0.60 to 0.70 is found to be almost similar.
3. Increase in ALR above 0.70 decreases the shear strength of joint rapidly until pure axial failure of the joint.
4. Axial failure of unconfined joint without establishing any shear capacity occurs at ALR of 1.00 to 1.10
5. Joint failure mode occurs up to ALR of 0.60 to 0.70 whereas above that joint fails in axial failure mode.
6. High axial load increases the inclination of shear cracks.
7. On average reduction in shear strength of BCJ due to reverse cyclic loading is around 14 % as compared to monotonic counterpart.
8. High axial load delayed the initiation of first shear and beam-joint interface crack. However, number of cracks in beam increases with rise in CAL.
9. Ductility of BCJ reduces with increase in CAL, this effect is more pronounced for ALR of 0.60 and above.

10. Several factors such as shear and flexural cracking, reinforcement slippage and loss of cover effects the stiffness degradation of joint.
11. High axial load increases the initial stiffness of BCJ and rate of stiffness degradation is found to be more in such cases.
12. Although initial stiffness increases with increase in axial load but post peak stiffness degradation trend is found to be similar up to ALR of 0.60.
13. Above ALR of 0.60 rate of stiffness degradation increases drastically due to more deterioration caused by local crushing and bond damage especially after initiation shear failure.
14. Energy dissipation capacity increases with increase in axial load up to 0.60 f'_c A_g.
15. Improvement in energy dissipation capacity because of high axial load is due to confinement provided by axial load against joint shear and improved bond-slip behavior of longitudinal reinforcement. However, the same is not true for very high axial load that is above 0.60 f'_c A_g where joint experiences local crushing or complete axial failure in such cases high axial load damages the joint in crushing and thus causes severe detrimental effects on shear strength.

8.1.3. Numerical Modelling of BCJs

1. Concrete damage plasticity reasonably predicts strength, ductility and crack patterns in BCJs
2. Model code of fib for concrete structures predicts the stress-strain curve relationship for concrete with reasonable accuracy.

3. Embedment technique to simulate bond behavior of reinforcement with concrete gives reasonable results without numerically costly iterations linked with surface formulations.

8.1.4. Proposed Shear Strength Equation for BCJs

1. The proposed shear strength equation considers all the effects like CAL, f'_c, joint aspect ratio and beam reinforcement ratio in predicting joint shear strength.
2. The proposed shear strength equation gives more representative and conservative estimates of joint shear strength for unconfined joints as dictated by validation results of experimental database.

8.2. Future Recommendations

1. This research deals with exterior BCJs which can be extended for other types of joint like knee and interior and corner joints.
2. Performance of BCJs with different magnitude of axial load on column can be evaluated for higher strength and various types of concrete like ultra-high performance concrete (UHPC).
3. This research work can be extended to evaluate performance of different retrofitting techniques such as CFRP sheets, steel jacketing, GFRP, AFRP, ultra-high strength concrete (UHPC) and shape memory alloys (SMA).
4. Different BCJs aspect ratios and beam-column eccentricities can be studied to advance the current research work.
5. Effect of column and beam reinforcement percentages can be evaluated for strength and failure mode under different axial load ratios.

REFERENCES

[1] A. G. Tsonos, ‘Lateral Load Response of Strengthened Reinforced Concrete Beam-to-Column Joints’, *Struct. J.*, vol. 96, no. 1, pp. 46–56, Jan. 1999.

[2] P. J. Granata and A. Parvin, ‘An experimental study on Kevlar strengthening of beam–column connections’, *Compos. Struct.*, vol. 53, no. 2, pp. 163–171, 2001.

[3] S. Hakuto, R. Park, and H. Tanaka, ‘Seismic Load Tests on Interior and Exterior Beam-Column Joints with Substandard Reinforcing Details’, *Struct. J.*, vol. 97, no. 1, pp. 11–25, Jan. 2000.

[4] Tarek H. Almusallam and Yousef A. Al-Salloum, ‘Seismic Response of Interior RC Beam-Column Joints Upgraded with FRP Sheets. II: Analysis and Parametric Study: Journal of Composites for Construction: (ASCE)’, *J. Compos. Constr., 11(6), 590–600.*

[5] Ghobarah, A. and El-Amoury, T., ‘Seismic Rehabilitation of Deficient Exterior Concrete Frame Joints: Journal of Composites for Construction: (ASCE)’, 2005.

[6] A. Prota, A. Nanni, G. Manfredi, and E. Cosenza, ‘Selective Upgrade of Underdesigned Reinforced Concrete Beam-Column Joints Using Carbon Fiber-Reinforced Polymers’, *Struct. J.*, vol. 101, no. 5, pp. 699–707, Sep. 2004.

[7] A. Mukherjee and M. Joshi, ‘FRPC reinforced concrete beam-column joints under cyclic excitation’, *Compos. Struct.*, vol. 70, no. 2, pp. 185–199, Sep. 2005.

[8] R. Park, ‘A summary of results of simulated seismic load tests on reinforced concrete beam-column joints,beam and columns with sub-standard reinforcing details’, *J. Earthq. Eng.*, vol. 6, no. 2, pp. 147–174, Apr. 2002.

[9] Pampanin, S., Bolognini, D and Pavese, A., ‘Performance-Based Seismic Retrofit Strategy for Existing Reinforced Concrete Frame Systems Using Fiber-Reinforced Polymer Composites: Journal of Composites for Construction: (ASCE)’.

[10] Bank, L., Brown, V., Cosenza, E., Davalos, J., Lesko, J., Machida, A., Rizkalla, S., and Triantafillou, T., ‘Fiber-Reinforced Polymer Composites for Construction—State-of-the-Art Review: Journal of Composites for Construction: (ASCE)’, 2002.

[11] ‘National Information Service for Earthquake Engineering (NISEE), Pacific Earthquake Engineering Center’, University of California, Berkeley, 2010.

[12] Uang, C-M., et al., ‘Ji-Ji Taiwan Earthquake of Sep.21, 1999: A Brief Reconnaissance Report’, Department of Structural Engineering, University of California, San Diego, 1999.

[13] Moehle, J. P., ‘State of research on seismic retrofit of concrete building structures in the US’, presented at the US-Japan Symposium and Workshop on Seismic Retrofit of Concrete Structures - State of Research and Practice, 2000.

[14] Gokgoz, E., ‘Experimental Research on Seismic Retrofitting of R/C Exterior Beam-Column-Slab Joints Upgraded with CFRP Sheets’, M.Sc. Thesis, Graduate Program in Civil Engineering, Bogaziçi University, 2008.

[15] A. GHOBARAH∗ and A. SAID†, ‘Seismic Rehabilitation of Beam-Column Joints Using Frp Laminates’, *J. Earthq. Eng.*, vol. 5, no. 1, pp. 113–129, Jan. 2001.

[16] Clyde, C., et al, ‘Performance-Based Evaluation of Exterior Reinforced Concrete Building Joints for Seismic Excitation’, University of California, Berkeley, CA, Technical Report PEER 2005-5, Jul. 2000.

[17] Barnes, M. and Jigoral, S., ‘Exterior Non-Ductile Beam Column Joints’, University of California, Berkeley, PEER/NEESREU Research Report, Aug. 2008.

[18] Wong, H.F., ‘Shear Strength and Seismic Performance of Non-Seismically Designed Reinforced Concrete Beam-Column Joints’, PhD Dissertation, Department of Civil Engineering, The Hong Kong University of Science and Technology, 2005.

[19] Antonopoulos, C.P. and Triantafillou, T.C., ‘Experimental Investigation of FRP Strengthened RC Beam-Column Joints’, *ACSE J. Compos. Constr.*, vol. V.7, No. 1, pp. 39–49, 2003.

[20] Pantelides, C., Okahashi, Y., and Reaveley, L., ‘Seismic Rehabilitation of Reinforced Concrete Frame Interior Beam-Column Joints with FRP Composites: Journal of Composites for Construction: (ASCE)’, 2008.

[21] Vollum RL, ‘Design and analysis of exterior beam column connections’, Phd thesis, Imperial College of Science Technology and Medicine-University of London, 1998.

[22] Bakir, P.G., and Boduroglu, H.M, ‘A new design equation for predicting the joint shear strength of monotonically loaded exterior beam-column joints’, *Engineering Structures*, vol. No. 24, pp. 1105–1117, 2002.

[23] Sarsam, K.F., and Phipps, M.E., ‘The Shear Design of In-situ Reinforced Beam-Column Joints Subjected to Monotonic Loading’, *Magazine of Concrete Research*, vol. 37, no. No. 130, pp. 16–28, 1985.

[24] Ilki, Alper, ‘Behavior of FRP-Retrofitted Joints Built with Plain Bars and Low-Strength Concrete’, *J. Compos. Constr.*, vol. 15, no. 3, pp. 312–326, 2011.

[25] Joint ACI-ASCE Committee 352, ‘Recommendations for Design of Beam-Column Connections in Monolithic Reinforced Concrete Structures’, 2002.

[26] Will, G. T., Uzumeri, S. M. and Sinha, S. K., ‘Application of finite element method to analysis of reinforced concrete beam-column joints.’, in *In Proceedings of Specialty Conference on Finite Element Method in Civil Engineering*, Canada, 1972, pp. 745–766.

[27] Noguchi, H., ‘Nonlinear finite element analysis of reinforced concrete beam-column joints’, in *In IABSE Colloquium*, Delft, The Netherlands, pp. 639–653.

[28] Baglin, P. S., and Scott, R. H., ‘Finite element modeling of reinforced concrete beam-column connections’, *ACI Struct. J.*, pp. 886–894, 2000.

[29] Gulsah Sagbas, ‘Nonlinear Finite Element Analysis of Beam-Column Subassemblies’, Graduate Department of Civil Engineering University of Toronto, Canada, 2007.

[30] Ahmed, D., ‘Retrofitting of exterior beam-column joints using CFRP’, MSc. Thesis, King Fahd University of Petroleum and Minerals, Saudi Arabia, 2012.

[31] N.Mitra, ‘Continuum Model for RC Interior Beam-Column Connection Regions’, presented at the The 14 th World Conference on Earthquake Engineering, Beijing, China, 2008.

[32] De Borst, R. and Nauta, P., ‘Non orthogonal cracks in smeared finite element model’, *Eng. Comput.*, pp. 35–46, 1986.

[33] Hordijk, D. A, ‘Local approach to fatigue of concrete’, PhD thesis, Department of Civil Engineering, Delft University of Technology, Delft, The Netherlands, 1991.

[34] Willam, K. J. and Warnke, E. P., 'Constitutive models for the triaxial behavior of concrete.', in *International Assoc. for Bridge and Structural Engineering*, 1975, vol. 19, pp. 1– 30.

[35] ACI committee 318, *318-14: Building Code Requirements for Structural Concrete and Commentary*. 2014.

[36] ASTM C39/C 39M-04a, 'Standard Test Method for Compressive Strength of Cylindrical Concrete Specimens', 2004.

[37] ASTM C 469-94, 'Standard Test Method for Static Modulus of Elasticity and Poisson's Ratio of Concrete in Compression', 1994.

[38] ASTM C 496/C 496M - 04, 'Standard Test Method for Splitting Tensile Strength of Cylindrical Concrete Specimens', 2004.

[39] Chen GM., 'Behaviour and strength of RC beams shear-strengthened with externally bonded FRP reinforcement.', Department of civil and structural engineering,The Hong Kong Polytechnic University, Hong Kong. China, 2010.

[40] Yang ZJ, Chen JF, Proverbs D., 'Finite element modelling of concrete cover separation failure in FRP plated RC beams.', *Constr Build Mater1713–13*, 2003.

[41] Yang ZJ, Chen JF., 'Fully automatic modelling of cohesive discrete crack propagation in concrete beams using local arc-length methods.', *Int J Solids Struct413–4801–26*, 2004.

[42] Yang ZJ, Chen JF., 'Finite element modelling of multiple cohesive discrete crack propagation in reinforced concrete beams.', *Eng. Fract. Mech.*, 2005.

[43] International Federation for Structural Concrete (fib), *fib Model Code for Concrete Structures 2010*, vol. 1. .

[44] V. Birtel, P. Mark, 'Parameterised Finite Element Modelling of RC Beam Shear Failure', presented at the ABAQUS Users Conference, 2006.

[45] *ABAQUS Documentation*. RI, USA.: Dassault Systèmes, Providence, 2011.

VITAE

Name : Umais Khan

Nationality : Pakistani

Date of Birth : 24-12-1989

Email : umais-khan@live.com

Address : Abbottabad, Pakistan

Academic Background : **Master of Science in Civil Engineering, May, 2016**

Thesis: Effects of Variation of Axial Load on Seismic Performance of RC Exterior BCJs

King Fahd University of Petroleum & Minerals, KSA

Bachelor of Engineering, Civil Engineering, October, 2012

Final Year Project: Review and Evaluation of Structural Fire Safety Measures in Pakistan.

National University of Sciences & Technology, Pakistan